The Effects of Different Deployment Strategies of Artemisinin Combination Therapies on Slowing Down the Spread of Antimalarial Drug Resistence: Investigation With Individual-Based Simulations

Thesis

THE EFFECTS OF DIFFERENT DEPLOYMENT STRATEGIES OF ARTEMISININ COMBINATION THERAPIES ON SLOWING DOWN THE SPREAD OF ANTIMALARIAL DRUG RESISTANCE: INVESTIGATION WITH INDIVIDUAL-BASED SIMULATIONS

by

Tran Dang Nguyen

A thesis submitted to the Open University U.K

For the degree of Doctor of Philosophy in the field of Life Sciences

Oxford University Clinical Research Unit

Hospital for Tropical Diseases

Ho Chi Minh City, Viet Nam

June 2015

DATE OF SUBMISSION: 30 JUNE 2015

DATE OF AWARD: 12 MAY 2016

Dedication

I dedicate this thesis to my parents for their unconditional love and support, and my wife, Nguyen Kieu My Oanh, for always be there and putting up with me while I was doing this PhD.

Acknowledgement

It appears somehow wrong to declare that this thesis is my work alone when I received a great amount of invaluable support over the past five years. First of all, I owe a tremendous amount of gratitude to my supervisor, Prof. Maciej Boni, for constantly providing encouragement and constructive feedback on my research as well as research skill development, especially scientific writing. Without his continued patience and guidance, it would never have been possible to finish this thesis nor would I have gained so much valuable research experience.

I would like to thank Prof. Nick White and Prof. Piero Olliaro for their scientific advice and knowledge as well as many insightful discussions and suggestions.

I would like to thank Ha Minh Lam, who developed a separated graphical user interface, so that I can live-view the output of the model during validation phase.

Abstract

Despite the success of recent global malaria control efforts, which have halved global malaria mortality since 2000, malaria is still one of the world's most deadly diseases causing an estimated half a million deaths, mostly among African children, and around a quarter of billion clinical episodes every year as reported in 2014 [1]. Drug resistance is one of the most important challenges to malaria elimination. To contain drug resistance, many efforts have been put forth including improvement of surveillance systems and mass treatment in order to stop or slow down the transmission of the resistant strain. To find out whether a population-level treatment strategy can have any benefit in containing drug resistance, mathematical models are an appropriate approach to this problem and individual-based models allow us to have a better understanding of the effect of individual heterogeneities on the outcome.

The first part of the thesis is about building and validating an individual based microsimulation. The model is implemented as an individual-based discrete-time event simulation model in C++. The behaviors and the state changes of human individuals are determined by relevant events and mathematical formulas. This integrated model combines components that reproduce the most important features of malaria transmission and epidemiology: the infectiousness of human populations; clinical model of acute illness; heterogeneities in individuals' age, biting-rate level, drug absorption, drug action, multiple parasite populations, and human immunity.

To validate this individual-based model, two types of validation have been done. The model's parameters were obtained from field or clinical data were used directly in the model. For those parameters that cannot be obtained directly from literature review, sensitivity analysis has been done to find how variation in parameter values affects certain key features of malaria epidemiology.

The second part of the thesis focused on the comparison between population-scaled treatment strategies. The results showed that using multiple first-line therapies (MFT) results in a lower number of treatment failures compared to other strategies where a single first-line ACT is

recommended. This result is robust to various epidemiological, pharmacological, and evolutionary features of malaria transmission. In addition, including non-ACT therapy in an MFT strategy seems to have a significant benefit in reducing the pressure on artemisinin-resistance evolution, delaying its emergence and slowing its spread.

The third part of the thesis focused on individual-level treatment strategies to combat artemisinin resistance. The results showed that lengthening an ACT course or using multiple courses of ACT can reduce the long-term number of treatment failures significantly.

The work reported here introduces a novel individual-based simulation that includes drug resistance evolution and the ability to be scaled up to millions number of individuals. The challenge that remains is to evaluate the feasibility of these novel treatment strategies given that they will need to be implemented in the real world of malaria control programs, their operations, human behavior, and economic realities.

Table of Contents

List of Tables

List of Figures

List of Abbreviations

ACT	Artemisinin Combination Therapy
AL	Artemether-Lumefantrine
AMU	Artemisinin Monotherapy Use
ASAQ	Artesunate-Amodiaquine
ASMQ	Artesunate-Mefloquine
ASSP	Artesunate-SP
CQ	Chloroquine
DDT	Dichloro Diphenyl Trichloroethane
DHA-PPQ	Dihydroartemisinin-Piperaquine
DES	Discrete Event Simulation
EIR	Entomological Inoculation Rate
GMPD	Geometric Mean Parasite Density
GUI	Graphical User Interface
HPC	Human Population Component
IRS	Indoor Residual Spraying
ITN	Insecticide-Treated Bed Net
LLIN	Long-lasting Insecticide-Treated Nets
MAC	Multiple Artemisinin Courses
MACR	Multiple Artemisinin Courses Randomization
MDA	Mass Drug Administration
MSAT	Mass Screen And Treat
MFT	Multiple First-line Therapy
MOI	Multiplicity Of Infection
NTF	Number of Treatment Failures
PK/PD	Pharmacokinetic/Pharmacodynamic
RDT	Rapid Diagnostic Test
SDC	Statistic and Data Collection
Seq Depl	Sequential Deployment
SP	Sulfadoxine-Pyremethamine
TME	Targeted Malaria Elimination
UTL	Useful Therapeutic Life
WHO	World Health Organization
ws60	60-day Window Size
ws120	120-day Window Size
ws180	180-day Window Size

Chapter 1

Introduction and Literature Review

Malaria is one of the world's most deadly diseases and is believed to have existed in humans for tens of thousands of years[2–4], and detailed records of malaria clinical symptoms, transmission routes, and treatment options began to be recorded at the end of the 19th century[5]. In the middle of the 20th century, malaria was endemic in more than 143 countries, with over half of the world's population at risk of infection[6,7]. The two major and geographically most expansive species were, and still are, *Plasmodium falciparum* and *Plasmodium vivax*, with three other human-adapted *Plasmodium* species accounting for an unknown proportion of infections[8]. In the 1950s and 1960s, rapid economic development in some regions of the world along with a World Health Organization (WHO) malaria eradication campaign helped shrink the global malaria map, but the disease is still endemic in most of Africa and parts of Asia and South America[9]. At the turn of the century, malaria caused approximately 300 million annual clinical malaria episodes and over one million deaths[10]. After a renewal of interest in global malaria control over the past ten years, case numbers have been cut approximately in half, and the number of malaria deaths is around 500,000 per year[1].

Treatments for malaria have existed for hundreds of years, and the 20th century saw an acceleration of discovery of new antimalarial drugs[11,12]. The discovery of these new drugs, however, was accompanied by the evolution of drug resistance in one or some of the parasite species that cause malaria[12,13]. Chloroquine (CQ), the most commonly used antimalarial in the 20th century, lost its efficacy in the 1970s and 1980s; this was followed by an increase in usage of sulfadoxine-pyremethamine (SP), and SP-resistance appeared soon thereafter[12–16]. Of the dozens of widely used antimalarials, only the artemisinin-class drugs have not been adversely affected by drug-resistance evolution, but recently a several *P. falciparum* genotypes partially-resistant to artemisinin have emerged in Southeast Asia[17–21].

As malaria elimination and eradication plans move forward in the 21st century, these massive global health efforts must be pursued alongside a rational drug management strategy that seeks to minimize both (1) the future expected level of drug-resistance, and (2) the number of malaria cases and deaths in the world each year. This complex problem is amenable to analysis by mathematical modeling, and my PhD thesis will develop an individual-based modeling system to predict long-term trends in malaria epidemiology and evolution, in the context of different antimalarial treatment strategies.

This chapter, after a brief introduction to malaria, reviews what is currently known about mathematical modelling for malaria including compartmental and individual-based models, and lastly describes the rationale and objectives of the thesis.

1.1 Malaria

Malaria is a vector-borne disease that caused by *Plasmodium* parasites. There are five species of *Plasmodium* that cause disease in human, namely *P. falciparum*, *P. vivax*, *P. ovale*, *P. malariae*, and *P. knowlesi*. Among those species, *P. falciparum* is the deadliest one which accounted for more than half of symptomatic cases and 90% deaths from malaria as estimated in Africa 1993 [22]. According to the World Malaria Report 2015, *P. falciparum* is the most prevalent on the African continent, and is responsible for most deaths from malaria [23].

P. falciparum is spread from human through human by female *Anopheles* mosquitoes [4]. Within the host, the parasites proceed through a series of developmental stages. When an infectious mosquito bites a person to take a blood meal, the mosquito can inoculate sporozoites (a particular developmental stage of *Plasmodium* species) into human's blood stream and these sporozoites invade the liver within half an hour. In the liver, they develop into around 30,000-40,000 merozoites over the duration of one to two weeks, after which they exit the liver cells to invade the red blood cells. Inside red blood cells, the merozoites continue to grow and divide, eventually reaching parasite population sizes approaching 10^{11} or 10^{12} parasites[24]. Some merozoites eventually develop into gametocytes, which are the only parasite stages that can be

taken up by mosquitoes during blood meals. Inside the mosquito, the gametocytes undergo sexual reproduction (haploid to diploid to haploid) and then develop into sporozoites that enter the mosquito's salivary glands after about ten days. At this point, the infected mosquitoes are infectious and the transmission cycle is re-initiated by biting a human and inoculating him or her with sporozoites.

During the transmission cycle, when asexual blood-stage parasites reach a total population size of around 10^8 or 10^9 [25], the host will experience symptoms that include fever, muscle aches, sweats, chills and vomiting[26]. The WHO-recommended treatment for symptomatic or clinical malaria is artemisinin combination therapy (ACT), which currently would be one of artemether-lumefantrine, artesunate-amodiaquine, dihydroartemisinin-piperaquine, artesunate-mefloquine, or artesunate-SP[27]. If a naïve patient does not receive any treatment or receives inadequate treatment, the infection can become severe and life-threatening. However, people who live in endemic areas acquire immunity through continuous natural exposure to malaria parasites, and this immunity can protect them from the severe effects of malaria or progression to symptoms[28,29]; the drawback of not experiencing symptoms is that these individuals are likely to not be treated and are thus likely to carry malaria parasites in their blood for prolonged periods[30,31].

1.2 Malaria Control Strategies

1.2.1 Vector Control and Protection against Mosquito Bites

To reduce the transmission between vectors and human, many attempts have been made to reduce the source of infection and to protect humans from infectious mosquito bites. The two most popular and effective methods in vector control are indoor residual spraying (IRS) and insecticide-treated bed nets (ITNs).

Indoor residual spraying is a widely used method that involves spraying insecticides on the wall inside a house. Mosquitoes usually rest on the wall after taking blood meal, so if the wall was

surfaced by insecticides it can kill mosquitoes before they can bite another person, and thus reduce the transmission of malaria[32]. However, this method has its flaws. Mosquitoes can easily evolve to become resistant to chemical insecticides, and thus national malaria control programs have to perform entomological surveys and change the chemicals frequently to maintain the efficacy of IRS. In addition, due to the irritation caused by IRS, mosquitoes (and their subsequent generations) have adopted new behaviors, e.g. new time or place of blood meal or new host, to avoid the exposure to insecticides and maintain their reproduction[33]. For example, studies conducted in Senegal [34] and Benin [35] showed that *A. gambiae* changed their biting habits from after midnight to about before 10 p.m. when most people are not yet under a bed net. The studies from Benin also showed that, just one year after the large-scale introduction of ITNs, *A. funestus*, which used to bite inside people's homes, began to take more frequent blood meals outdoors; the proportion of outside bites increased from 45% before intervention to >75% after the intervention [35].

Mosquito nets help prevent mosquitoes biting people when they are sleeping, as *A. gambiae*, the major malaria vector species in Africa, usually have their blood meal at night [36,37]. Hence, the use of mosquito nets can reduce the transmissibility of infectious mosquito to human. However, a simple net is not a sufficient shield from infection and it is often soaked with insecticide to kill mosquitoes when they land on the net. These insecticide-treated nets (ITNs) also have the advantage of also providing some protection to other people, including people in the same room but not under the net. The use of ITNs has been shown to be an effective method to prevent malaria in children and pregnant women. Under research study conditions, ITNs usage has been associated with significant reduction in malaria morbidity and all-cause child mortality[38–41]. However, due to the lack of knowledge of people living in the endemic areas, there are some concerns about the misuse of ITNs, i.e. using nets for window curtains, drying fish, or fishing, etc[42,43]. Those misuse may lead to a reduction in the efficacy of ITN control programs.

1.2.2 Treatment Strategy in Individual-scaled and Population-scaled

Prophylaxis is a recommended method of malaria prevention for people that are going to travel to a malaria-endemic area. Due to the fact that *Plasmodium* species are resistant to one or more antimalarial drugs the choice of prophylaxis medications highly depends on location. Another possible prevention strategy is vaccination. Although malaria vaccines have been under continuous development for several decades and they still cannot offer full protection from infection. As of mid 2015, there is no malaria vaccine that has been qualified or recommended by WHO.

Two traditional low-cost treatments for malaria are chloroquine (CQ) and sulphadoxine-pyrimethamine (SP). However, due to drug resistance, those drugs are ineffective in Asia and some parts of Africa for treatment of both *P. falciparum* and *P. vivax* infections[15]. These drugs have been replaced by artemisinin-based drugs over the past decade, and artemisinin derivatives have become standard treatment as WHO recommendation[27]. Although artemisinin is a powerful drug with very high parasite killing rate, it has a very short drug half-life. To improve the efficacy and to reduce the risk of resistance emerging to artemisinin, a combination of artermisinin with a longer half-life partner drugs is now recommended as the best use of artemisinin drugs. Some popular combinations that are used in many countries are Artemether Lumefantrine (AL), Dihydroartermisinin Piperaquine (DHA-PPQ), Artesunate Amodiaquine (ASAQ). Since 2006, ACTs have been globally recommended by WHO and artemisinin monotherapy has been actively discouraged [44]. However, partial resistance to artemisinin drugs has emerged as mentioned in the first reports coming from Southeast Asia in 2008 [17,21,45,46]. The genetic cause of this resistance appears to be K13-propeller gene mutations and these have been recently identified as being under positive selection [19].

One of the best known population-scale strategies to reduce and potentially eliminate malaria is mass drug administration (MDA)[47]. MDA is a strategy in which everybody in a population is treated during the same time period (a few days or a week, typically) with a curative dose regardless of whether the treated person is infected or symptomatic. However, there are some

concerns that using MDA may result in sub-therapeutic levels of drug in a large number of persons and thus increase the risk of developing drug resistance[48]. This strategy is currently being implemented in 11 villages in Southeast Asia in a clinical trial study known as "Targeted Malaria Elimination" (unpublished study).

One major concern for MDA strategies is that they may not be very effective in high transmission areas where individuals are very likely to be bitten and reinfected shortly after the MDA strategy has completed. A recent comparison of mathematical models by the World Health Organization [49] showed that MDA strategies can be effective in low transmission regions, but less so in high transmission regions as the application of MDA is normally followed by a rebound in prevalence. Historically, vector control has been viewed as the best-choice control strategy for high transmission regions [50].

Another variation of the MDA strategy is a "mass screen and treat" strategy (MSAT) [51]. All people in a population are screened with a high-sensitivity malaria diagnostic test (normally RDT) and those with positive results will receive treatment. This intervention is based on the assumption that people who are gametocytaemic will have sufficient parasite density to be detected at the time of screening.

Another hypothetical population level intervention strategy is the deployment of multiple first-line therapies (MFT)[52]. While most national treatment policies recommend a single first-line therapy for uncomplicated malaria, an MFT policy would recommend the simultaneous deployment of different first-line therapies for different patients, as this type of public health policy may delay the emergence of resistance and thus result in a lower number of treatment failures[52]. This strategy is based on the concept that it is difficult for a pathogen to adapt to a constantly changing environment. Thus, in using MFT in a population, the parasites would experience difficulty evolving drug resistance as they have higher chance of encountering different drugs upon each successive new infection.

1.3 Mathematical Model for Malaria

Many mathematical models have been developed to evaluate malaria public health policies. Some models focus on vector control and thus must have detailed vector dynamics in the model, while other models may evaluate treatment strategies and may be more focused on drug-resistance details, pharmacokinetics, and pharmacodynamics. This leads to two current trends in developing malaria models, those focused on vector interventions and those focused on drug-based interventions.

1.3.1 Compartmental Model

The very first mathematical model for malaria was developed by Ronald Ross in 1911 at the same time as his discovery that malaria parasites are transmitted by mosquitoes [53]. Ross wrote down many equations for the different parts of the malaria transmission cycle. His approach included both humans and mosquitoes and was centered around (1) a 'happenings rate' that described the frequency of occurrences of mosquito bites on humans and (2) a basic reproduction number that described, under static or equilibrium conditions, the number of secondary malaria infections generated by a single human case, as a function of the life course of the parasite in mosquitoes and humans. In Ross's models that allowed for recovery, the happenings rate was accompanied by a recovery rate and the resulting system took the shape of a traditional Susceptible-Infected-Susceptible (SIS) model. Using these equations, Ross was able to show that reduction of the happenings rate below a certain threshold would stop transmission causing the parasite to die out (if the reduction were permanent). A reduction in the happenings rate could be achieved in multiple ways, for example by shortening the life of a mosquito or by increasing the recovery rate in humans and thus reducing the chance that an uninfected mosquito becomes infected after a bite. Ross's approaches and methods have been reviewed in many places (e.g. Fine 1975 [54], Smith and Mckenzie 2004 [55]) and his happenings rate still forms the basis of how dynamical epidemiological models are structured.

Forty years later, Ronald Ross's equations began to be modified by George Macdonald. Macdonald added an exposed state to the mosquito component [56] and began fitting his EIR equation to field data [57]. This modification was based on the knowledge of the parasite development period inside the mosquito. The results from this model implied that the crucial part of malaria transmission is the survival of the infected mosquito. Macdonald suggested that the worst conditions known in Africa could therefore be overcome by an increase in the daily mortality of the vector from about 5% to about 45%. This provided the rationale for a WHO-coordinated campaign that used DDT to kill mosquitoes in order to eliminate malaria in Africa [58,59]. Macdonald worked explicitly on elimination models looking at population growth rates in both *P. falciparum* and *P. vivax* [59], the observed and modeled rates of decline when transmission is interrupted [60], and later stochastic computer models aimed at evaluating control strategies [61].

Data collected through the global WHO malaria eradication program of the 1950s and 1960s led to many new analyses on basic malaria epidemiology and a second effort in the 1970s of controlling and understanding malaria in certain parts of West Africa (notably Garki, Nigeria). Dietz et al [62] used periodic biting and prevalence surveys to fit a mathematical model to one year of malaria transmission data in Garki, and this work gave the community its first statistical estimates of recovery rates (infection duration) in a population where immunity to malaria could be gained and lost and could influence the rate of recovery. Bekessy et al [63], Cohen and Singer [64], and Singer and Cohen [65] adopted an approach based on Markov models describing host states, and performed inference on the model's transition probabilities. These analyses also used Garki data and were able to infer age-specific recovery rates. This level of inference was at the limits of what could be done, based on the data and computational methods available at the time.

The next natural step in the evolution of malaria models should have been the evaluation of interventions based on the well-parameterized models that emerged from the 1970s focus on detailed longitudinal studies. However, mathematical modeling was yet to mature into the

computation-intensive, connected, fast-moving field that it became at the beginning of the 21st century. Simplified models were still being used to evaluate things such as household-based intervention strategies [66]. A theoretical focus on model analysis rather than data analysis put certain practical malaria intervention questions out of reach [67]. And a lack of experience in drug treatment modeling caused some very useful intervention models to be overlooked because they were conceptually ahead of their time [68] (Curtis and Otoo, 1986;13 citations in its first 10 years after publication).

In 1983, Nedelman [69] conducted a deeper investigation on the Dietz et al. model (1974) in order to achieve better understanding on the model's assumptions, such as constraints on parameters, inoculation and recovery rates, and data-fitting methods. Nedelman assumed that the inoculation rate is proportional to the vector density and that the proportion depends on the following rationale, that the expected lifetime of a mosquito should be relatively short to both the human infectious duration and the expected time until a naïve mosquito becomes infected. The fitting results showed some inconsistencies with Dietz et al. model, that could be due to the fact that Nedelman used a different approach in estimating the inoculation rate; instead of directly using the entomological data, Nedelman calculated the inoculation rate based on the estimation of human and mosquito susceptibility, using infant infection data and sporozoite rate data. The hypothesis that the inoculation rate is proportional to vector density was tested by the fitting ability of the new model. Although this approach provided a better understanding on the construction of the estimate of inoculation rate, Nedelman's estimates resulted in poorer fits than the original Dietz estimates in some cases. Therefore, it is unclear which model is better at describing the mechanisms of malaria transmission.

In 1989, Halloran et al. [70], based on the Dietz's model, developed the first malaria model to have the ability to evaluate the effect of malaria vaccine programs by introducing acquisition and loss of stage-specific immunity. As expected, the results showed that the prevalence of malaria wanes after implementing a vaccination program and increases if the program is stopped. If the vaccination program cannot eliminate malaria, the total transmission during the

rebound phase overshoots the pre-program prevalence and the magnitude of the rebound increases as the proportion of the population vaccinated increases. Elimination of transmission could be achieved when the proportion of the vaccinated population reaches a certain threshold; however, it was difficult to have confidence in the exact value of the threshold vaccination level due to there being many assumptions about malaria immunity and the effect of the vaccine. One of the biggest drawbacks of this model is that the vaccines were assumed to be 100% effective, which is unrealistic, as through 2016 there is still no highly efficacious vaccine available.

Another mathematical model for vaccination and vector control was developed by Aron in 1987[71]. The analysis of this model showed that malaria elimination can be achieved by combining both vaccination and transmission control that reduce the R0 to below unity. When malaria control cannot eradicate the disease, this can lead to a perverse situation because the prevalence of symptomatic disease may increase. This is based on the assumption that the immunity is maintained by repeated exposure to infections; any intervention that affects or interrupts the transmission will reduce the immunity level in the population which leads to a change in the age distribution of clinical malaria, especially among adults. Aron also had a concern about the effects of the control program that would be sensitive to immunological assumptions made in the model, for example the relative contribution of immune individuals to the force of infection and the rates of waning and acquisition of immunity as the transmission setting changes.

Until 1991, there was no malaria mathematical model that included both population-level antimalarial treatment coverage and drug resistance (to the best of my knowledge). In 1991, Cross and Singer published a hybrid epidemiological and genetic model that allowed for the selection of resistant strains to occur based on the effectiveness of the drugs used [72]. The model was calibrated with the field data of pyrimethamine resistance in Tanzania [73]. The results from the model suggested that sparing use of new anti-malarial drugs is recommended to minimize the selective pressure on the parasite. However, due to the complexity of the model, some

epidemiological features were omitted. The model did not take immunity acquisition or the resistant strain's cost of resistance into account.

A latent period in humans was introduced to malaria models by Anderson and May in 1991 [74]. The model reconfirmed the conclusion by Macdonald [56] that an intervention that targets adult mosquitoes was more effective than the one that targets larval stages. These models also included age structure by considering the population density in the infectious class as a function of age. Then, the age-structured model was incorporated with a simple immunity model so that the model could reproduce the age-prevalence curve that was observed in data. However, this age dependence of infection approach did not make the model fit well when results showed a very long duration of infection. This was due to the limitation of the model which did not take into account the interaction between age and immunity as well as some other epidemiological features.

The 1990s saw an increase in mathematical modeling publications relative to the 1980s. Although it was not yet possible to run large-scale individual-based simulations, numerical simulations for ordinary differential equation models could now be easily obtained and discrete-time models could be implemented easily. Antibiotic resistance emerged as an area of focus for mathematical modelers, and in malaria the first drug-resistance models began to be published after Curtis and Otoo [68]. The initial approach to drug resistance in malaria was rooted in population genetics (Dye 1991 [75], Dye and Williams 1997 [76], Hastings 1997 [77], Hastings and Mackinnon 1998 [78], Mackinnon and Hastings 1998 [79], Koella 1998 [80]) and the focus was on identifying mechanisms that were critical to understanding the evolutionary epidemiology of malaria drug resistance. From these papers, we learned about the importance of the cost of resistance, multi-clonality, linkage, recombination, immunity and the step-wise nature of mutation.

Most compartmental models are not able to have simple features in different heterogeneities in the human population, e.g. age structure, immunity, within-host parasite density and diversity, relative attractiveness to mosquitoes, or heterogeneity in the PK/PD model. The reason for this

is that those variables are most commonly modeled on the individual level but compartmental models are designed to look at groups of individuals. To meet these challenges, individual-based models are used to introduce heterogeneity at the individual level.

1.3.2 Individual-based Model

By the beginning of this century, computational power was sufficient to run both large-scale individual-based models and large compartmental models. The last decade and a half have seen a wide expansion in the use of mathematical models, as development and run-time have both become much shorter since 2000.

McKenzie developed a discrete-event simulation for malaria in 1998 and 2001[81]. This model was developed in order to estimate the elimination probability of malaria in populations by utilizing computer techniques to extend classical compartmental models at the individual level. This can be considered as the first basic individual-based model for malaria. To simulate malaria transmission as well as the *P. falciparum* life cycle within hosts and vectors, a single "time-line" variable was used to schedule an event at a specific time. This model only keeps track of individual states, but not parasite density and it does not allow superinfections. There is no clinical or asymptomatic state in the model. An individual can be in one of four states: susceptible, infected/exposed, infectious and recovered with waning immunity. A simple immunity model was introduced into the simulation where individuals are at a certain probability of re-infection based on their current immunity level (ranging from zero to one). An individual has fully effective immunity at the beginning of an infection, and the level of immunity wanes exponentially to zero after the individual reaches the end of the infectious state.

Later in 1999, McKenzie extended his model to allow superinfection of multiple species, *P. falciparum* and *P. vivax*, in the transmission model[82]. The model shows that a misdiagnosis of a single *P. vivax* infection for a mixed-species infection can lead to a significant increase in *P.*

falciparum parasite density after treatment for *P. vivax*. The number of individuals is 500 and the number of vector varies from 5000 to 50000 in their evaluations.

Another individual based model was developed in 2003 by Gu et.al[83]. Gu's model included a simple immunity model and human immigration to consider the effect of importation of new cases in a scenario of malaria elimination. Multiple intervention strategies, from reducing transmission through bed net use to active case detection and treatment of diagnosed malaria infections, were employed. The results showed that local elimination could be achieved in a low transmission area. For high transmission areas, however, the probability for elimination was low even with a high coverage of whichever intervention strategy was used. In addition, the results also showed that a small level of immigration of new infections (>0.3% population size) would prevent local extinction of malaria. This model simulated both human and vector individuals and was based on an SIS model. The initial population size is 500 which is relatively small.

One of the most important models of the past fifteen years was developed by a team of researchers at the Swiss Tropical Institute; it is an individual-based model that is able to simulate the effect of different types of intervention strategies for malaria control [84–87]. The model is called Open Malaria and its source code is available for free online access [88]. Open Malaria is an individual-based model with a five-day time steps that looks at different aspects of the malaria transmission process in order to evaluate the impact of different types of vaccines. Each individual keeps track of within-host asexual parasite densities. This is an important feature which allows mathematical modelers to investigate the effects of parasite density on the transmission process. High parasite densities are predicted to be associated with clinical malaria, which helps to model the treatment seeking process and to extend the model to have severe and a malaria-induced mortality feature. The parasite densities determine the infectiousness of individuals to mosquitoes. The original version of the individual based model is the "non-vector" version, the vector component, which is a compartment model, was integrated into the original model later in 2008 to evaluate ITNs, IRS intervention strategy [86,89].

By separating the model into different processes, the Open Malaria model can evaluate four types of vaccines. Pre-erythrocytic vaccine acts on reducing the EIR experienced by individuals in the model. The asexual blood-stage vaccine can be simulated by a function that reduces the parasite densities. The transmission blocking vaccine can be modeled by modifying the individual infectivity function, and anti-toxic vaccine reduces the morbidity and mortality rate[84].

For each epidemiological process, the model was validated/fitted with multiple different types of data. The model used the seasonal measured EIR from field data as the input to the transmission process [90]. The malaria therapy data were used to fit the relationship between asexual parasite density and infectivity to vectors [91]. Age-prevalence and incidence data from different sites in Africa were used to validate the immunity behavior of the model [85]. Due to the high computational demands and the complexity of the fitting process, different sub-models were fitted separately [84].

The PK/PD model was introduced into the model in order to evaluate intermittent preventive treatment against malaria in infants (IPTi) using SP [92]. Open Malaria also includes a drug resistance model but no evaluation has been published on this topic [93]. As of writing, the model does not appear to simulate mutation or genetic recombination, hence it cannot simulate resistance evolution. The model does have heterogeneity in biting rate in individuals, as implemented via a differential biting rates according to age and body surface area. The computation cost for a simulation with 10,000 individuals with 1-day time step is said to be around 2 hours.

Another important individual-based model was developed over the past 7-8 years by modelers at Imperial College in London. Based on a compartmental model developed by Filipe et.al. [94], that has both human and vector components, Griffin's model used individual-based approach to model the human components and a stochastic compartmental model to describe the vector component [95]. The initial purpose of the model was to evaluate vector control interventions, thus the vector model included 3 different species of mosquito, i.e. *An. funestus*, *An. arabiensis*,

and *An. gambiae*. So that, the model has the flexibility to investigate different geographically location where the distribution of the species is different. The transmission rate of the model was controlled by the emergence rate of the mosquitoes which can vary the ratio of vectors to humans. However, there is literally no way to validate the fitted number of mosquitoes to match with the epidemiology data.

Turning into human component, the model implemented three different types of human immunity to malaria; i.e. infection-blocking immunity, clinical immunity, and parasite clearance immunity. Three different assumption on immunity acquisition functions were used in the model, namely that immunity increases with age only, immunity increase linearly with exposure, and immunity is acquired with exposure but limited to new infections. The immunity status of each individual is calculated based on transmission intensity, age, and relative biting rate of the individual, which means that individuals with the same age and the same relative biting rate will have the same immunity status. Thus, in the model, the individual does not directly acquire immunity through infections and the individual's immunity status does not reflect the true infection history of an individual. For example, if there is a sudden drop in transmission rate that is caused by an intervention, the immunity will decrease immediately according to the transmission rate; this is implausible.

The model has heterogeneity in the biting rates which assigned to each individual following a log-normal distribution. However, the Griffin model does not have a clear discussion about the role of relative biting rates on the malaria transmission dynamic. In addition, the model does not explicitly keep track of the within host parasite density and thus will not provide an adequate evaluation on many treatment interventions.

The population size is assumed to be static overtime, which means that there is no age structure shifting in the simulation. There is no clear information on birth, death or age changing over time of an individual, which is an important feature where immunity in the model is implemented, as age-dependent immunity is said to be acquired immunity over the lifetime of an individual.

The model's parameters were fit with the age-stratified prevalence and clinical incidence data. The fitting results showed that the infection-blocking immunity is acquired with exposure bit limited to new infections and clinical immunity is acquired with exposure. The model can reproduce the log-linear relationship between EIR and prevalence in collected data. There is a close correlation between the posterior estimate of EIR and the measure EIR.

The model is a closed-source model, and a GUI software is available [96]. However, the population size in the GUI software is fixed to 1,000 for faster performance. With a small population size, the disease tends to died out when population prevalence is less than 0.1%. Finally, I was not able to observe the performance of the model for higher population size, but is mentioned in other papers that the model takes a few hours to simulate 90 years with 100,000 individuals [97].

Improvements to the model were introduced in 2014 which included the improved fitting to the clinical incidence [98]. There were modifications to the function of immunity to help the model fit to data, however there were no changes in the underlying mechanism in the model.

In summary, Griffin's model is good at evaluating vector control interventions (e.g. ITNs or IRS) but not suitable for evaluating the action of antimalarials due to the lack of a within-host model, within host PK/PD heterogeneity and drug resistance mechanism.

A third important model developed over the past decade is the Epidemiological Modeling (EMOD) model or "kernel" developed by Institute of Disease Modelling in Seattle. The EMOD source code is freely available [99]. Initially, EMOD was an individual-based model that focused on simulating the mosquito life cycle and ecology [100]. The main purpose of the model was to evaluate the vector control interventions (e.g. ITNs, IRS). Thus, EMOD had many details on the mosquito life cycle that took into account different stages of vector development. To simulate the infection process to mosquito, a simplified human disease model was used, with 22-day latent period from bite to infectiousness. The model allowed a maximum of five simultaneous infections within an individual. This model provides a flexible framework that is

able to explore the effects of a combination of multiple vector control interventions on the dynamics of vector population and disease transmission.

Immunity to malaria was introduced in the human component in 2012 [101]. Instead of looking at age-dependent immune factors to fit with the age-pattern prevalence data, EMOD uses the parasite antigenic diversity to explain the age-trend data [102]. The model has the ability to keep track of a population with different number of merozoites-surface antigens, PfEMP-1 variants, and minor antigenic epitopes associated with infected red blood cells. Thus, the clinical progression and parasitological immunity is determined by the adaptive immune response to specific antigens. This approach provides a better explanation on immunity acquisition through time compared to other models.

The PK/PD model was introduced to EMOD in 2015 in order to compare the used of DHA-PPQ and AL in a mass drug administration program [103]. The results showed that MDA with an ACT which has a longer half-life partner drug would have resulted in better outcomes under high transmission with moderately high coverage. In addition, adding primaquine in MDA will have the largest effect in reducing prevalence when coupled with long-lasting prophylactic ACT. The PK model was described by a 2-compartment pharmacokinetic, fast decay rate for distribution phase and slow decay rate for elimination phase of the drug concentration; and the PD model followed the Hill equation [104].

According to the model's document, EMOD uses a 24-bit barcodes to represent different parasite strains [105]. It also has the recombination feature within mosquito when mosquito bites an infected individual carried more than one strain. However, in the current version, the parasite strains are only used to show the distribution of parasite strains in population across multiple transmission seasons. Different parasite strains have no effect on the antigenic presentation and drug action on resistance strains.

In brief, the EMOD model should play an importance role in malaria eradication policy by having the ability to estimate the impact of ecology, vector behavior and the risk of re-introduction of disease from migrations to a location where elimination has been achieved .

In a recent publication, Open Malaria, Griffin and EMOD model were used to evaluate the public health impact and cost-effectiveness of the phase-3 malaria vaccine candidate called RTS,S/AS01 [106]. Basically, there is are no major differences in the underlying mechanisms of these models. These three models underwent a harmonization and validation exercise which illustrated their ability to represent similar patterns for some key features of malaria epidemiology, e.g. EIR-prevalence, prevalence-incidence, and age-incidence relationships. However, in all models, the human population was fixed as a non-growing static population with 100,000 individuals. This mean that the immunity status of an individual is determined by his age and the transmission setting, but not by the history infection of that individual. This way of implementation could be used to evaluate the short-term effects of a vaccination intervention but may not be the optimal way for evaluating long-term effects, due to the fact that any intervention that reduces exposure in children would shift the burden of malaria into older age groups.

As shown in a Lancet publication in September 2015, all three models were run with a 5-day time step [97]. To simulate the dynamic of the malaria transmission, 5-day time step is an acceptable duration. However, to evaluate intervention that involves antimalarial acting and resistance, a smaller time-step, at least 1-day time step, is a must to maintain the realism of the simulation.

With a small population size, the outcomes have a wide range of variability. With larger population size, results are more predictable and closer to their expected values. So far, the number of individuals in the published individual-based model were set to be around 100,000 individuals to have a suitable running time for large scale analysis. Thus, there is a need for a malaria simulation that can comfortably run with a larger number of individuals, with better computational performance and equal or better epidemiological realism.

In summary, the key projects in this area have been the OpenMalaria project run out of the Swiss Tropical Institute [84], the development of individual-based models by a team of researchers at Imperial College [95], and the development of EMOD software (started in the year 2011). None of these large projects have begun focusing on drug resistance (however, between 2014 and 2016 this has begun to change), and for this reason during my PhD I set out to build an individual-based model similar to existing ones, but with a focus on drug resistance evolution and drug-resistance management strategies.

1.4 Rationale of the Thesis

It is clear that there are limitations of using mathematical models, for example, to predict the effects of antimalarial drugs on malaria transmission and host immunity due to the lack of knowledge on malaria immunology. As eradication plans are moving forward, a broad and sustainable policy is crucial to guarantee that reductions in malaria transmission are achieved and maintained. However, it is widely known that any long-term treatment policy with a high coverage would lead to rapid evolution of antimalarial resistance. Without the help of large-scale planning from mathematical models, we would be facing the risk of emerging and wide-spread antimalarial drug resistance, or more specifically, the loss of artemisinin efficacy that would endanger the health of hundreds of millions of people where artemisinin combination therapy is still the primary treatment for malaria. Thus, despite of its limitation and caveats, mathematical models are important auxiliary tools in helping contain the risk of drug resistance. In addition, mathematical modeling is the only way to evaluate population-level treatment strategies since we cannot run a clinical trial for twenty years in order to compare long-term outcomes on drug resistance evolution.

Moreover, to evaluate the effects of individual heterogeneity, an individual-based model is the appropriate approach, when compared to compartmental models, because individual-based models keep track all different individuals in the population while compartmental models only keep track of groups of individuals who have similar characteristics.

Because drug resistance mutations occur at the individual level, individual-based simulation is an appropriate method to capture the whole picture of resistance evolution and the spread of drug resistance in the population.

The compartmental model developed by Boni et.al. shows potential results for MFT which, according to that paper, is associated with a lower number of treatment failures compared to other strategies[52]. In this thesis, I aim to re-evaluate these results with an individual-based model.

1.5 Aims

The aims of this thesis are:

- to build and develop an individual-based modeling framework for *Plasmodium falciparum* malaria
- to compare the use of multiple first-line therapies (MFT) to the status quo strategies
- to determine if there is a benefit to using artemisinin combination therapies (ACT) in an MFT strategy, and if drug diversity in the partner drugs is sufficient to delay the onset of artemisinin resistance
- to experiment and combine other new treatment strategies (for instance, Multiple Courses of ACT for a single patient)

This thesis is focused on the following objectives:

- Firstly, an individual-based simulation is developed. This model should have not only high performance that can be run with millions individuals for 30 years, but also extensibility which would allow the model to adapt to changing requirements in later stage of development (Chapter 2 and Chapter 5).
- Secondly, this model has to be validated by acquiring parameter values directly from the real data or exhibiting key features of malaria epidemiology (Chapter 3).
- Thirdly, the model should be able to compare the benefit of using MFT to other strategies (fixed-time cycling and sequential adaptive cycling) (Chapter 4).

- And fourthly, the model should be upgraded to evaluate new treatment strategies where a dosing schedule can be lengthened or manipulated to allow the use of multiple ACTs in one course of treatment (Chapter 5 and Chapter 6).

The simulation is open-source and freely available at https://github.com/merlinvn/OUCRU-Malaria-Sim-v3.0.2

Chapter 2

Software Design for Malaria Simulation

2.1 Introduction

Software design and development play an important role in developing individual-based simulations for malaria or any other diseases. When simulations like these need to be run with millions of individuals that need to be updated regularly, the design of the system has to fulfill the following characteristics: robustness, extensibility, memory efficiency, and optimization for performance. This chapter will focus on the technical part of the model's design.

First of all, the C++ programming language was chosen instead of Java or C# due to its features that can improve the performance of the simulation significantly. The C++ language allowed me to build a native executable machine code program which is by default two to four times faster than Java or C# programs that run in a virtual machine [107]. Moreover, the individual-based model consists of millions of objects that need to be initiated and manipulated during running time, and C++ does not have extra computational overhead when creating objects and thus is more efficient in terms of its memory usage. C++ also allows the simulation to have its own manual resources and memory management; these features will be described in the following sections.

Section 2.2 provides an overview structure of the individual-based model. The whole model was broken down to multiple components in order to maintain the flexibility and robustness of the system.

Section 2.3 through 2.6 describe technical designs of some programming techniques and patterns that are crucial to develop a high performance simulation. Section 2.3 contains the description of a novel scheduler design where a combination of single time-step and discrete event scheduler was developed. Section 2.4 describes the design of parasite genotype that

allowed the drug resistant evolution occurs in the simulation. Section 2.5 and 2.6 describe programming techniques about data structures and memory management that help improving the performance of the simulation significantly.

2.2 System Design

Individual-based models for infectious diseases attempt to mimic a complex system, and all the requirements of the model and the details of this system may not be known at the beginning. For example, in malaria, individuals that are negative in a blood-smear test may in fact be harboring parasites, but we may not know how likely this is; this could be a result from in test sensitivity, detection threshold of the microscopy technique or host infectivity, but we do not know precisely from the beginning and changes are likely to be introduced during model development. Thus, in order to maintain the robustness and flexibility of the system, the whole model is broken down to multiple components as shown in Figure 2.1, so that each component can focus on its own function. By separating components, changing internal behaviors of one component will not have any significant impact on other components in the system. In addition, by employing inheritance and polymorphism concepts in object-oriented programming, components are designed in a flexible and reusable way to allow the system to adapt easily to changes when the model evolves in later stages of development.

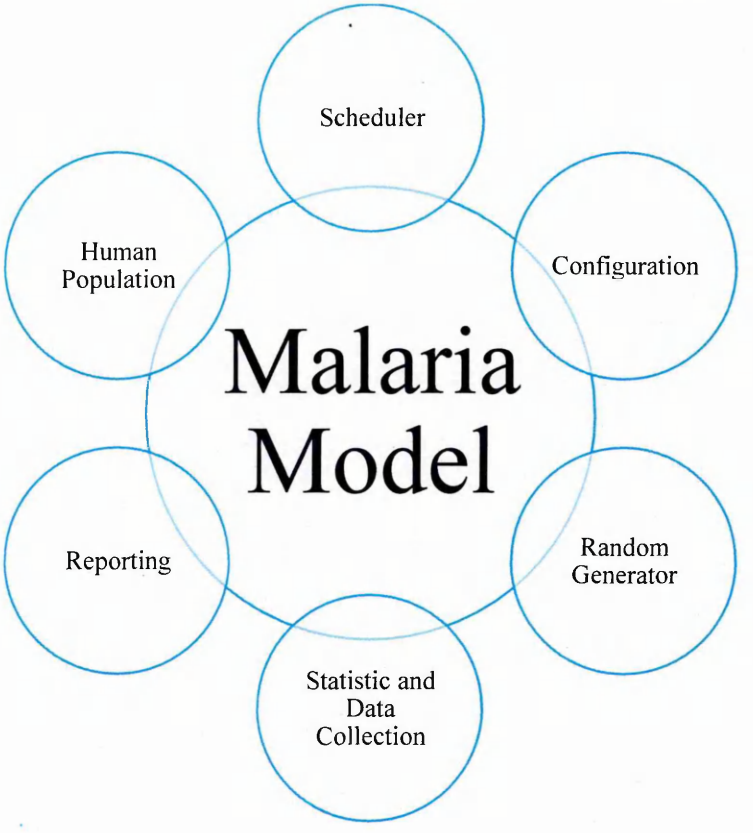

Figure 2.1. Individual-based simulation system design.

2.2.1 Malaria Model Component

To connect all the components together, a centralized class called "Malaria Model" is used. This class is the centralized component that contains and controls other components of the simulation. The main functionality of the malaria model class is to initialize other components at the beginning of the simulation and to act as a proxy or intermediary for other components of the system to communicate with each other easily.

All properties and methods of model class are shown in Figure 2.2. This central class has a lifetime that is the same as the lifetime of the simulation and the flow activity of this component is shown in Figure 2.3. A simulation is started by initiating a malaria model class, then setting options and parameters to the model object with the values that are read from the input file. The model object will call its "initialize" method that will set up other components with the initial values.

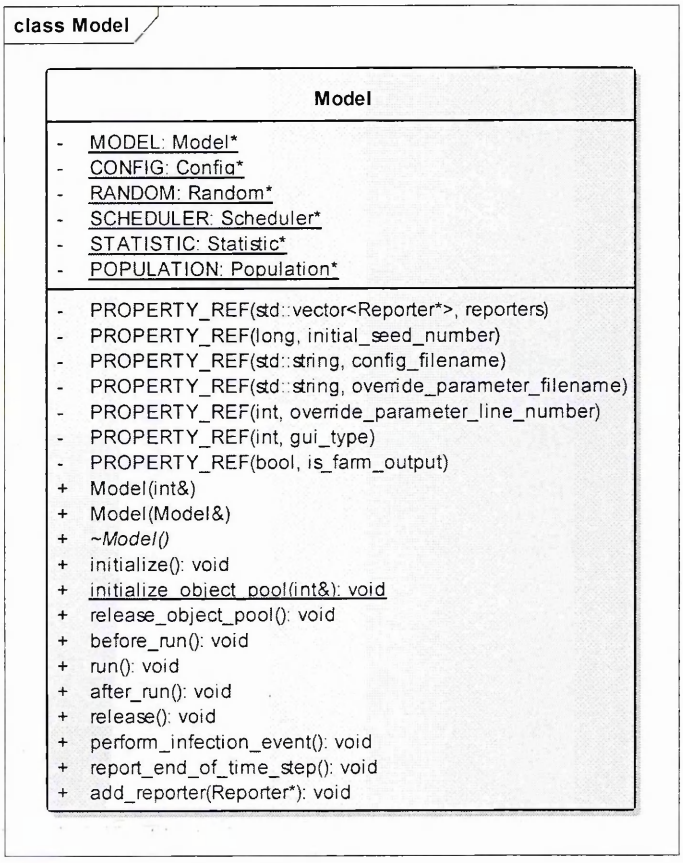

Figure 2.2. Model class diagram

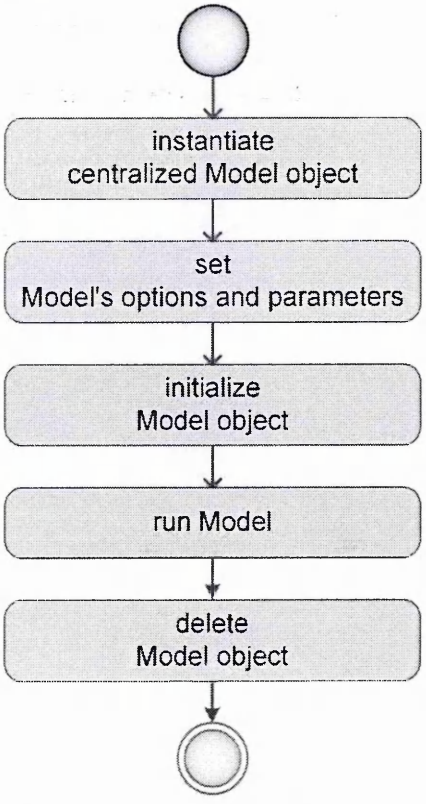

Figure 2.3. Flow activity of a simulation

2.2.2 Scheduler Component

In a naïvely constructed individual-based model, the model would have to loop through all individuals at each time step to determine if each particular individual needs to be updated during that time step, even if the only activities occurring at that time step are infections of only some specific individuals, e.g. find and infect ten new individuals. This process is both time consuming and inconvenient from a design perspective as the model becomes more complex and more different types of actions need to be performed. To solve this problem, the Discrete Event Simulation (DES) methodology has been applied to our individual-based model [108]. DES describes the system as a discrete sequence of events in time, where each event is associated with an object that will perform an action at a specific time point.

Hence, the Scheduler component is designed to keep track of the current simulation time and maintain a list of events which allows the events to be executed at a specific time point; in addition, this component schedules and cancels events in the future. The detail design of this component will be described in Section 2.3.

2.2.3 Random Generator Component

The Random Generator component is a utility class that provides a simpler way to draw random numbers by using functions in the Gnu Scientific Library (GSL) [109]. Here, the random generator algorithm gsl_rng_mt19937 or Mersenne-Twister-19937 is used in the simulation and the seed number is converted from the current time, or it can be manually set from the command line. The class design diagram of Random Generator component is shown in Figure 2.4.

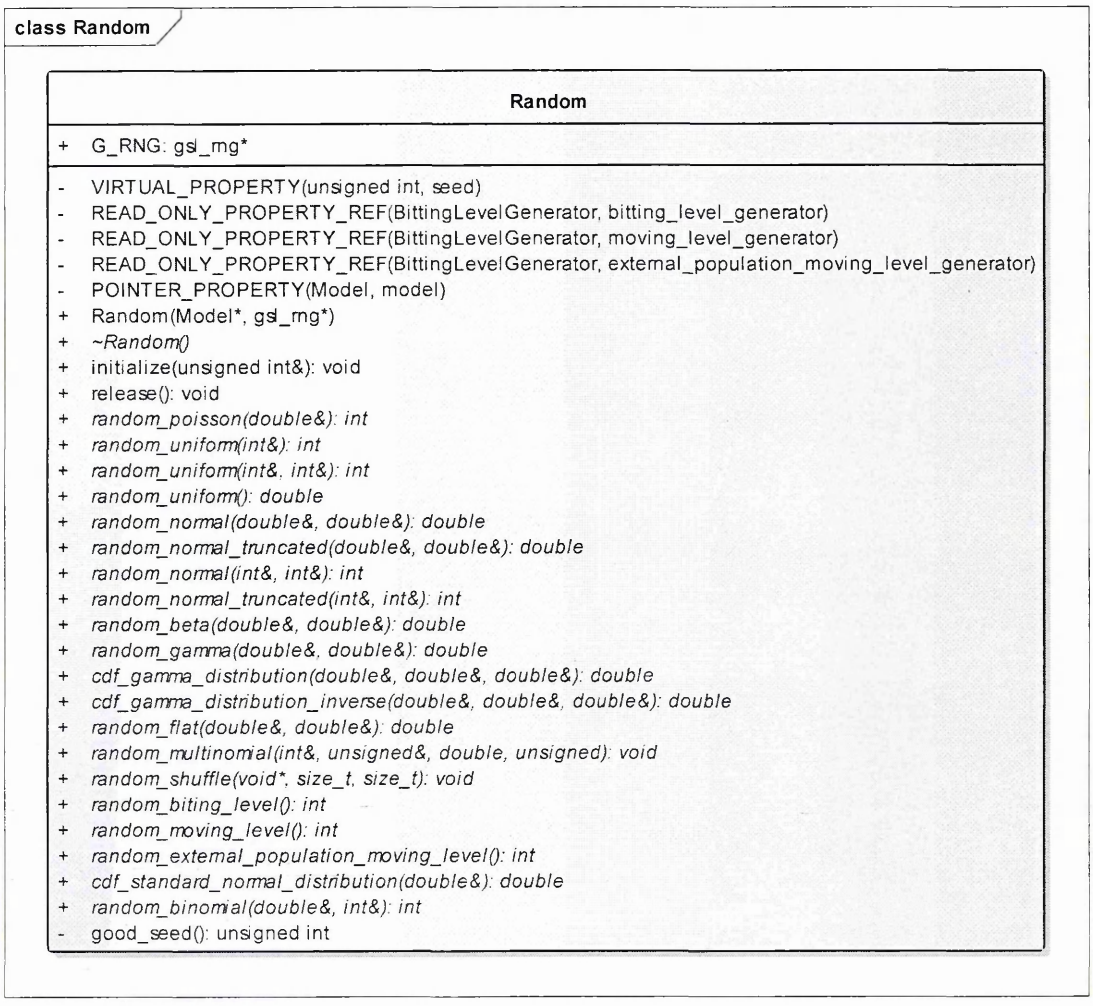

Figure 2.4 Random class diagram.

2.2.4 Configuration Component

The main function of the Configuration component is to store all parameters and initial conditions that will be used later by other components in the simulation. For the ease of use, all initial parameters and initial conditions are stored in a text file with YAML format [110], and read to memory when the Configuration component is initialized by the main Model component. Here, the YAML format is used instead of XML or ini format due to its human readability, standardization, and portability across multiple programming languages. The detail design of the Configuration class is described in Figure 2.6. Example of YAML-format input file is shown in the Figure 2.5.

```
# total days the simulation is run, including the burn-in period
# where the system goes to equilibrium
total_time: 11300

# length of burn-in period
start_treatment_day: 4000

# probability that a person receives treatment
p_treatment: 0.8000

#comments
number_of_locations: 1
number_of_age_classes: 15

# THE MAIN TRANSMISSION PARAMETER THAT DETERMINES R0 AND EIR
# if there is more than 1 location just separate by a comma
#beta: [2.5 , 0.1 , 0.2, 0.0015]
beta: [0.4 , 1.4 , 1.4, 1.4, 1]

seasonal_beta:
  a: [0, 0.25, 0.25, 0.25]
  phi: [200, 200, 200, 200]

# population size by location
# this is only population of susceptible individuals!
population_size_by_location: [1000000, 1000 , 1000, 1000, 500]

#probability for an infectious bite to make an infection
#maybe range from 0.1 to 0.3...
p_infection_from_an_infectious_bite: 0.1

# ageStructure
age_structure: [1, 2, 3, 4, 5, 6, 7, 8, 9,10,11, 15, 20, 60, 100]

#[0,1) [1,2) .....
ageStructureReport: [0, 1, 2, 3, 4, 5, 6, 7, 8, 9, 14, 19, 60, 100]
```

Figure 2.5. Example YAML-format input file.

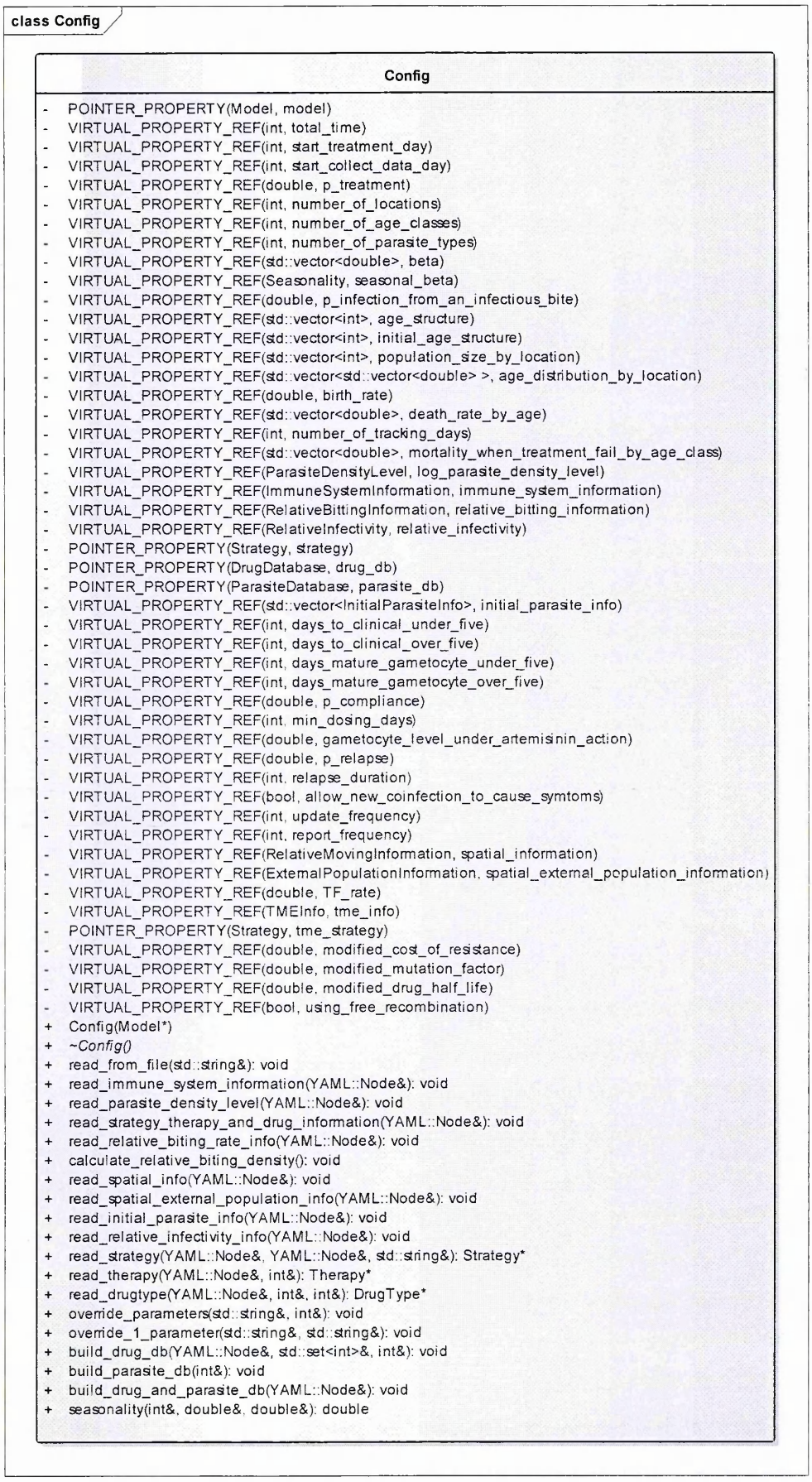

Figure 2.6. Configuration Component class diagram

2.2.5 Statistic and Data Collection Component

The main function of the Statistic and Data Collection (SDC) component is to keep track and analyze all the data that are generated during the simulation running time. For instance, when an individual was bitten by a mosquito in the simulation, the SDC records it by adding one in a variable called *total_number_of_bites* that is used later to calculate the EIR.

The analyzed data are mainly used by the Reporting component to generate the model output.

2.2.6 Reporting Component

Due to the requirements that the model needs to be able to generate multiple types of output, e.g. output to file, console, GUI or a group of processors on a farm, the Reporting component was designed in a way that allows the flexibility to add new reporting types as well as allows multiple type of Reporters to work at the same time without interfering with each other. The design of Reporter class and subclasses are shown in Figure 2.7.

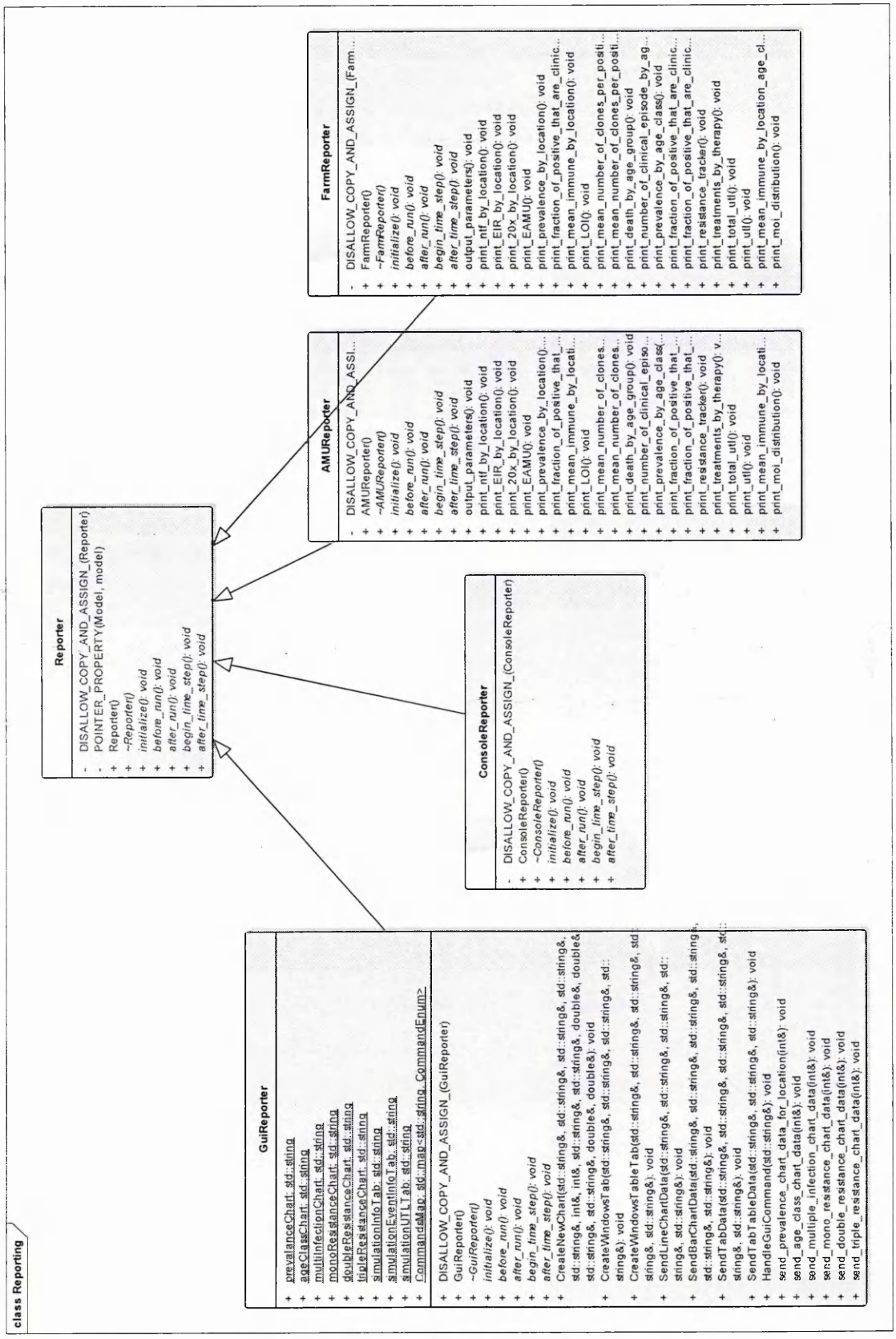

Figure 2.7. Reporter class diagram.

2.2.7 Human Population Component

The Human Population Component (HPC) organizes and keeps track of all individuals in the simulation. By employing the Object Index technique (described in Section 2.5), the HPC can classify individuals into different groups based on the characteristic of the individual, e.g. grouping by location, host-state, or age-class. Moreover, by having multiple nested groups, the HPC can query individuals with specific information. For example, the HPC can directly access a list of symptomatic individuals who live in location 0, and are aged between 15 and 20, without having to scan all individuals in the population and pick out the ones that satisfy these criteria.

Individual information

An individual in the simulation is represented by a Person class and has heterogeneous characteristics. Each individual will have a different age, age-class, birthday, attractiveness to mosquitoes, and other features; this will allow us to evaluate the effect of different age-patterns or biting patterns on the outcome of the model. The detail design of Person class is shown in Figure 2.8.

Each individual has a variable that describes his or her current infection status with malaria. The following states are used in the simulation: Susceptible, Exposed (having liver-stage parasites), Symptomatic, and Asymptomatic.

Individuals in the simulation have their own immune system. The details of the immune system will be described in Section 3.9.

Each individual has a list of asexual parasite populations. The purpose of this list is to allow a person to have multiple malaria infections (i.e. coinfection). Each infection or "clone" or "parasite population" is a genetically identical clonal population, and each person can be infected with multiple clonal populations that differ from each other by genotype and parasite density. Thus, each asexual parasite population will keep track of all the information about parasite density and genotype. The resistant genotype representation will be described in

Section 2.4. This way of implementation also allows multiplicity of infections to occur in the simulation.

Each individual has a set of drug concentrations to represent multiple different drug levels that are circulating within host. Theses drug concentration levels will be used in the PK/PD model (described in Section 3.8)

Figure 2.8. Person class diagram.

2.3 The Combination of Time-Step and Discrete-Event Simulation (details of scheduler and event)

The simulation is required to allow some daily activities that can apply to the whole population, i.e. potential infection activity, birth and death activity, importation, migration. In addition, the system also has activities that act independently on each individual, i.e. introducing parasites to the blood from the liver, progressing to a symptomatic clinical state, or the maturation of gametocytes. To fulfill these requirements, a modified discrete-event simulation (DES) is developed by combining designs of time-step model, that performs executions at each time step, and discrete-event simulation to allow the simulation to have a quick and convenient way to schedule and update both daily and time-specific activities.

The heart of a discrete-event system is the scheduler that is used to schedule and perform an event at a specific time point. In other discrete-event systems, the scheduler is implemented by using single-dimension vector (or a priority queue) because those systems do not have a fixed time step. However, in malaria simulation, all of the individual-related events are independent and the simulation has a fixed daily time step. Hence, to improve the performance, a modified event lists in the scheduler is used to achieve the feature that allows both daily behaviors and time-specific activities to be scheduled and executed in advance. Here, a two-dimensional vector is used to arrange generic event pointers at multiple time-points, as shown in Figure 2.10. The length of the first dimension of this vector is equal to the total number of days that the simulation will be run and the index of the first dimension represents a single day in the simulation. The second dimension of the vector is used to store all the events that will occur on the same day. Figure 2.9 shows all different events that will occur in the simulation.

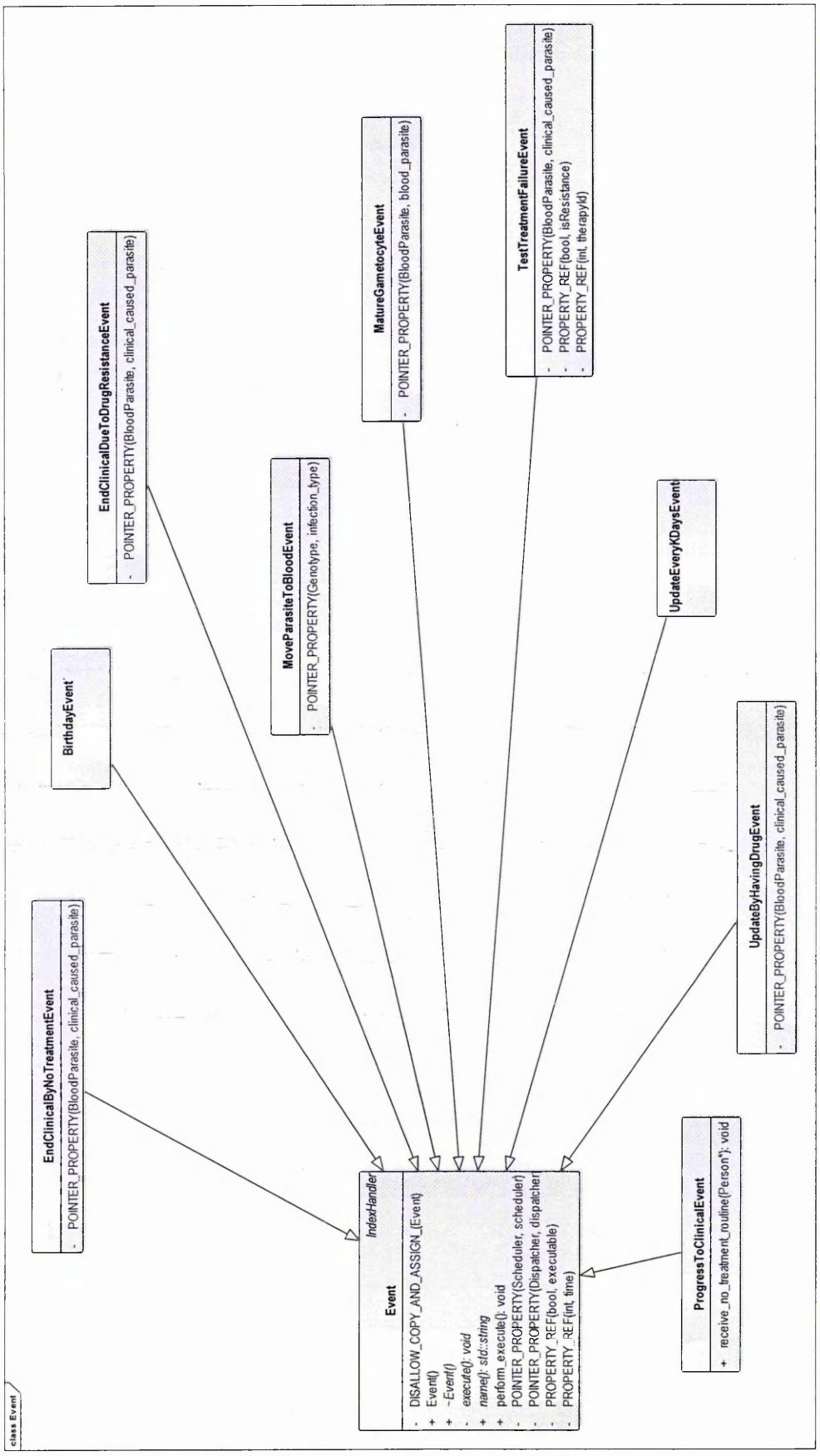

Figure 2.9. Event class hierarchy.

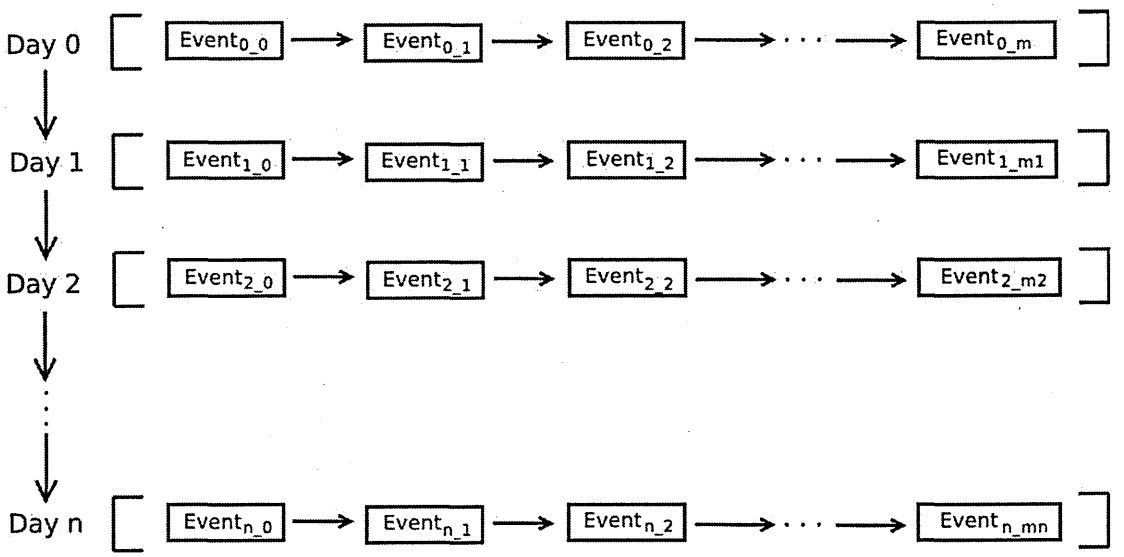

Figure 2.10. Overall view of the Scheduler. Scheduler was implemented by a two-dimensional vector of Event pointer. The vertical dimension represents for days (time step) in the simulations while the horizontal dimension represents all the events that will occur in a particular day.

2.4 Parasite and Drug Resistant Genotype design

Each clonal parasite population within individual, described in Section 2.2.7, is associated with a specific genotype. A proper design for genotype representation will not only allow the occurrence of the mutations but also improve the performance of the simulation.

To model drug-resistant genotypes, a bit-string data structure from the C++ Boost library has been used[111]. Each position in the bit-string represents a particular drug that is used in the simulation, and the values represent the resistance mutation to that drug that have occurred or not (0 means non-mutant and 1 means mutated).

Example of resistant genotypes when using three different drugs:

- Naïve strain genotype: [0,0,0]
- Single resistant genotypes: [0,0,1], [0,1,0], [1,0,0]
- Double resistant genotypes: [0,1,1], [1,0,1], [1,1,0]
- Triple resistant genotypes: [1,1,1]

If the parasite becomes resistant to a particular drug, the drug will have no efficacy on the treated patients that carry the resistant parasite. The genotype representation will be modified to allow partial resistance in Section 5.2.

2.5 Object Index for Faster Calculation and Reducing Memory Usage

In the traditional way of counting how many individuals have symptoms at a specific time point, the simulation has to loop through all individuals in the population and increase the counter for each individual that is in a symptomatic state. This process would be time consuming when it needs to be done at each time step during the infection event for the whole population. However, at every time point, the simulation only needs to update the state of individual carrying parasites. Hence, a convenient way to group individuals into separated groups could improve the performance of the simulation significantly.

In the model, I use a technique called "object indexing" that utilizes multi-dimensional array of pointers in order to group individuals having similar properties; such as states, age classes, or biting level. For each object index in the simulation, an individual will have a separate member variable that is associated with that index. This variable stores the position of the individual pointer in the deepest nested vector of the index. This variable is used when the simulation wants to randomly access an individual through the object index and it also helps improve the performance in adding and removing pointer in the index.

To add a new object pointer to the object index, the program just adds the object pointer at the end of the object index. To remove an object pointer at a specific position in the object index, the object index swaps that object pointer with the last pointer in the index, then removes the last pointer. With the "swap and remove last" technique, the performance improves significantly in comparison with the method that removes and shifts left all objects from the removed position to the last position: *O(1)* vs. *O(n)* in term of computational complexity. C++ code to add and remove object pointer in the object index is shown in Figure 2.12.

Here, a technique called the "Observer" design pattern [112] is used to allow the object index classes to automatically update the multidimensional array pointer whenever a change occurs to the individual. For example, in a model that has multiple different object indexes, when an individual changes his state from susceptible to exposed, the individual object makes a signal

to inform all object indexes in the model; the object index that is responsible for grouping by host state will capture that change and update the underneath pointer array. There are currently three different objects indexes in the simulation: *AllObjects*, *IndexedByBitingLevel*, and *IndexedByStageAgeClass*, shown in Figure 2.11. The *AllObjects* index object manages all individuals in the model. The *IndexedByBitingLevel* index object, which uses a one-dimensional array pointer, groups individuals by each individual's biting level (i.e. how likely a mosquito is to bite that particular individual because of his or her innate attractiveness to mosquitoes), and it is used at every time step to distribute new malaria cases. The *IndexedByStageAgeClass* index object used two-dimensional array to group individuals into stage and age class. An example usage of this index object is to count how many symptomatic individuals there are in age class 5, or to select randomly three individuals that are susceptible in age class 2.

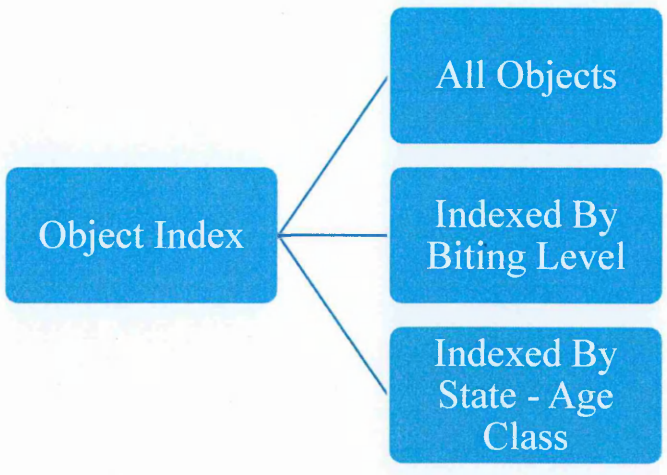

Figure 2.11. Person Index Hierarchy

```
void PersonIndexByLocationBittingLevel::add(Person* p, const int& location, const int& bitting_level) {
    vPerson_[location][bitting_level].push_back(p);
    p->PersonIndexByLocationBittingLevelHandler::set_index(vPerson_[location][bitting_level].size() - 1);
}

void PersonIndexByLocationBittingLevel::remove_without_set_index(Person* p) {
    vPerson_[p->location()][p->bitting_level()].back()->
PersonIndexByLocationBittingLevelHandler::set_index(p->PersonIndexByLocationBittingLevelHandler::index());
    vPerson_[p->location()][p->bitting_level()][p->PersonIndexByLocationBittingLevelHandler::index()] =
vPerson_[p->location()][p->bitting_level()].back();
    vPerson_[p->location()][p->bitting_level()].pop_back();
}
```

Figure 2.12. Example C++ code for adding and removing a person pointer of the PersonIndexedByBittingLevel object.

2.6 Memory Management with Object Pool

Throughout the lifetime of the simulation, a large number of short-lived objects are created and deleted; e.g. parasite population objects, event objects, person objects. When creating an object, the program has to allocate a free memory location for this new object; when the program deletes this object, the memory will be deallocated. The processes of allocating and deallocating memory are time consuming, especially when millions of objects are spawned and released. To improve the performance, a technique called "Object Pools" is used. The pools create objects at the beginning of the simulation. Whenever the program needs to allocate an object, it asks the corresponding pool for one. When the program is done with the object, it returns the object to the pool. The object pools automatically increase their size when the number of using objects excesses the number of pre-created objects in the pools.

A dedicated Object Pool object, shown in Figure 2.13, is assigned to each class that needs to apply the object pools technique, e.g. the parasite object pool object is only used to manage parasite objects. All the created objects are stored in the *AllObjects*, a vector of pointer arrays, and all of the ready-to-use objects are stored in *freeList*, a vector of pointers. Each time the simulation requests an object, the pool gives the last object pointer in the *freeList* vector, and pushes back the object when the simulation returns it to the pool. Basically, the pool does not explicitly keep track of objects that are in use and the program has to return objects correctly to the pool when the simulation finishes with them. In a simple program which constantly

creates and deletes 10,000 individuals 10,000 times, the object-pool version achieves five to six times faster computation than a version with *ad hoc* memory allocation and freeing.

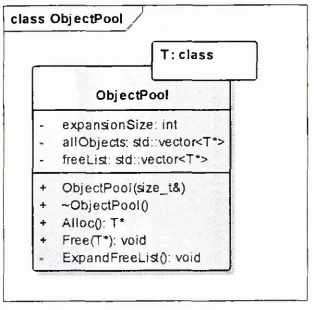

Figure 2.13. Object Pool class diagram

Chapter 3

Model Construction and Model Validation

This chapter is an expanded version of the supplementary appendix to a manuscript titled "Optimal population-level deployment of artemisinin combination therapies." This manuscript was published on *Lancet Global Health* in November 2015. In order, the authors on this manuscript are myself, Piero Olliaro, Arjen Dondorp, J Kevin Baird, Ha Minh Lam, Jeremy Farrar, Guy E Thwaites, Nicholas J White, and Maciej F Boni.

The first section of the chapter contains a description of the biology and epidemiology implementation of the individual-based model ("microsimulation"); this description includes details on the mechanisms and assumptions in the model that are related to transmission, clinical progression, immunology, pharmacokinetics and pharmacodynamics, evolution, and demography.

Sections 3.2 through 3.8 contain descriptions of model parameters where model inputs can be directly obtained from field or clinical data.

Sections 3.9 through 3.15 describe model validations for behaviors that cannot be input directly into the model. For example, clinical episodes decrease with age more quickly in high-transmission settings than in low-transmission settings, but the model cannot be forced to exhibit this behavior; this behavior is a consequence of the interaction between population-level immunity and entomological inoculation rate (EIR). In the sections below we validate that these qualitative features of malaria epidemiology are observed in our model.

Due to the complexity and high computational requirement of the individual-based simulation, I do not do rigorous model fitting, but instead I used model calibration, through visual comparison of data and model outputs, to find suitable ranges for unknown parameters. The model is then validated against collected data by showing that the model, with these 'calibrated' parameters, can illustrate key epidemiological features of malaria.

3.1 Model Description

The model is an individual-based stochastic microsimulation developed in C++ using a daily time-step and asynchronous updating. Individuals in the model carry certain basic attributes such as age, attractiveness to mosquitoes, presence/absence of malaria symptoms, level of parasitaemia (possibly none), the number of independent clonal parasite populations circulating in their blood, the presence/absence of parasites in the liver (before a blood-stage infection), level of acquired immunity to malaria, and drug levels in the blood. These are described in more detail below. The population size in the model is set to one million, as larger population sizes showed no difference in qualitative dynamics. Typical simulations for our present analysis were run to equilibrium with no treatment, which was done so that all simulations would settle to the same endemic equilibrium before the application of any treatment strategy, allowing for a fair comparison of the different strategies. After treatment was initiated – for a fraction f of symptomatic malaria cases (known as the "treatment coverage") – the simulations were run for another twenty years. The treatment coverage parameter f was varied between 0.5 and 0.9 in the simulations. Asymptomatic cases were not treated in our simulations. The microsimulation is meant to model the dynamics of *Plasmodium falciparum.*

Blood-stage Parasitaemia. Each host i is associated with an asexual parasite density D_i, which is the sum of the densities of the individual clonal parasite populations in that host. If there are c_i clonal parasite populations inside host i, then we let $j = 1,\ldots, c_i$ index these clonal populations. We let R_j be the resistance profile of clonal population j, where R_j is the set of drugs to which the corresponding parasite population carries resistance (using the index-set notation of Andreasen et al [113]). As an example, $R_3 = \emptyset$ indicates that the third clonal population in this host does not carry any drug resistance genes, and $R_4 = \{1, 2\}$ indicates that the fourth clonal population in this host carries resistance to drugs 1 and 2. The parasite density inside host i is then described by the equation 1.

$$P_i = \sum_{j=1}^{c_i} w_{R_j} \delta_{j,i} \gamma_{j,i} \qquad (1)$$

where w_{R_j} is the relative fitness of a resistant parasite with resistance profile R_j; the fitness of a sensitive parasite is defined as $w_\emptyset$=1. The quantity $\delta_{j,i}$ is the parasite density of clone j in host i, and $\gamma_{j,i}$ is the relative gametocyte production of clone j, with one corresponding to normal production and zero to no production. Typically, $\gamma_{j,i}$ is set to zero for the first four (children) or six (adults) days of an infection, and then fixed at one after gametocytes begin to be produced; this is slightly earlier than true gametocyte production, the reason being that we do not model the tail-end of a cured infection when asexual parasitaemia is zero but gametocytaemia stays positive for one week or more [114]. Essentially, the model shifts the gametocytaemic period to be several days earlier so that infected hosts have the same number of transmissible days as they would for real infections. This adjustment does not affect our simulations as we do not model gametocytocidal drugs such as primaquine. The force of infection of resistant type R at time t, denoted as $\Lambda_{t,R}$, is calculated from equation 2.

$$\Lambda_{t,R} = \beta \sum_{\text{all hosts } i} g(P_i) \cdot b_i \cdot \left(\frac{w_R \sum_{j:R_j=R} \delta_{j,i} \gamma_{j,i}}{P_i} \right) \qquad (2)$$

where b_i is the biting attractiveness of host i (drawn from a gamma distribution with coefficient of variation equal to 2.0 [115]), the function g describes the saturation of transmission probability with increasing parasite density [91] (see Section 3.2), and β is a scaling factor that we vary to obtain a particular entomological inoculation rate (EIR) in a given simulation. The parameter β does not represent any particular epidemiological quantity such as biting or mosquito population size; it is a non-dimensional quantity that allows us to scale the force of infection to get a particular prevalence or EIR. Recombination can occur when a mosquito bites a host with multiple clonal infections. We assume that interrupted feeding on multiple hosts does not occur; the frequency of interrupted feeding by non-infected mosquitoes has been estimated to be as high as 10% [80,116,117] but our previous modeling analysis [52] indicated a weak relationship between outcrossing rate the evaluation criteria we measure here. It is assumed that drug resistance genes are located on different chromosomes. The parasite densities in the above

equation already take into account a single generation of segregation and recombination that occurs inside the mosquito.

Parasitaemia levels are set to 20,000 parasites per microliter at the beginning of a symptomatic episode of malaria (this is relaxed in Chapter 5). Asymptomatic cases have their parasitaemia levels initialized at 1000 parasites per microliter, after which the parasite population size is slowly reduced by the immune system; the minimum and maximum durations of asymptomatic parasitaemia observed in the model are 60 days and 281 days [85,118,119], and this varies with the host's immune status. The progression of an asymptomatic case to a clinical case is determined by the host's immune status, the details of and justifications for this process are described in section 3.9. For a multi-clonal infection presenting with clinical malaria, symptoms are caused by one clonal parasite population (typically, the most recent bite) reaching a density of 20,000 parasites per microliter, while the other parasite population sizes stay at levels of <1000 parasites per microliter.

Transmission model. Genotype-specific forces of infection are stored in the simulation for 11 days, and new infections are generated by drawing a Poisson number of hosts based on each genotype's force of infection 11 days ago (this 11-day lag mimics the course of parasite development in the mosquito [120–122]). Once this number has been drawn, the specific hosts to be infected are chosen with replacement relative to their biting weights b_i, and seven days later, after growth and development of liver-stage parasites, these hosts will have a newly emerged blood-stage parasite population (50,000 total parasites).

Immunity Model. We implement an immunity model in each host that describes the general level of acquired immunity that a host has to *P. falciparum* malaria; specific immunity is not modeled. This model's immunity variable M ranges from zero to one, and it is meant to be interpreted on a relative scale. Its two biological effects are that a higher level of immunity increases parasite clearance rate and decreases the chances that a new infectious bite leads to a

clinical episode of malaria, similar to Filipe et al [94]. The immunity-dependent parasite clearance rate is defined by the equation 3.

$$P_{t+K} = w_R[c_{min} \cdot (1 - M_t) + c_{max} \cdot M_t]^K \cdot P_t \quad (3)$$

where P_t is the parasite density at time t, w_R is the fitness of the given strain (1 for the drug-sensitive strain, $1 - c_R$ for a single-drug resistant strain; see drug-resistance description below), and $(1-c_{max})$ and $(1 - c_{min})$ are the daily immunity parasite reducing rate for fully-immune and non-immune individual respectively. The values of c_{min} and c_{max} are calculated as the equation 4 and 5.

$$c_{max} = 10^{-\frac{\log_{10}(parasite\ density\ assymptomatic) - \log_{10}(parasite\ density\ cured)}{duration\ of\ infection\ for\ fully\ immune\ individuals}} = 0.9572 \quad (4)$$

$$c_{min} = 10^{-\frac{\log_{10}(parasite\ density\ assymptomatic) - \log_{10}(parasite\ density\ cured)}{duration\ of\ infection\ for\ immunologically\ naïve\ individuals}} = 0.8036 \quad (5)$$

The parasite density is typically updated asynchronously every seven days (K=7) in the simulation; validations were done to ensure this is not very different from daily updating. If an individual has another event occurring (e.g. new infection, clearance of a different parasite clone) then the parasite density is updated earlier than the scheduled 7-day interval. The parameters in this equation are calibrated so that infections are a maximum of 281 days and minimum of 60 days. Details of this calibration are presented in Section 3.3. The effect of immunity of symptoms development is described in Sections 3.9 and 3.10.

Clinical/Symptomatic Malaria. When an individual in the model acquires a new malaria infection, that host will progress to clinical or symptomatic malaria with probability P_{clin}. This probability is immunity dependent and will be described in detail in Sections 3.9.

Pharmacokinetics and pharmacodynamics (PK/PD). Drug action was modeled with a standard concentration-effect curve, and drug clearance was modeled with a standard exponential decay (Section 3.8). Daily killing rates, or parasite reduction ratios, were obtained from past PK/PD studies [123–132]. Variable drug absorption was included so that different individuals had different starting concentrations of drug (this allowed treatment to fail

sometimes); the coefficient of variation of the starting drug concentration was varied between 0.1 to 0.4. This coefficient of variation and the slope of the concentration-effect curve were varied for each specific therapy, to obtain a desired efficacy at 28 days. As an example, the maximum daily killing rates for artemether, artesunate, and dihydroartemisinin were set to 99.9% per day. For artemisinin combination therapies, the standard deviation for the initial concentration of both drug components was set to 0.4, resulting in an efficacy of 95%, and these parameters were used for ACTs in the simulations presented here.

Drug resistance evolution. Evolution in clonal parasite populations is modeled by allowing a parasite population to mutate from sensitive to resistant to drug x, only in the presence of drug x; as in previous modeling studies, this model behavior really represents the fixation of a new mutant, but we keep the terminology of a "mutation rate" to be consistent with past modeling literature. In the simulation, mutation occurs on a daily basis with a certain daily probability. For the majority of drugs, these probabilities are unknown. Hence, the probabilities in the model are set so that resistance evolves, under high drug coverage, during the 20-year time span that the model is run. These mutation parameters were set to be the same for all resistant genotypes, including those encoding resistance to the partner drugs, as the relative magnitudes of these mutation rates are unknown. In the model version presented in Chapter 3 and Chapter 4, drug-resistant genotypes are completely resistant to the action of the drugs they are resistant to.

Mutation rates from drug-sensitive to drug-resistant genotypes are a function of the drug concentration. When the drug concentration is zero, the mutation rate is set to zero. When the drug concentration is a full dose, the mutation probability is μ. We introduce a parameter k to determine whether the probability of drug resistance emerging and fixing is higher or lower at intermediate drug concentrations. Under a simple linear model, the mutation probability falls linearly with drug concentration (k=0.5) so that the mutation rate is $\mu/2$ at half concentration. We also test a model where the mutation probability is twice as high at half-concentration than

at full concentration (k=2), and another where the mutation probability is four times as high at half-concentration (k=4).

Each resistant genotype is assigned a fitness cost c_R (that varies between 0.1% and 1.0%), and for multiple-resistant genotypes fitnesses are multiplicative. The fitness component in the force of infection (showed in equation 2) is defined as equation 6.

$$w_R = 1 - c_R \tag{6}$$

3.2 Gametocytaemia and Infectivity

Ross and colleagues developed a statistical model that described the relationship between host infectivity to mosquitoes and asexual parasite density and fit that model with data from 392 neurosyphilis patients treated with malaria therapy [91]. In their model, the relationship between gametocyte density and asexual parasite density was described as equation 7.

$$\ln(y_g) \sim Normal(\ln(\rho \mathrm{P}), \sigma_g) \tag{7}$$

where y_g is the density of functional female gametocytes in an individual, P is the asexual parasite density, ρ is the parameter that tells us the proportion of asexual parasites that have developed into gametocytes, and σ_g is the standard deviation. Then the probability that at least one functional gametocyte is taken up is defined as equation 8.

$$\Pr(y_g > y_g^*) = \Phi\left[\frac{\ln(\rho \mathrm{P}) - \ln(y_g^*)}{\sigma_g}\right] = \Phi\left[\frac{\ln(\mathrm{P})}{\sigma_g} + \rho^*\right] \tag{8}$$

where y_g^* is the gametocyte density (per microliter) required for a mosquito to take up at least one functional gametocyte during one blood meal; Φ is cumulative distribution function (CDF) of the standard normal distribution and $\rho^* = \frac{\ln(\rho) - \ln(y_g^*)}{\sigma_g}$. If the volume of the blood meal is assumed to be 3μl [133] then $y_g^* = \frac{\rho}{3}$. And, if the sex ratio between male and female gametocytes is 1:1 then the probability that a mosquito is infected by taking up both male and female gametocytes is $\Pr(y_g > y_g^*)^2$. According to the results from Ross et al.'s study [91], $\rho =$

0.00031 ($95\%\ CI$: $0.00027 - 0.0036$) and $\sigma_g = 3.91$ ($95\%\ CI$: $3.72 - 4.10$) were the statistically fitted values to the neurosyphilis dataset.

In our simulation, we use this Ross et al (2006) function $\Pr(y_g > y_g^*)^2 = \left(\Phi\left[\frac{\ln(P)}{3.91} - 1.7852\right]\right)^2$ as $g(P)$ function that used in equation 2 to describe the per-bite infectivity of an individual with an asexual parasite density Y. An individual with a parasite density of 10/µl will have approximately a 1% chance of infecting a mosquito. An individual with a parasite density of 1000/µl will have approximately a 25% chance of infecting a mosquito.

3.3 Duration of Infection

The duration of infection is the amount of time that it takes for an untreated individual to clear all blood-stage parasites. This duration is dependent on how high or low an individual's immunity is. Finding a plausible range for the duration of infection is crucial to a malaria model.

Using the malaria therapy data, Maire et al [85] computed the duration of an untreated infection. Of patients whose infection duration was longer than two months, the log-mean of the untreated infection durations for 47 patients was 5.13 (σ=0.80), which corresponds to a mean of 169 days ($\pm$ 1σ range: 76 – 376). Eyles and Young [118] described the course of malaria infection in 22 neurosyphilitic patients with malaria therapy and presented an average duration of infection of 222 ± 117 days for patients where the entire course of continuous and intermittent parasitaemia was followed until they were defined as cured or cleared (6 months of zero parasitaemia). For a larger group of 38 patients, the initial course of continuous parasitaemia was calculated as 121 ± 58 days. These patients were normally untreated and occasionally received quinine treatment during clinical episodes.

In the World Health Organization's Garki Project Report [119], the daily clearance rate ranged from 0.002 to 0.018 (approximately, according to the Figure 31 of the report), corresponding to an infection duration between 55 and 500 days (in the absence of interventions). This graph

also shows an increasing clearance rate with age which is likely due to the development of immunity in older individuals.

In our simulation, we define the duration of infection as the number of days that an untreated or inadequately treated individual clears all blood-stage parasites (by action of the immune system only). By comparing and combining all 3 references above [85,118,119], we select 60 days and 300 days as the suitable lower and upper limits for infection duration, for fully immune and immunologically naïve individuals, respectively (see Section 3.9 for the immunity model in the simulation). Because immunologically naïve individuals acquire some level of immune protection during the course of a malaria infection, a 300-day parasitaemia is never observed. The maximum observed parasitaemia in the simulation is 281 days for a naïve 1-year-old child and 197 days for a naïve 20-year-old individual.

3.4 Probability that an Infectious Bite Causes an Infection

From February 1986 to October 1987, Beire et al conducted an epidemiological and entomological investigation of malaria incidence in 809 children in Saradidi (western Kenya) to investigate the relationship between *P. falciparum* incidence and EIR [134]. Using clinical incidence reports and EIR measurements from household vector studies, the authors found that 7.5% (1 in 13) of sporozoite inoculations produced new infections in children in Saradidi. The measured EIR during this period was 0.75 infective bites per person per night or 273 bites per person per year.

A parallel study in Saradidi [135] indicated that adults were less susceptible to malaria compared to children given the same level of exposure. In the same village during a high-transmission period, 57 of 62 children (92%) experienced parasitaemia within 56 days and all children developed parasitaemia by day 84, while only 16% (day 56) and 58% (day 84) of adults developed parasitaemia. All participants received radical cure at the beginning of the study. Thus, the probability of developing parasitaemia after receiving an infectious bite likely

depends on an individual's level of immunity (possibly sporozoite-blocking immunity, but this is not known).

In our simulation, we use a single parameter to define the probability that an infectious bite causes a new infection, as there are still not enough data to accurately measure the age dependence of this parameter. We keep this probability constant at 10% across all age groups.

From experiments, changing this probability mainly affects the association between EIR and prevalence and the MOI distribution. With high probabilities, the model failed to replicate the log-linear relationship between EIR and prevalence as well as the MOI pattern describe in the Section 3.12 and 3.14. In later analysis in Section 4.4.10, this probability is modified to be age-dependent and this modification does not have any impacts on the main results.

3.5 Age-specific All-cause and Malaria Mortality

Considering DSS data from seven sites in sub-Saharan Africa from 2001-2005 [136], malaria mortality ranged from 2.5 to 8.2 deaths per 1000 children per year. Age-specific mortality rates are shown in Figure 1 of this paper. Extracting these numbers from the graphs and averaging across sites, we obtain the table 3.1.

Combining this with a longitudinal data set on 60,000 individuals in Burkina Faso from 1999 to 2003 [137], we summarize age-specific all-cause mortality and age-specific malaria mortality in the table 3.2.

With these two datasets, we construct an age-specific mortality pattern (table 3.3) (malaria attributable and non-malaria attributable) that we would expect to observe in a high-transmission region.

Age	All-cause Mortality	Malaria Mortality
0.1	170.2	27.4
0.3	58.7	23.8
0.6	60.6	28.3
0.9	62.4	31.5
1.1	52.3	23.4
1.4	43.7	19.6
1.6	37.8	16.2
1.9	31.4	13.4
2.6	21.3	19.2
3.5	10.1	9.6
4.4	5.0	4.2
5.4	4.9	2.7
6.5	3.8	1.9
7.5	3.0	1.2
8.5	2.7	1.8
9.4	2.9	1.7
10.4	2.2	1.0
11.5	2.1	1.5
12.5	2.2	1.6
13.4	2.3	0.9
14.4	1.8	0.8

Table 3.1. Averaged age-specific mortality (per 1000 person-years) from seven sites in Burkina Faso, Ghana, Kenya, Tanzania, and Mozambique

	<1 year	1-4 years	5-14 years	15-59 years	> 60 years	Reference
All-cause mortality	60.5	23.6	2.8	5.9	54.7	Becher et al
Malaria mortality	23.4	10.4	0.7	0.4	10.2	Becher et al
All-cause mortality	80.84	28.79	2.98	No data	No data	Abdullah et al
Malaria mortality	26.86	15.09	1.77	No data	No data	Abdullah et al

Table 3.2. Annual mortality (per 1000) by age group, data extracted from Becher et al [137] and Abdullah et al [136].

Age-Group	0-1	1-2	2-3	3-4	4-5	5-6	6-7	7-8	8-9	9-10	10-15	15-20	20-60	>60
All-cause Mortality	80.84	37.29	20.94	12.14	6.65	4.54	3.88	3.16	2.88	2.60	2.25	5.9	5.9	54.7
Malaria Mortality	26.86	18.36	14.07	11.02	5.51	2.93	1.92	1.63	1.59	1.53	1.27	0.4	0.4	10.20
Non-Malaria Mortality	53.98	18.94	6.87	1.12	1.14	1.61	1.95	1.53	1.30	1.07	0.98	5.5	5.5	44.5

Table 3.3. Expected age-specific mortality per 1000 persons per year in a high-transmission region.

The mortality not attributable to malaria is input directly into the demographic part of the simulation; however, malaria mortality depends on transmission and must be input as a per-case probability of death. In the simulation, we count failed treatments and non-treatments, but we do not distinguish between severe malaria and uncomplicated malaria in these cases. Using summary information from the WHO [138], we assume that the percentage of symptomatic malaria cases that progresses to severity is 5% for the 0-5 age group and 1% for individuals over five years of age.

In a meta-analysis of malaria clinical trials conducted through 2002, Myint et al summarized the mortality rates for uncomplicated and severe malaria, for which the probabilities of death were 0.03% and 13.9%, respectively [139]. These numbers are for treated patients. The assumptions in Goodman et al [138] have the under-five case fatality for severe malaria at 19.2% if treated and 50% if untreated; the over-five case fatalities used are 10% for treated patients and 25% for untreated patients. Depending on how many of the treated patients were receiving failing treatments and how many would progress to severe malaria under these circumstances, the malaria mortality for a "treated patient population" should be, approximately, between 0.1% and 1.0% of all malaria cases. For untreated patients, the total malaria mortality rate could be as high as 2.5% in under-fives and 0.5% in over-fives.

In our simulation we set the mortality rate for untreated malaria to 4% for age group 0-1, 2% for age-group 2-5, 0.4% for age-group 6-10, and 0.1% for older age groups. Successfully treated cases in our simulation result in zero mortality, and unsuccessfully treated cases have the same mortality profile as untreated cases. It is important to remember that mortality rates in south Asia, southeast Asia, and the Americas may differ from the parameterized values here using African data, due to different clinical setting and different levels of familiarity with malaria and malaria case management. When evaluating our comparison criteria (Section 4.2.2) we decided not to include mortality as one of the reported measures, as the mortality measure correlated very closely to our `failed treatment measure' (NTF).

3.6 Age Structure

The current implementation of our individual-based simulation is not intended to represent any particular country; however, we must choose a population age structure for the simulation. In the current implementation, we use the population age structure of Tanzania, obtained from the web site of the Tanzanian National Bureau of Statistics (see table 3.4). The initial population size for each age 0 to 14 will be calculated based on these numbers; for other ages, the population size for each one-year age band is obtained by equally dividing the age classes below.

Age	Population	% of Total Population	Age Group	Population	% of Total Population
0	1,499,389	3.34%	**15-24**	8,562,875	19.06%
1	1,349,091	3.00%	**25-34**	6,302,172	14.03%
2	1,477,998	3.29%	**35-44**	4,340,066	9.66%
3	1,456,609	3.24%	**45-54**	2,716,946	6.05%
4	1,490,745	3.32%	**55-64**	1,544,557	3.44%
5	1,412,917	3.14%	**>65**	1,736,851	3.87%
6	1,420,161	3.16%			
7	1,394,553	3.10%			
8	1,279,389	2.85%			
9	1,152,017	2.56%			
10	1,340,272	2.98%			
11	951,527	2.12%			
12	1,443,723	3.21%			
13	1,022,836	2.28%			
14	1,034,229	2.30%			

Table 3.4. Population distribution of Tanzania

In 2013, the birth rate of Tanzania is estimated at 37.25 births per 1000 population per year. Note that with a birth rate of 37.25 births per 1000 population and the death rate as described in Section 3.5, the population size of the simulation will double after 30 years.

As in the Griffin papers [95], Tanzania was chosen as a malaria-endemic country with a representative population structure as Tanzania is neither small nor isolated (e.g. Equatorial Guinea, Comoros), is not severely overpopulated (Nigeria, Bangladesh), and has a mixture of rural and urban areas.

3.7 Parasite Density Levels

3.7.1 Asymptomatic Hosts

In a study of 314 asymptomatic children in Kampala, Uganda, Nsobya et al [140] showed that, at the enrollment point of the study when all children were asymptomatic, the asexual parasite densities had a range between 16 and 71840 parasites per microliter, with a geometric mean parasite density (GMPD) of 2630 parasites per microliter.

In a study from Gabon in 1995, 10 children aged from 5 to 11 with positive thick-film blood smears for *P. falciparum* and no symptoms for at least 5 days were followed daily for 7 days and then every 2 to 3 days until symptoms appeared [141]. The duration of the asymptomatic state for the 10 children ranged from 7 to 38 days and parasitaemia remained low (ranging from 10 to 10,000 parasites per microliter) during the asymptomatic state and usually increased with the appearance of symptoms (in 8 of 10 children). However, some children had more than 2500 parasites per microliter for several days without developing symptoms. The appearance of symptoms, in all 10 children, was coupled with the occurrence of a new parasite genotype. An immunological hypothesis consistent with this observation is that the children had a moderate amount of specific immunity to their resident parasites, but this immunity was not strong enough to prevent a clinical episode caused by a newly acquired parasite. The short duration of asymptomatic parasitaemia in this study is likely due to the fact that the study was conducted in a high EIR area (EIR $\approx$ 50) where new infectious bites occur frequently.

Data from a study conducted in Madagascar from 1996 to 2005 show age-stratified histograms of parasite density among 541 asymptomatic *P. falciparum* malaria patients (Figure 5 in their paper) [142]. Across all age groups, the majority of asymptomatic cases had parasite densities lower than 500. A relatively high parasite density (>500parasites/μl) was observed in ~50% of children under ten and ~25% of individuals older than ten. A very high asymptomatic parasitaemia (>5000 parasites/μl) was observed in ~15% of under-tens and <2% of individuals over the age of ten.

In our simulation, we use 1000 parasites/μl as the initial parasite density for an asymptomatic individual. During the asymptomatic phase, parasite density decreases according to the host's level of immunity until it reaches 0.002 parasites per microliter which we define as the "cure level" where parasitaemia in the simulation is set to zero.

3.7.2 Symptomatic Hosts

It is generally accepted that the total parasite burden for a symptomatic patient varies from 10^{10} to 10^{12} parasites [24]. Hence, for symptomatic adults and children we set the initial parasite density at 20,000 parasites/microliter (10^{11} total parasites), assuming that an adult individual has 5 liters of blood. For children the total parasite burden will be lower than 10^{11} parasites per symptomatic infection.

3.7.3 Detection Level of Microscopy

A review of malaria diagnostic tools shows that the detection limit of microscopy has been estimated to be 4-20 parasites/microliter; however, in field conditions, a detection level of around 50-100 parasites/microliter is more realistic [143]. In our simulation, the detectable parasite density is chosen as 10 parasites/microliter and this threshold is used to determine the blood-slide prevalence, as show in Figure 4.1.

3.8 Pharmacokinetics / Pharmacodynamics

Each individual is assigned a relative drug concentration value (relative to the initial concentration) for each drug that he or she has received during a treatment. We use a basic pharmacodynamic (PD) model (showed in equation 9) to describe the exponential waning of drug concentration[144]:

$$C=C_0 \cdot e^{-k_1 t} \tag{9}$$

where t is time in days, k_1 is the elimination rate constant, and C_0 is the maximum initial concentration after dosing. When an individual is treated, the initial drug concentration C_0 will

be drawn from a normal distribution with mean of one and standard deviation ranging from 0.1 to 0.4; C_0 will be constrained to be within the range [1-3*sd, 1+3*sd]. The variation in C0 mimics patient variability in drug absorption and/or patient variability in body size. By adjusting the value of the standard deviation, we can vary the efficacy of a particular drug (explained below).

The relationship between k_1 and drug half-life is given by the equation 10.

$$k_1 = \frac{\ln 2}{t^*} \tag{10}$$

where t^* is the half-life of the drug.

To formulate the pharmacokinetic (PK) model, a modified version of the standard Michaelis-Menton equation (which is known as Hill's equation) was used [145,146]:

$$p(C) = p_{max} \cdot \left(\frac{C^n}{C^n + EC_{50}^n}\right) \tag{11}$$

is the fraction of parasites that are killed in a given day. The value C is the current drug concentration, p_{max} is the maximum fraction of parasites that can be removed by a drug in one day, EC_{50} is the concentration level corresponding to 50% effect, and n is the slope of the concentration-effect curve. In the simulation, the parasite density is updated according to the equation 12.

$$P(t) = \big(1 - p(C)\big) \cdot P(t-1) \tag{12}$$

We can consider the term $(1 - p(C))^{-1}$ as the parasite reduction ratio and $(1 - p_{max})^{-1}$ as the initial parasite reduction ratio. In the simulation, estimated *in vivo* PRR values of different drugs, as shown in Table 3.5, correspond to the following p_{max} values for antimalarial drugs.

Antimalarial drugs	**PRR/day**	p_{max}
Artemnisinin, artesunate, artemether	10^2 – 10^2.5	0.99 – 0.9968; see also [147] for a higher estimate
4-Aminoquinoline (Cholorquine, Amodaquine), halofantrine	10 – 10^2	0.9 – 0.99
Quinine, mefloquine, sulfadoxine-pyrimethamine	10^0.5 – 10^1.5	0.68 – 0.9684

Antimalarial antibiotics (doxycycline, clindamycin), desferrioxamine	10^0.35 – 10^0.5	0.55 – 0.6838

Table 3.5. Maximum parasite killing rates for different antimalarial drugs[123].

Intuitively, one would expect to vary the pharmacodynamic parameters p_{max}, EC_{50}, and n to vary the efficacy. However, the PD process outlined in equation (12) is very deterministic as parasite numbers are very high; i.e. there is very little variability in outcomes when equation (12) is simulated forward stochastically. Therefore, the 7-day efficacy, 14-day efficacy, 28-day efficacy measures will all be either 0% or 100%, regardless of how the three PD parameters are varied. As another option for introducing variability, we may like to draw the parameters p_{max}, EC_{50}, and n from a distribution to introduce some variation, but estimates of these parameters (i.e. means) are already difficult to obtain from data and choosing/estimating the right distributions is difficult. The simplest choice is to introduce stochasticity into the parameter C_0, as it is known that patients have different body sizes and different absorption rates. By choosing C_0 randomly for each patient and simulating 10,000 patient treatments, we can measure the x-day efficacy, for any x, of a particular set of PD parameters. If C_0 were to remain fixed, all of the efficacy measurement from a 10,000-patient simulation would be 0% or 100%.

Drug half-life values were obtained from a 2001 WHO Report on antimalarial drug use [148] and several other sources (shown in the table 3.6).

Drug	Half-life (t^*)
Chloroquine	10 days
Amodiaquine	9 (7-12) days [149]
Sulfadoxine	8 days
Pyrimethamine	4 days
Proguanil	16 hrs
Quinine, quinidine	10-12 hrs
Mefloquine	10-40 days
Halofantrine	1-6 days
Artemisinin derivatives	4-11 hrs (DHA: 11-12 hrs)
Lumefantrine	3-6 days [150]
Piperaquine	33 days [151]

Table 3.6. Half-lives of antimalarial drugs.

To find specific values of n and EC50 for a particular drug or drug combinations, we fixed the drug half-life and p_{max} value which are known, and we adjusted n (ranging from 10 to 25 with step equals 1), EC50 (ranging from 0.4 – 0.6 with step equals 0.1), and the standard deviation of the initial drug concentration (ranging from 0.1 to 0.4 with step equals 0.1) until the PK/PD profile of that drug (for 10,000 treatments) or combination corresponded to the treatment efficacy measured from clinical trials. For example, for artemether-lumefantrine, we set a half-life of zero days (i.e. drug is completely out of the system on the following day), n=25, EC_{50}=0.6, p_{max}=0.999 [147] for artemether, and a half-life = 4.5 days, n=21, EC_{50}=0.6, p_{max}=0.99 for lumefantrine. This corresponded to a treatment efficacy of 94.9%, when using a standard deviation of 0.4 for C_0.

Note that the one-day time step in the simulation is a major limitation for modeling the clearance artemisinin and its metabolites, as these molecules are cleared from the system very quickly. The model essentially approximates the action of artemisinin derivatives for one day, and then assumes that the compound is completely absent from the system in the next time step if the patient is not dosed again.

3.9 Model of Immunity and Symptoms

Using M as the variable describing the general immune level ($0 < M < 1$), the equation for immune acquisition while a host maintains a blood-stage infection is defined in equation 13.

$$1 - M(t_2) = \left(1 - M(t_1)\right) e^{-a_2(a)\cdot(t_2 - t_1)}, \tag{13}$$

where the rate of immune acquisition (a_2) increases with age. We model this age dependency by allowing the rate a_2 to increase by 1% every year for hosts over the age of ten. For hosts under the age of ten, we use a convex function to describe the slower immune acquisition observed in children. For children under ten ($1 < a < 10$), the age-specific immunity acquisition rate is defined by equation 14.

$$a_2(a) = (a/10)^{\kappa} \times (1.01)^{a} \times 0.00125, \tag{14}$$

where a is treated as an integer and κ determines the convexity of the function (this is fit from Figure 3.1 and Figure 3.2 below). Individuals younger than six months have maternal immunity (see below) with no immune acquisition; individuals between 6 and 12 months no longer have maternal immunity and acquire immunity when infected at a rate a_2 that is half as fast as the rate for one-year olds. The parameter κ sets the convexity age-specific immune acquisition – for low κ the immune-acquisition rate of children quickly reaches the normal level observed in adults, and for high values of κ children will have slow immune acquisition rates until they reach an age of nine or ten. We varied κ between 0.1 and 5.0 to determine how it affected rates of clinical presentation, and in our simulations we use $\kappa = 1.0$.

For individuals older than ten, the immune acquisition rate is defined by equation 15.

$$a_2(a) = (1.01)^{a-10} \times 0.0013809 \tag{15}$$

Using these parameters, a naïve ten-year old child would reach a state of 80% immunity (M=0.8) in about three years. A naïve 30-year old adult would reach this state after about 2.5 years. Assuming κ=1.0, a persistently infected two-year old would reach 80% immunity by age nine, and a persistently infected five-year old would reach 80% immunity by age ten. Figure 3.1 shows the immune acquisition by age under different kappas.

Immunity wanes according to the equation 16.

$$M(t_2) = M(t_1)\, e^{-a_1(t_2-t_1)} \tag{16}$$

where a_1 is set to 0.0025. This corresponds to 90% immune loss after 2.5 years [94]. Newborns are given maternal immunity (M=1) which wanes linearly over six months and is then set to zero.

The level of immunity M determines the duration of parasitaemia (see Section 3.3) and the probability that a new infectious bite leads to symptomatic/clinical malaria. Our model most closely resembles the immunity model in Filipe et al. [94], which describes two types of immunity in individuals that are acquired and lost at different rates. In our model, there is a single

immunity variable but this variable M determines two clinical phenotypes (probability of developing symptoms and rate of parasite clearance) that are acquired and lost at different rates as they are non-linear functions of M.

Note that the behavior and structure of our immunity model will not exactly mirror that of the 2007 Filipe model, as their model is compartmental and immunity is modeled as a population-level variable. For example, in our model a naïve individual can become infected and acquire a higher degree of immunity, associated with faster clearance, over the 6-month duration that he/she is clearing parasites; but in a compartmental model with a population-level immunity variable this host would remain naïve and a slow-clearer as long as the EIR and prevalence in the population remained low.

The probability of progression to symptoms, as a function of M, is modeled as equation 17.

$$P_{clin} = \frac{0.99}{1+(M/M_{\text{mid}})^z} \tag{17}$$

The value 0.99 is the maximum probability when an individual is immunologically naïve; the parameter z describes the relationship between the level of immunity and the likelihood of developing symptoms, and z is varied between 2.0 and 8.0 to determine its effects on patterns of clinical malaria; we set M_{mid} to 0.4 as in the Filipe paper [94]. Figure 3.2 shows the probability of progressing to clinical disease after in infectious bite, based on host's immune level and the parameter z.

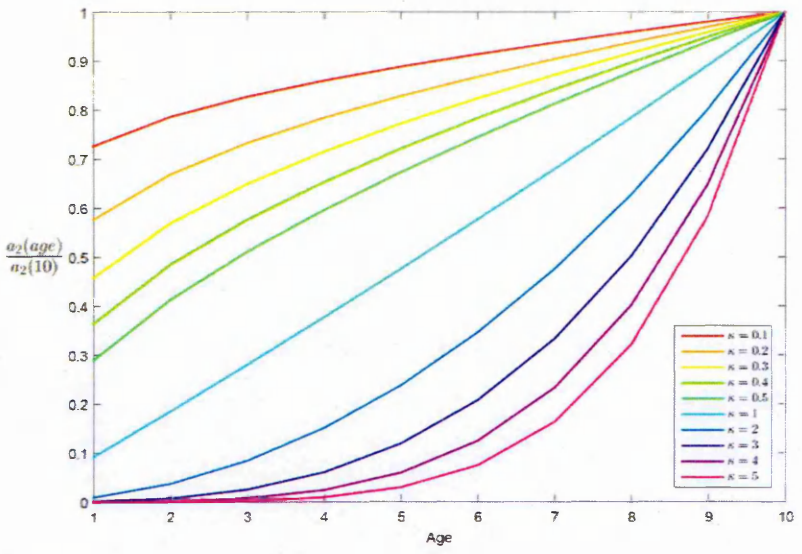

Figure 3.1. Immune acquisition by age under different kappas. The y-axis shows a child's relative immune acquisition rate when compared to a ten-year old. Ten different lines are drawn for different values of the κ parameter ranging from 0.1 to 5.0.

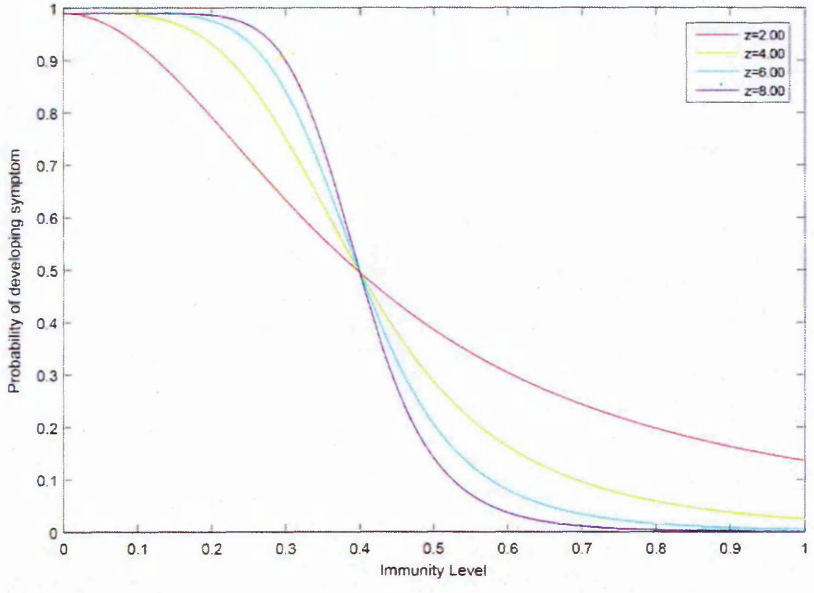

Figure 3.2. The probability of progressing to clinical disease after in infectious bite, based on host's immune level and the parameter z.

3.10 Incidence of Clinical Episodes by Age

Because there is no single measure of immunity, and because some of the unknown parameters from Section 3.9 (a_1, z, and κ) are impossible to measure directly, we perform a model calibration to determine suitable parameter values so as the age-stratified annual incidence of clinical episodes in the simulation matches what is observed in the field.

If immune acquisition is rapid and if immunity has a strong effect on protecting individuals from severity/symptoms, then the age distribution of clinical cases should have a spike in the younger age groups with a rapid drop off as age increases. If immune acquisition is slow with weak effects of symptoms prevention, the age-distribution of clinical cases would look flat in low-transmission areas and nearly-flat (slowly decreasing with age) in higher transmission areas. Essentially, as EIR increases children acquire immunity more quickly, and a larger fraction of clinical episodes should be observed in the younger age classes.

We use eight sites (from five publications) that report incidence patterns of clinical episodes by age for varying levels of EIR. The table below shows the annual incidence of clinical malaria episodes for 2-year olds, 10-year olds, and 17-year olds for these eight sites. These age groups were chosen for convenience based on the available data. The numbers in the table 3.7 are approximations as it is only necessary to see roughly how the age-specific clinical episodes change relative to one another when the EIR is changed.

		Clinical Episodes Per Year		
		Age		
Study Reference	**EIR**	**2**	**10**	**17**
Mwangi et al[152]	10	1.60	0.50	0.35
Saute et al [153]	18	0.42	0.13	no data
Trap and Rogier [154]	30	2.10	2.70	1.20
Mwangi et al [152]	37.5	1.55	0.30	0.25
Guinovart et al[155]	38	0.87	0.28	no data
Trap and Rogier [154]	200	5.00	0.60	0.30

Table 3.7. EIR and clinical episodes/year by for ages 2, 10, and 17, extracted from 4 referenced studies.

Figure 3.3 and Figure 3.4 show the ratio, from the table above, of clinical episodes in 2-year olds to clinical episodes in 10-year olds. These data are compared to our simulation output.

Simulation results show that the ratio of clinical episodes in age-group 2 to age-group 10 has a positive log-linear relationship with EIR. The square distance between the model output (selected EIR values only) and the field data with $\kappa = 1$ and $z = 4$ is at a minimum when $f = 0.0$ (figure 3.3) and this is the third best among 40 other κ-and-z combinations when $f = 0.5$ (figure 3.4). With $f = 0.5$, the best 3 minimum square distances are 24.2, 24.3 and 25.11 with the three

combinations $\kappa = 0.4$ and $z = 4$; $\kappa = 0.5$ and $z = 4$; and $\kappa = 1$ and $z = 4$, respectively. Thus, we chose the combination $\kappa = 1$ and $z = 4$ as the closest match to the data points shown in the last panel of Figure 3.3 and Figure 3.4, and we fix $\kappa = 1$ and $z = 4$ in our simulations.

We also verified that the EIR-prevalence relationship (Section 3.12) and EIR-multiplicity of infection relationship (Section 3.14) were not sensitive to the values of z and κ.

After choosing a particular immune acquisition behavior for our model ($\kappa = 1$ and $z = 4$), we test whether the model reproduces the expected age-specific clinical pattern under different transmission scenarios. The burden of clinical disease should shift from the older age-group to the younger age-groups as transmission rate increases, and this is indeed what we observe in Figure 3.5 (no treatment) and Figure 3.6 (50% treatment coverage).

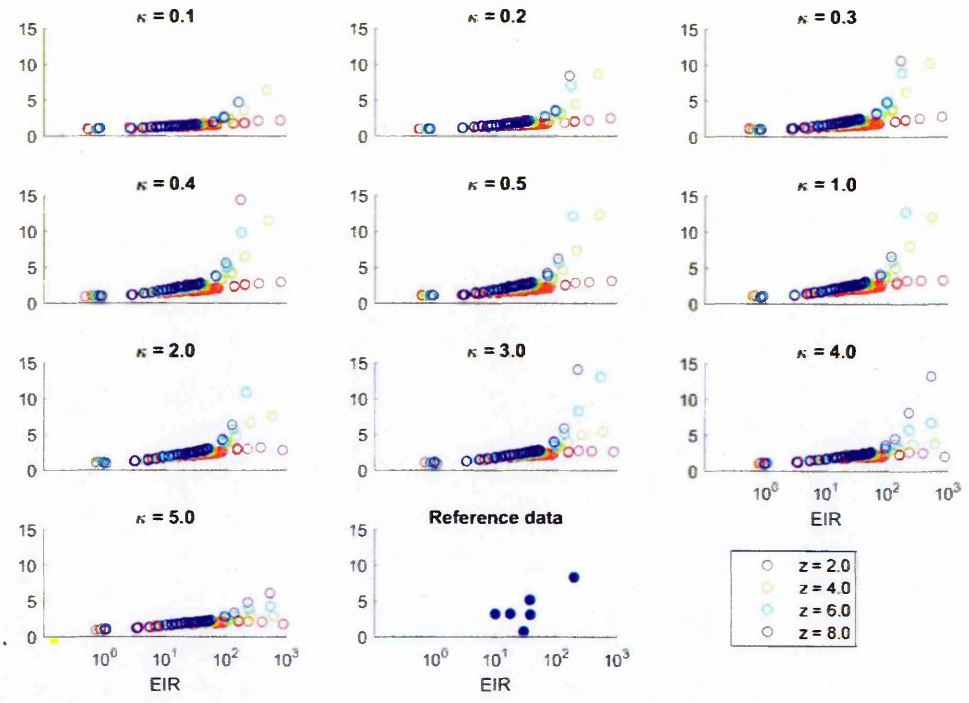

Figure 3.3. The ratio of the number of annual clinical episodes in 2-year olds to the number in 10-year olds under different transmission intensity. Ten simulations were done for each combination of κ (different panels) and z (different colors). The last panel shows the data from Table 3.7. In these simulations the treatment coverage was $f = 0.0$

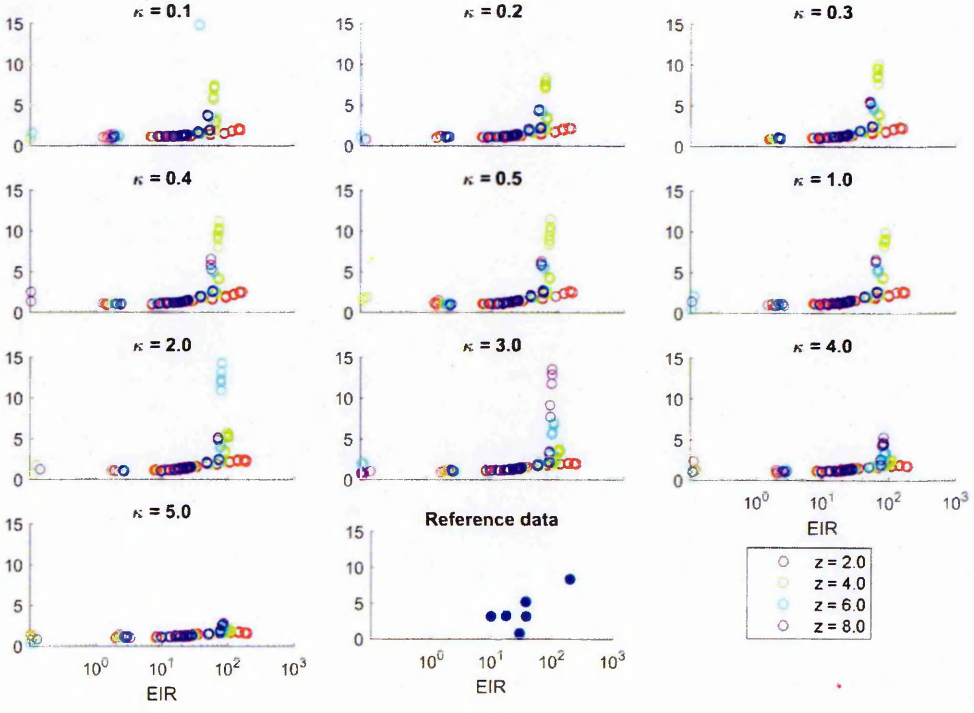

Figure 3.4. As Figure 3.3, in these simulations the treatment coverage was $f = 0.5$ with a drug with a 7-day half-life.

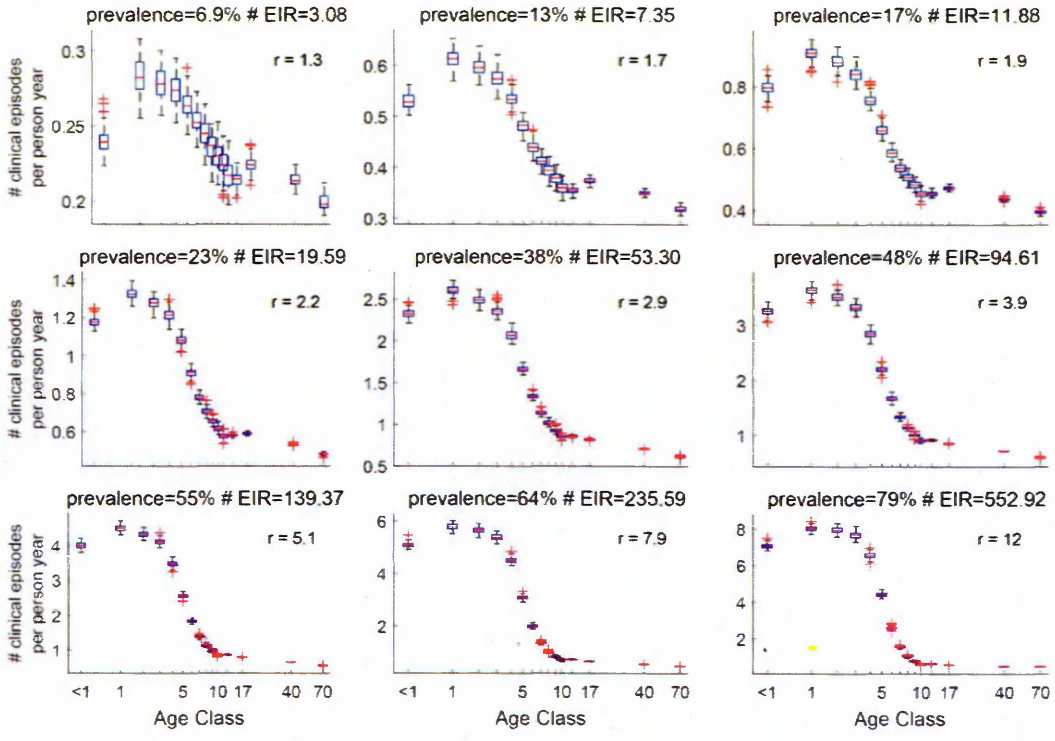

Figure 3.5. The age-specific clinical pattern under different transmission intensity (EIR increases from left to right and from top to bottom). The *r*-values in the top right corner show the ratio of clinical episodes ratio between two-year olds and ten-year olds in the simulation. Boxplots show medians and interquartile ranges from 100 simulations. All simulations run with $\kappa = 1$ and $z = 4$. In these simulations the treatment coverage was $f = 0.0$.

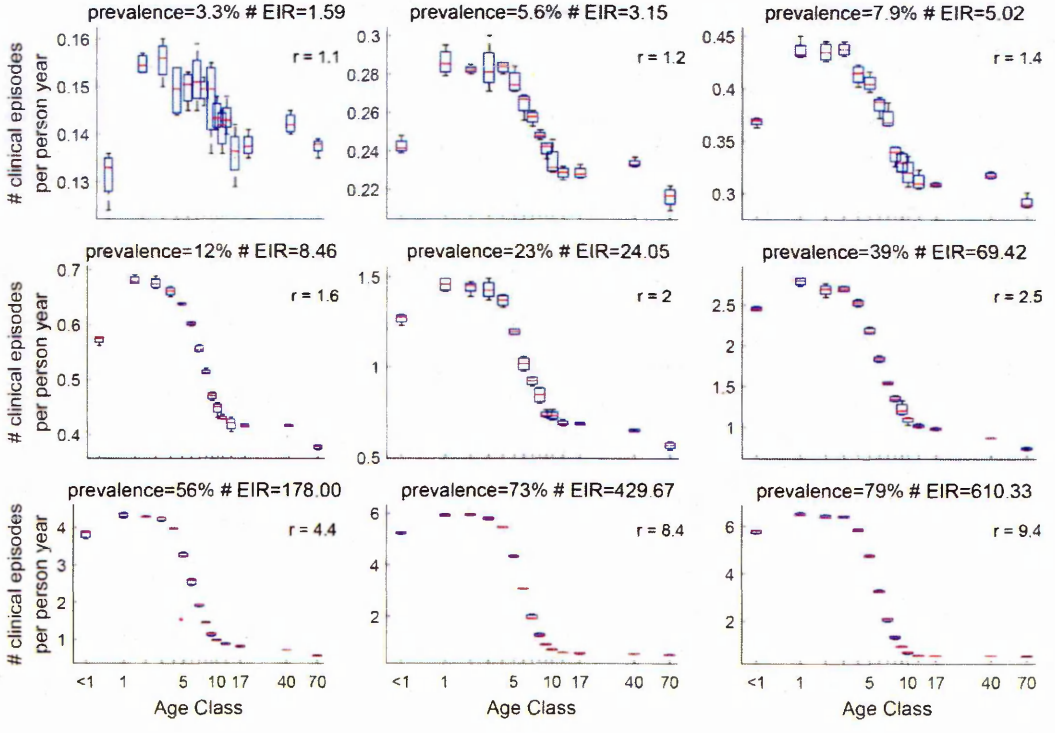

Figure 3.6. As Figure 3.5, in these simulations the treatment coverage was $f = 0.5$ with a drug with a 7-day halflife.

3.11 Prevalence of Symptoms and Blood-Slide Prevalence (φ value)

For all age classes, we are interested in the ratio of symptomatic cases over all infected cases (what we call the "φ value") as this will give us a measure of the selection pressure on the parasite population as only symptomatic cases are treated. We would expect that for φ decreases as EIR increases, as in the model described by Boni et al [52]. Very few data exist on this measurement. A recent review on asymptomatic parasitaemia and transmission showed that φ ranges from 0.40 to 0.01, as prevalence increases from 1% to 85% [156]. Yekutiel reports φ as being between 0.06 and 0.17 [157]. In two other studies, it appears to be below 0.20 [158,159]. Note that this ratio is very sensitive to the denominator, which is very sensitive to the detection method used in each study.

In our simulations, the range of φ does stay below 0.20, and φ decreases with EIR. However, we also observe a complicated interaction between φ and age. As shown in Figure 3.7 and Figure 3.8 below, the φ-value for younger age groups (<10) increases as EIR increases; the explanation for this is that in high transmission areas, children are bitten more often and experience symptoms more often.

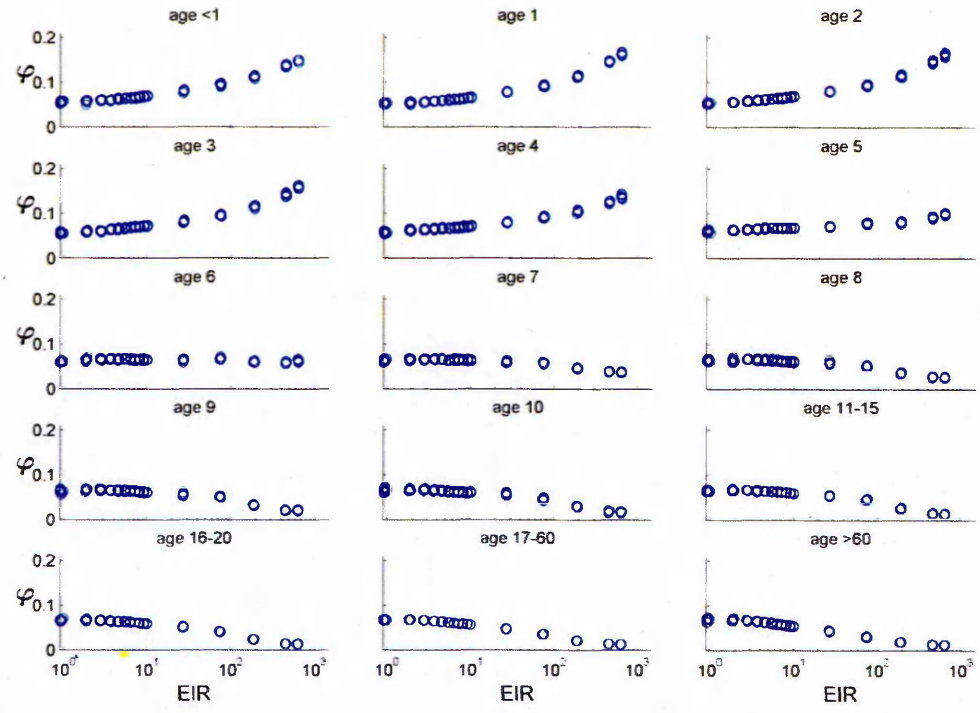

Figure 3.7. The φ-value by age-group. 400 simulations were run to equilibrium at EIR levels ranging from 0.6 to 550. In these simulations treatment coverage was set to $f = 0.0$. Immune acquisition parameters: $\kappa = 1$ and $z = 4$.

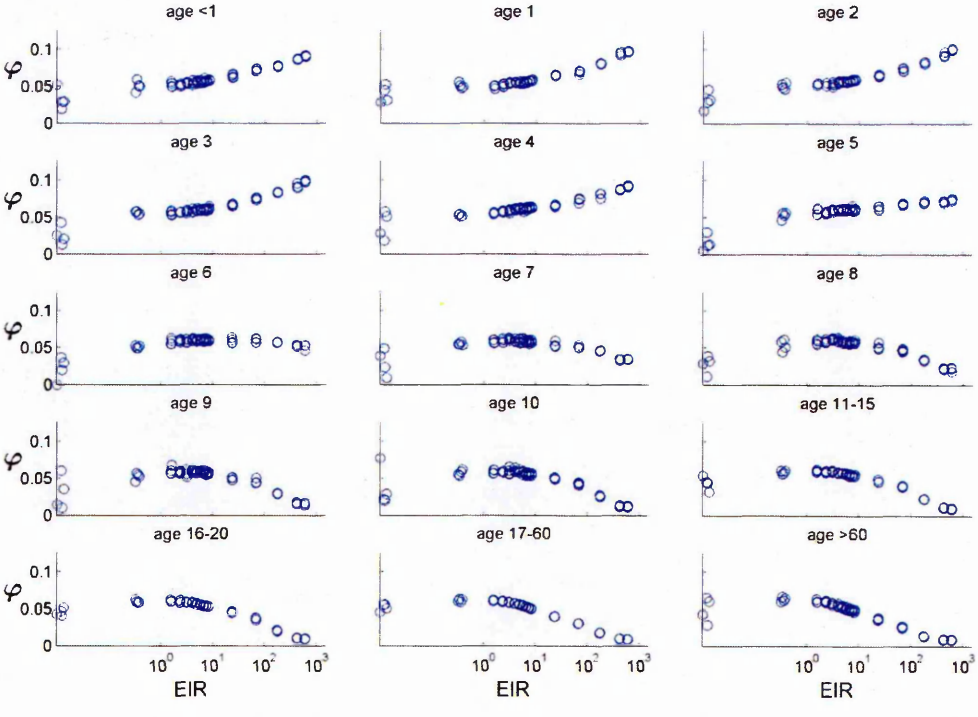

Figure 3.8. As Figure 3.7, with treatment coverage was set to $f = 0.5$ with a single 7-day half-life drug of approximately 80% efficacy.

3.12 Relationship between EIR and Malaria Prevalence

It is well known that the relationship between the entomological inoculation rate (EIR) and malaria prevalence (PR) should be non-linear, as prevalence will saturate close to 100% as EIR increases. Beier et al (1999) reviewed data from 31 sites in Africa and suggested a linear relationship between log(EIR) and prevalence (their Figure 1) [160]. Similarly, Hay et al [161] analyzed data from 22 countries across Africa between 1980 and 2004 and also found the log-linear relationship between EIR and PR. Figure 3.9 and Figure 3.10 show this relationship for our model. Saturation at high EIR is seen as expected, and a general log-linear relationship (bottom panel) is seen between EIR and prevalence.

As a second validation, we consider an EIR-PR relationship (showed in equation 18), proposed by Smith et al (2005), which includes biting rate heterogeneity [115].

$$PR = 1 - \left(1 + \frac{b\varepsilon}{rk}\right)^{-k} \tag{18}$$

where ε is EIR, b is the probability that an infectious bite results in an infection, r is the host's clearance rate, and $1/k$ is the variance of a unit-mean gamma distribution describing heterogeneity in biting rates. This model fit the data [161] better than five other models they proposed.

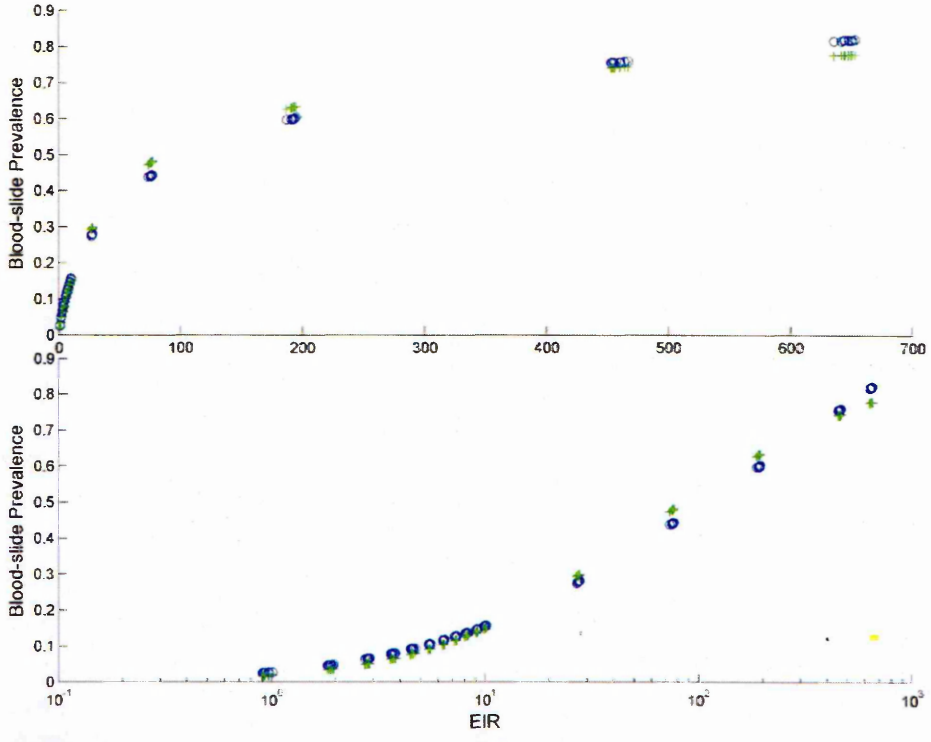

Figure 3.9. Relationship between EIR and blood slide prevalence. Model output shown in blue circles. Relationship between EIR and blood slide prevalence shown on linear scale (top) and log scale (bottom). The model was run with Γ-distributed relative biting rate with a coefficient of variation equal to 2.0. Treatment coverage is $f = 0.0$. The green crosses represent the fitted data from the Smith et al model with $b/r = 0.0194$, $1/k = 0.447$ [115].

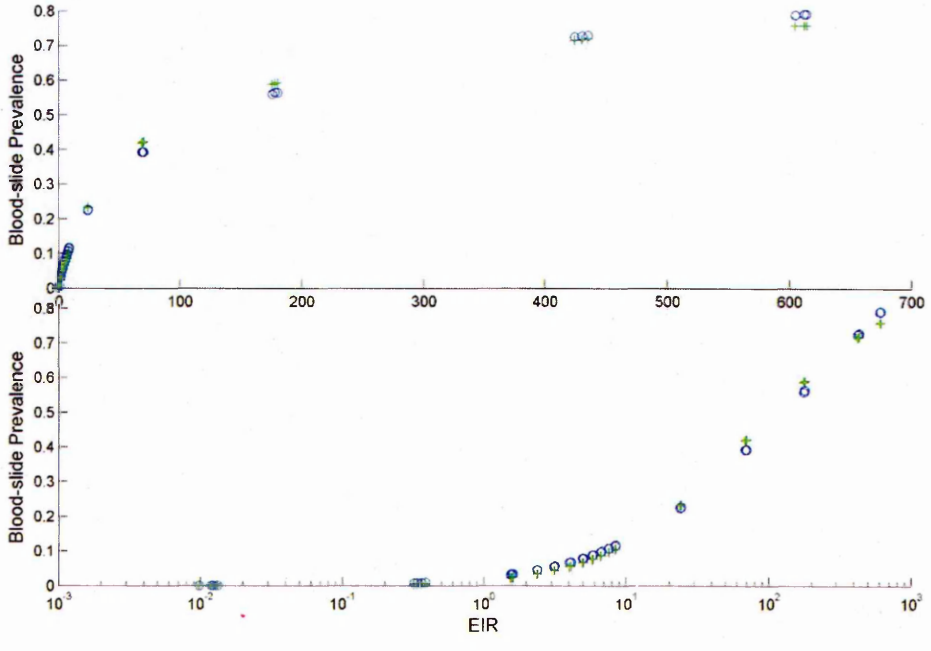

Figure 3.10. As Figure 3.9, treatment coverage is $f = 0.5$ with a single 7-day half-life drug of approximately 80% efficacy. The green crosses represent the fitted data from the Smith et al model with $b/r = 0.0194$, $1/k = 0.447$ [115]

3.13 Prevalence by Age

As discussed in previous sections, it is believed that immunity is acquired slowly in the 2-10 age group, with individuals over the age of ten acquiring immunity (as a result of parasitaemia) at approximately the same rate. A result of this assumption is that older age groups should have faster clearance rate and lower prevalence compared to younger age groups, as is observed in the field [119]. A decrease in transmission or prevalence may lead to a shift in peak risk of malaria infection to older age groups [162–164]. Age-specific prevalence data, summarized by Smith et al [165], show the shift in peak prevalence from older age groups to younger age groups as transmission increases. In a hypoendemic area, the prevalence appeared to be distributed equally across all the age groups. Our model exhibits the expected age-specific prevalence patterns as shown in Figure 3.11 and Figure 3.12.

3.14 Multiplicity of Infection

The multiplicity of infection (MOI) data from Owusu-Agyei et al [166] is used to validate the distribution of the number of parasite clones within each host. The EIR in the Owusu-Agyei study is estimated at approximately 300 bites per person year. We generate two model scenarios with this high level of transmission (Figure 3.13 and Figure 3.14) and plot the multiplicity of infection (MOI) distribution from the equilibria reached in these simulations, alongside the data from the Owusu-Agyei paper (green squares below).

The shape of MOI distribution depends on the transmission intensity. In a low-transmission setting, most infected individuals have a single parasite clone present in their blood, while in high-transmission areas the majority of individuals have multiple clones present. Arnot [167] showed a relationship between EIR and the average number of malaria parasite clones per infection with a positive linear association on a log-log scale. Our model output shows a similar pattern (not shown here), but there are simply too few data points from the field on the EIR-MOI relationship to determine what the null shape of this distribution should be.

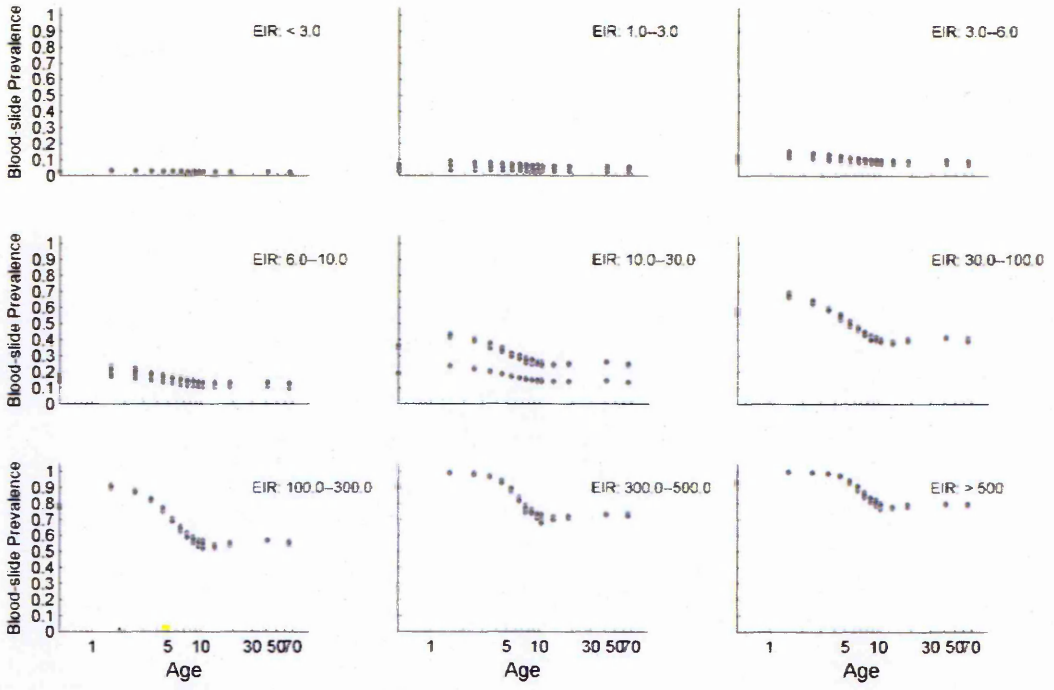

Figure 3.11. Age-specific blood-slide prevalence for different transmission intensities; κ = 1, z = 4, treatment coverage f = 0.

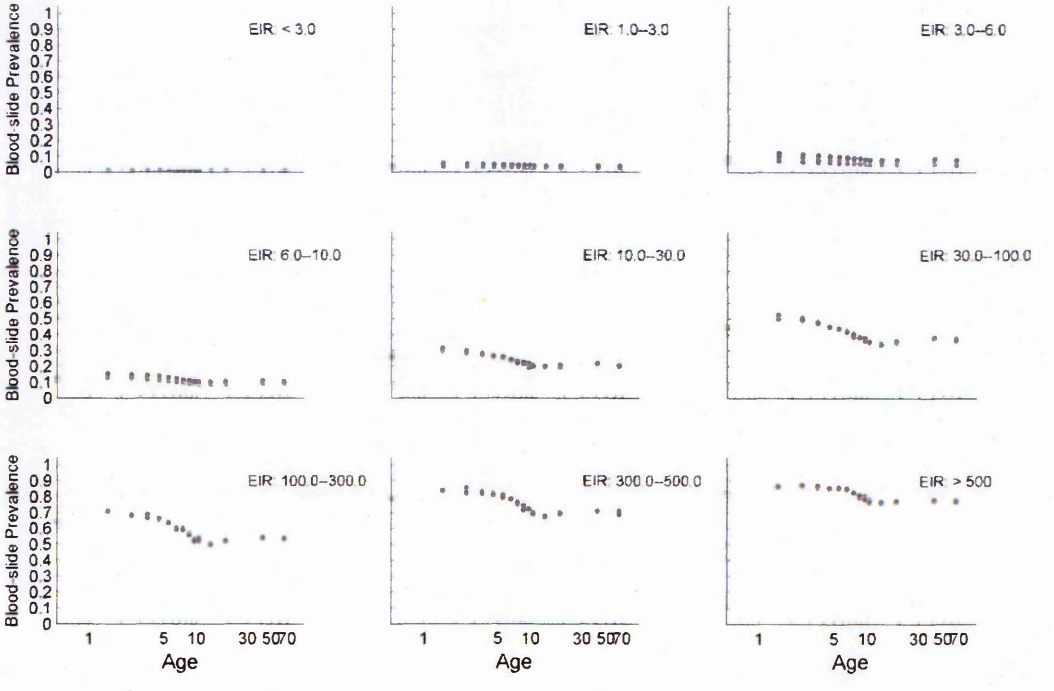

Figure 3.12. Age-specific blood-slide prevalence for different transmission intensities; κ = 1, z = 4, treated coverage f = 0.5, with a single 7-day half-life drug of approximately 80% efficacy.

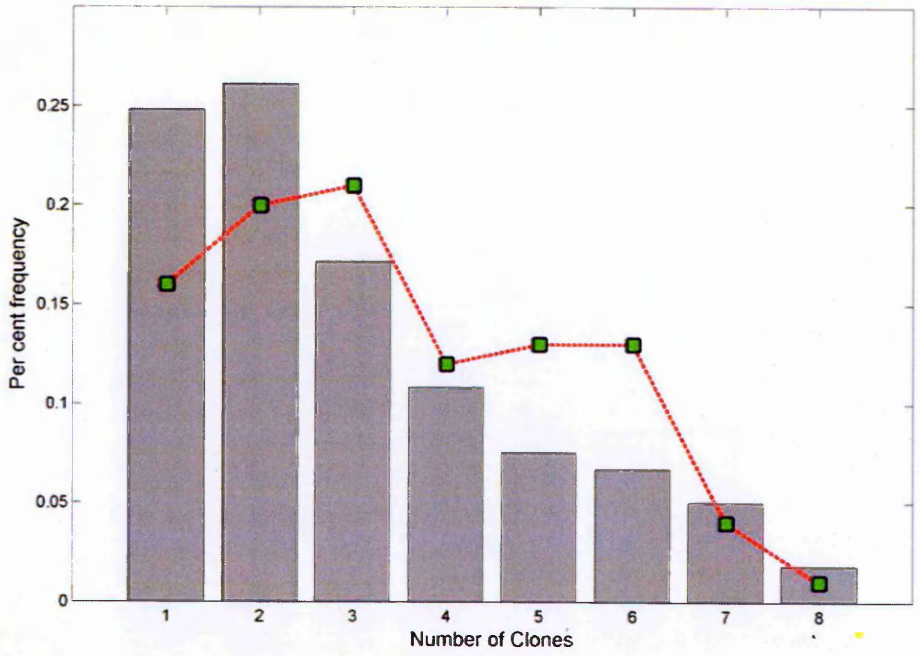

Figure 3.13. Distribution of number of clones per infection. The bar graph shows the output from our simulation with EIR = 290 while the dashed line (green squares) represents the data from Owusu-Agyei's study with EIR approximately 300 ($\kappa = 1$, z = 4, $f = 0.0$).

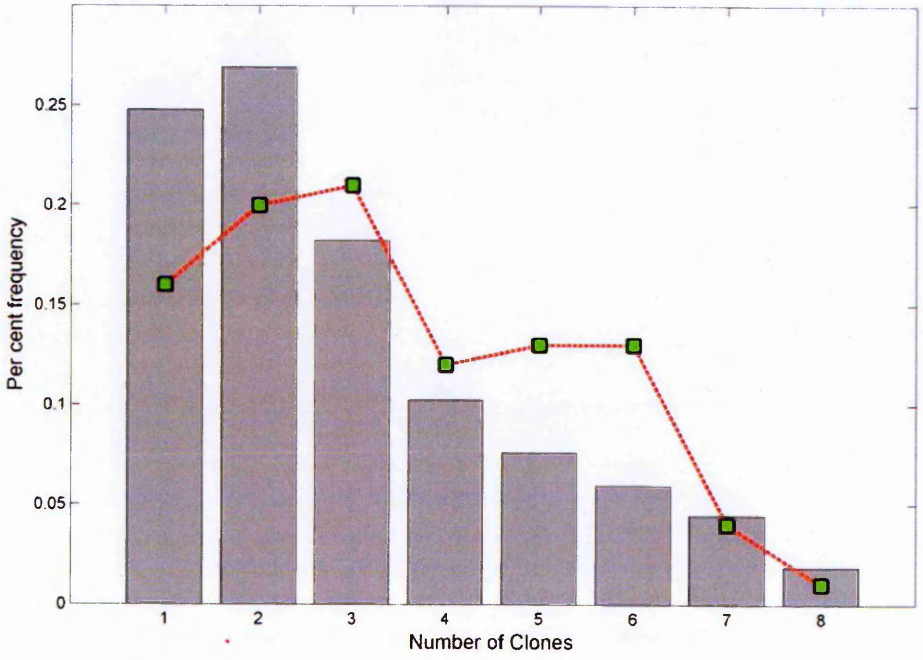

Figure 3.14. Distribution of number of clones per infection. The bar graph shows the output from our simulation with EIR = 335 while the dashed line (green squares) represents the data from Owusu-Agyei's study with EIR approximately 300 ($\kappa = 1$, z = 4, $f = 0.5$, with a single 7-day half-life drug of approximately 80% efficacy).

3.15 Biting-Rate Heterogeneity and Prevalence

Heterogeneity in transmission was modeled by assigning a relative biting level (b_i) to each host, which describes that host's relative attractiveness to mosquitoes. The higher an individual's relative biting level, the more frequently mosquitoes will bite that individual. A convenient and classic formulation of transmission heterogeneity is the "20/80 rule" [168] which states that in many epidemiological scenarios with transmission heterogeneity 20% of the population is responsible for approximately 80% of transmission.

The relative biting levels (b_i) in our simulation follow a gamma distribution. In the Smith et al paper [115], the inferred coefficient of variation (mean 1, variance 4.2) is approximately 2.05, and we set this coefficient of variation as our default. Sensitivity analyses (Section 4.4.3) are conducted with coefficients of variation set to 1.0 and 2.0.

The effect of the standard deviation on the 20/80 rule is shown in the figure 3.15 and 3.16.

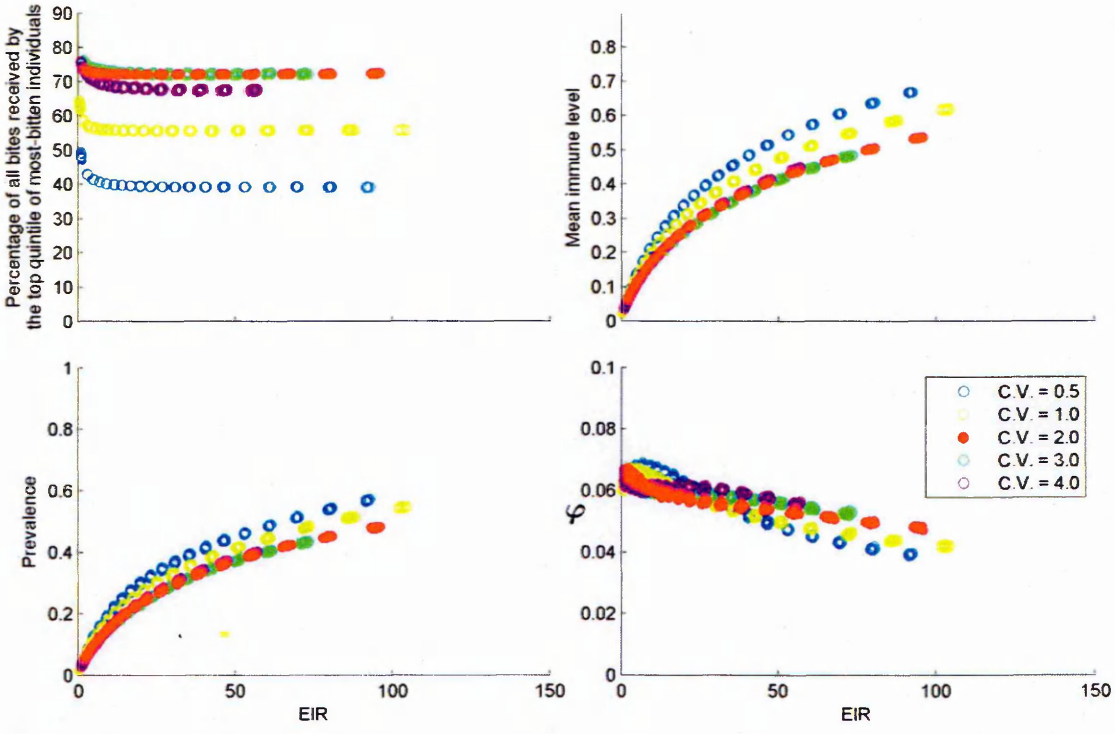

Figure 3.15. The sensitivities of four key model relationships to the standard deviation in relative biting rate. Treatment coverage f is set to 0.0.

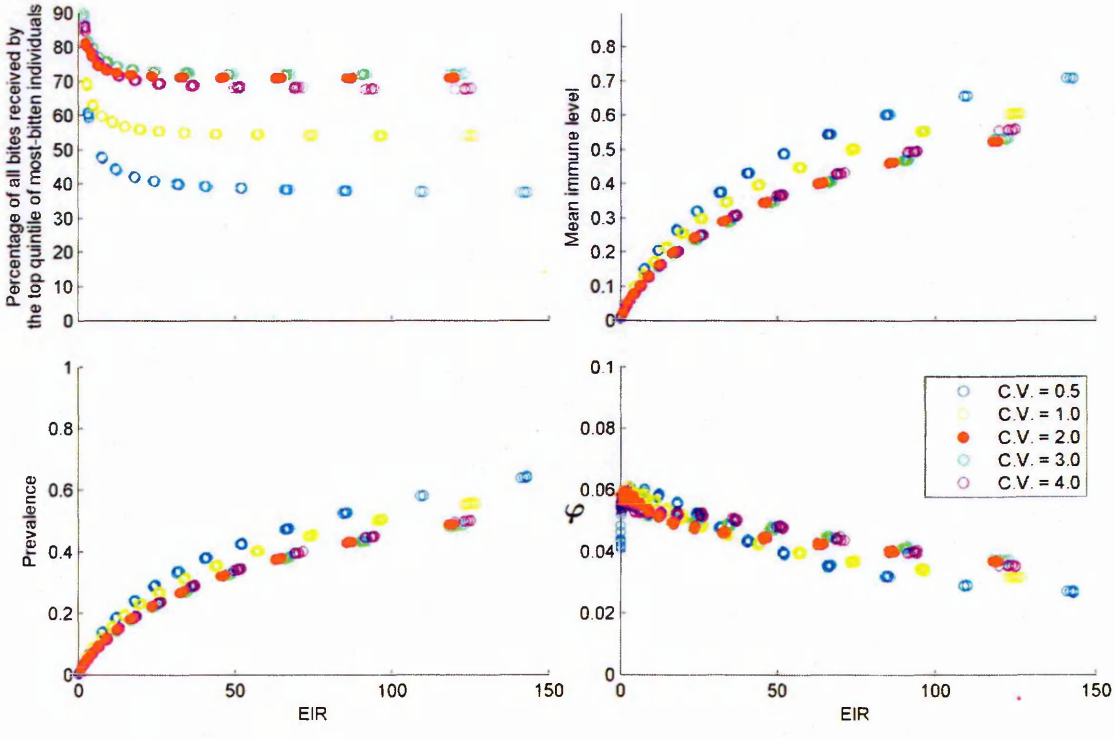

Figure 3.16. The sensitivities of four key model relationships to the standard deviation in relative biting rate. Treatment coverage f is set to 0.5.

Chapter 4

Optimal Population-Level Deployment of Artemisinin-Combination Therapies

This chapter is an expanded version of the main text of a manuscript titled "Optimal population-level deployment of artemisinin combination therapies." This manuscript was published on Lancet *Global Health* in November 2015. In order, the authors on this manuscript are myself, Piero Olliaro, Arjen Dondorp, J Kevin Baird, Ha Minh Lam, Jeremy Farrar, Guy E Thwaites, Nicholas J White, and Maciej F Boni.

In this chapter, the individual-based individual is used to evaluate which population-level approaches to distributing ACTs are most effective at (1) reducing the cumulative number of treatment failures over twenty years and (2) minimizing the risk that a novel artemisinin-resistant genotype emerges.

Section 4.2.1 describes drugs and strategies that are used to compare in the simulation, while Section 4.2.2 describes four evaluation criteria that are used.

Section 4.4.1 shows the results of the compared strategies.

Section 4.4.3 shows the sensitivity analyses. These sensitivity analyses were performed to determine the effects of differences in transmission setting, treatment coverage, partner-drug half-life, the fitness cost of drug resistance, and the relationship between drug concentration and resistance evolution. Sensitivity analyses were carried out with populations of 500,000 individuals (for quicker simulation runs).

4.1 Introduction

Over the next decade, significant public health effort and financial resources will be expended to eliminate malaria in as many parts of the world as possible[169]. In this endeavor, multiple

antimalarial tools will be used, including antimalarial treatment for clinically acute cases, antimalarial chemoprophylaxis in at-risk populations, insecticide treated nets (ITN), household insecticide use, improved diagnostics, and expansion of health service delivery[170]. For some of these interventions, we will need to be concerned with long-term diminishing returns as drug or insecticide resistance emerges and as mosquitoes adapt their behavior to ITN use and insecticide application. Efforts to maximize the effects of elimination campaigns are important, and so too are those aimed at minimizing the chances of an emergent drug or insecticide resistance phenomenon occurring during this period[171]. Such an event would seriously undermine the ambition and progress of any malaria elimination program.

Since 2005, the World Health Organization (WHO) has strongly endorsed first-line use of artemisinin-based combination therapies (ACTs) for uncomplicated falciparum malaria because of their safety and rapid action against asexual blood stages including some transmission stages[27,172]. In addition, the WHO discouraged artemisinin monotherapy to reduce recrudescence rates and to decrease the probability of *de novo* artemisinin resistance emerging in individual patients. The partner drug in a coformulated ACT always has slower elimination than the rapidly eliminated artemisinin derivatives, offering protection during the course of treatment against the *de novo* emergence of an artemisinin-resistant genotype. For artemisinin resistance to emerge, a parasite must be capable of surviving exposure to both artemisinin and the partner drug – a highly improbable event unless the infecting parasite population already carries resistance genes to the partner drug.

Despite these precautions aimed at preserving the efficacy of artemisinin-based therapies, the dangers of artemisinin resistance still warrant serious concern. A partially-resistant, slow-clearing *P. falciparum* phenotype emerged in Cambodia in the 1980s or 1990s[17,19]. This same phenotype was later observed on the border between Thailand and Myanmar[45], in southern Vietnam near the Cambodian border[173,174], and is now established in much of mainland Southeast Asia[174,175]. Slow parasite clearance is now strongly associated with a group of polymorphisms in the *P. falciparum* kelch propeller domain[19,174]. In devising strategies to

contain or extinguish this resistant genotype, we must also consider the potential for future resistance and that a fully artemisinin-resistant genotype could emerge in the next decade.

Artemisinin pressure on parasites is likely to increase over the next decade as (*i*) ACTs will remain the most commonly used antimalarial therapies, (*ii*) existing partner-drug resistance is likely to spread to areas where the corresponding ACTs are used, and (*iii*) artemisinin monotherapies are still likely to be used to some extent in contravention of strong WHO and national-level health policy recommendations. In addition, in individual patients, underdosing with artemisinin-based drugs may be a concern as subtherapeutic doses create an environment favorable to the fixation of drug-resistant genotypes[176]. Underdosing may occur as a result of substandard drugs[177], insufficient absorption, poor adherence practices, or the prescription of subtherapeutic doses especially in hyperparasitaemic cases (who require higher doses than patients with lower parasite densities) and young children or pregnant women (who have lower drug exposures)[176,178]. For these reasons, additional measures should be taken to ensure that the evolutionary selection pressure for artemisinin-resistant genotypes is as low as possible for as long as possible.

A key biological principle underpinning potential strategies for slowing down the evolution and spread of a novel mutant is that evolution occurs more slowly in heterogeneous or variable environments[179]. Combination therapy takes advantage of this principle by introducing drug heterogeneity into a pathogen's environment and forcing the pathogen population to adapt to multiple new environmental features simultaneously. This same principle can be applied at the population level, by having a parasite encounter different drugs in different individuals. The two commonly explored approaches to achieving this effect are drug cycling – where a single therapy is used population-wide for a certain amount of time before it is replaced with a different therapy – and the simultaneous distribution of multiple therapies in a population. Both of these strategies have been evaluated with mathematical models for bacteria[180–182] and malaria[52,183–185], and the strategy of simultaneous distribution is generally found to be more effective at delaying resistance evolution and keeping prevalence low for a longer period. One

of the reasons is that under a strategy of simultaneous distribution of different drugs the parasite's environment is more variable[52,182]. In this scenario, even if a *de novo* resistant parasite were to emerge in a single host, it would have difficulty establishing itself in the population as there would be at least a 50% chance that the parasite's next host would not be treated with the same drug. Under a drug cycling strategy, this effect would be as strong only if the drugs were being cycled in and out very rapidly, on the order of the generation time of the infection.

Here, we evaluate the optimal distribution of ACTs at the population level (see evaluation criteria in section 4.2.2), specifically focusing on a strategy of multiple first-line therapies[52] (MFT) – in which therapies are simultaneously recommended as first-line and are prescribed to individual patients according to some random factor (e.g. day of week, true randomization) – and comparing it to strategies of cycling or sequentially deploying single first-line ACTs. The optimal strategy in this chapter is simply the best strategy among the three presented; these three were chosen as they are all relatively simple strategies that could be implemented on a large scale. We developed and validated (Chapter 2 and Chapter 3) an individual-based microsimulation to answer this question, and our model represents an advance over previous efforts to address this question, as it accounts for key features of malaria epidemiology that affect patterns of resistance evolution: age-specific immune acquisition, biting rate heterogeneity, drug pharmacokinetics and pharmacodynamics, asexual parasite density, multiplicity of infection, and recombination.

4.2 Strategy Comparison and Evaluation Criteria

Assuming that three ACTs with different partner drugs are available for treatment, three population-level treatment strategies were compared in the simulations. The half-lives and efficacies of the therapies in the simulation were set to mimic the characteristics of artesunate-amodiaquine (ASAQ), artemether-lumefantrine (AL), and dihydroartemisinin-piperaquine (DHA-PPQ) [148–151].

4.2.1 Strategies

Multiple first-line therapies (MFT). In a strategy of multiple first-line therapies, one-third of individuals are treated with one ACT, one third with a different ACT, and the final third with the remaining ACT. If the treatment coverage parameter is $f = 0.6$, this means that 40% of individuals would not be treated for a symptomatic malaria infection (due to lack of access, inability to pay, not reporting to a clinic or pharmacy, etc.). The model would then assign 20% of individuals to be treated with the first ACT, 20% to the second ACT, 20% to the third ACT, and 40% to no treatment.

Five-year cycling. In a 5-year cycling strategy, a single ACT is used in the population at any one time and the ACTs are rotated out and switched every five years. We compared several cycling strategies in a previous publication [52] (2-year cycling, 3-year cycling, etc). Here, we choose five years as a feasible schedule which could be implemented at a national level in an endemic country. Shorter cycling periods are of course associated with improved outcomes, as they create more variability for the parasite population and slow down the pace of resistance evolution. The shorter the cycling period, the closer this strategy approximates an MFT strategy.

Sequential Deployment. The third strategy is meant to mimic the status quo approach of rotating therapies out when they begin to fail. We call this 'sequential deployment', and under this strategy switches occur when the treatment failure rate (using a 60-day moving average) reaches 10%, the WHO criterion for replacing first-line therapies [27]; a one-year delay is built in to this strategy as it is known that switching first-line drugs at the national level can take a significant amount of time and effort [186]. This is optimistic, but we used this one-year delay to compare the best possible sequential deployment strategy against the two alternatives. In a previous publication, this strategy was called 'adaptive cycling' [52].

Multiple first-line therapies with one non-ACT component. For the Figure 4.6, we evaluated an MFT strategy with two ACTs (ASAQ and AL) and one non-ACT therapy. The

non-ACT component in this strategy was a combination therapy whose components have 7-day and 10-day half-lives, mimicking the pharmacodynamics of chloroquine and sulfadoxine-pyremethamine.

4.2.2 Evaluation Criteria

Four evaluation criteria are used:

NTF. The number of treatment failures per 100 individuals per year over the 20-year course of the simulation. This measure is discounted with a 3% annual discounting rate. Non-treatments are counted as treatment failures; if this were not done, then policies with low coverage (f) would appear optimal as they would treat the fewest people and drive resistance evolution at the slowest rate.

AMU. Artemisinin monotherapy use is a risk measure describing how exposed to resistance evolution the artemisinins are under a particular strategy. "Exposed" in this context means "not protected by the partner drug". To compute the AMU measure, we run a separate set of simulations with the artemisinin-resistance mutation parameter set to zero, and we count all treated cases in which an individual with parasites resistant to partner-drug x is treated with an ACT containing the same partner drug x. We call this type of treatement *de facto* artemisinin monotherapy use because only the artemisinin component is acting in this situation. AMU is simply an absolute count of all cases of *de facto* artemisinin monotherapy use during a 20-year simulation.

We reported three types of AMU measures in our simulation: by person, by parasite clone, and by person but weighted by the number of parasite clones. Consider an individual with 5 clonal *P. falciparum* infections in the blood, two of which carry amodiaquine resistance. If this person were treated with ASAQ, then we could count this as 1 AMU ('by person' measure), 2 AMU ('by parasite clone'), or 2/5 AMU (weighted measure). All three measures had similar

behaviors when comparing treatment strategies. In Figure 4.5, we present the weighted measure.

We do not discount the AMU measure as we are trying to compare the relative probabilities across treatment strategies that, over a 20-year period, a novel artemisinin-resistance genotype could emerge and establish itself. Alternatively, AMU can be thought of as the total amount of "selection pressure via artemisinin monotherapy" present during a 20-year period. Comparisons using a discounted AMU measure were qualitatively identical to those shown in Figure 4.5.

UTL. In an MFT strategy, this is the time until the treatment failure rate reaches 10%. Treatment failure is computed in all simulations as a moving average over the past 60 days as this is what is likely to be picked up by surveillance systems. For the cycling and sequential strategies, the UTL is defined as the total time during the 20-year simulation that the treatment failure rate is below 10%. Note that the treatment failure rate computed in the simulation includes the usual expected treatment failure even when the parasite population is drug-sensitive. For this reason, the UTL would not be a useful measure for a drug or therapy with 91% efficacy as 10% treatment failure could be reached very quickly.

$T_{.01}$. The time at which the "genotype frequency of resistant alleles" reaches 1% in the population. If four drugs are being used in the population, then each parasite can be a single-resistant, a double-resistant, a triple-resistant or a quadruple-resistant. If p_1 is the frequency of single-resistant genotypes, p_2 the frequency of double-resistant genotypes, etc., then the "genotype frequency of resistant alleles" is defined as equation 19.

$$\frac{1}{4}p_1 + \frac{1}{2}p_2 + \frac{3}{4}p_3 + p_4 \tag{19}$$

The frequencies are calculated across parasite clones. This quantity is equivalent to the probability that if a parasite genotype is chosen at random and a drug is chosen at random, that the parasite will carry resistance to that drug.

When comparing two strategies, we test statistically for rank differences in the outcome measures (Mann-Whitney Test) as well as differences between the medians, 25th percentiles, and 75th percentiles (Mood's Test). To summarize, we present the maximum of these four p-values, unless stated otherwise.

4.3 Ecological Rationale for MFT

Basic ecological and evolutionary theory has demonstrated the rationale for using multiple first-line therapies. First, as described by Bergstrom et al [182], deploying multiple drugs simultaneously creates a more variable environment for the pathogen and makes any specific type of resistance evolution more difficult. Second, as described in Boni et al [52], cycling strategies have a particular detrimental effect on driving drug resistance, because each individual cycle drives the evolution of a particular resistant genotype. Hence, at the end of a cycle, we may observer one resistant genotype at a very high frequency in the population. When the second "drug cycle" begins and when the second drug-resistant type emerges, this newly emerged genotype will only have to outcompete resistants that have persisted from the previous treatment period. This is an easier evolutionary competition to win than one where drug-resistant genotypes have to outcompete wild-types. Cycling strategies, therefore, make resistance evolution (for all resistant types) easier by strongly driving the evolution of the first drug-resistant genotype. Third, as we will show later in this chapter, cycling strategies are susceptible to epidemiological rebounds and MFT strategies are not. Figure 4.1 shows what occurs at the end stages of each cycle: prevalence increases above the expected level at endemic equilibrium because of a temporary excess of susceptibles in the population. Epidemiological rebounds can occur under many disease dynamic scenarios. For malaria, they can be associated with a substantial increase in morbidity and mortality, and they should be avoided if possible.

4.4 Results

4.4.1 Strategy Comparisons.

The deployment of multiple first-line therapies (MFT) had consistently better population-level outcomes than either cycling strategy, and the superior performance of MFT was robust to a variety of transmission, clinical, and evolutionary settings. As noted in previous modeling efforts[52,182], an MFT strategy creates a more variable environment for the malaria parasite, which results in delayed resistance emergence and slower drug-resistance evolution. This is true even when allowing for free recombination among resistance loci, which was previously raised as a potential concern when evaluating the benefits and drawbacks of MFT strategies[187]. Figure 4.1 shows typical evolutionary-epidemiological trajectories for malaria under the three treatment scenarios we evaluated.

A strategy comparison in a low-transmission setting corresponding to an EIR of 1.3 infectious bites per person per year (Figure 4.3) shows significant variation, due to the stochastic nature of the model, in the number of treatment failures (NTF) and the time until resistance emergence ($T_{.01}$); note that in some high-coverage settings treatment drives the parasite population to a 'sticky elimination'[188]. When resistance does evolve ($0.5 \leq f \leq 0.7$), MFT strategies have median NTF values that are between 16% and 41% lower ($p < .003$; Mood's test) than either sequential or cycling strategy; this difference is larger for higher costs of resistance. In addition, elimination was observed more often under MFT strategies as these strategies preserve full drug efficacy for longer than either cycling strategy. Figure 4.4 shows that low NTF values are closely associated with longer times to emergence. MFT strategies exhibit a higher mean and more variation in their associated time-to-emergence (an expected outcome from a waiting process), resulting in a higher proportion of simulations in which resistance emerges very late or not at all during the 20-year model simulation.

Because these model simulations rely partially on the prediction of rare events (the emergence of artemisinin resistance), we ran a separate set of simulations to quantify the risk of artemisinin

resistance using the AMU criterion: the total number of cases during the 20-year simulation where a partner-drug resistant infection was treated with an ACT (Figure 4.5). Excluding one comparison set in this figure, the median AMU outcomes for MFT strategies were between 28% and 78% lower ($p < 10^{-5}$; Mood's test) than for either cycling strategy, suggesting that MFT strategies may carry a much lower risk of selecting for *de novo* artemisinin resistance. Essentially, MFT strategies delay and decelerate partner-drug resistance evolution, thus prolonging the time that artemisinin-based drugs are used as combination therapies with both components effective.

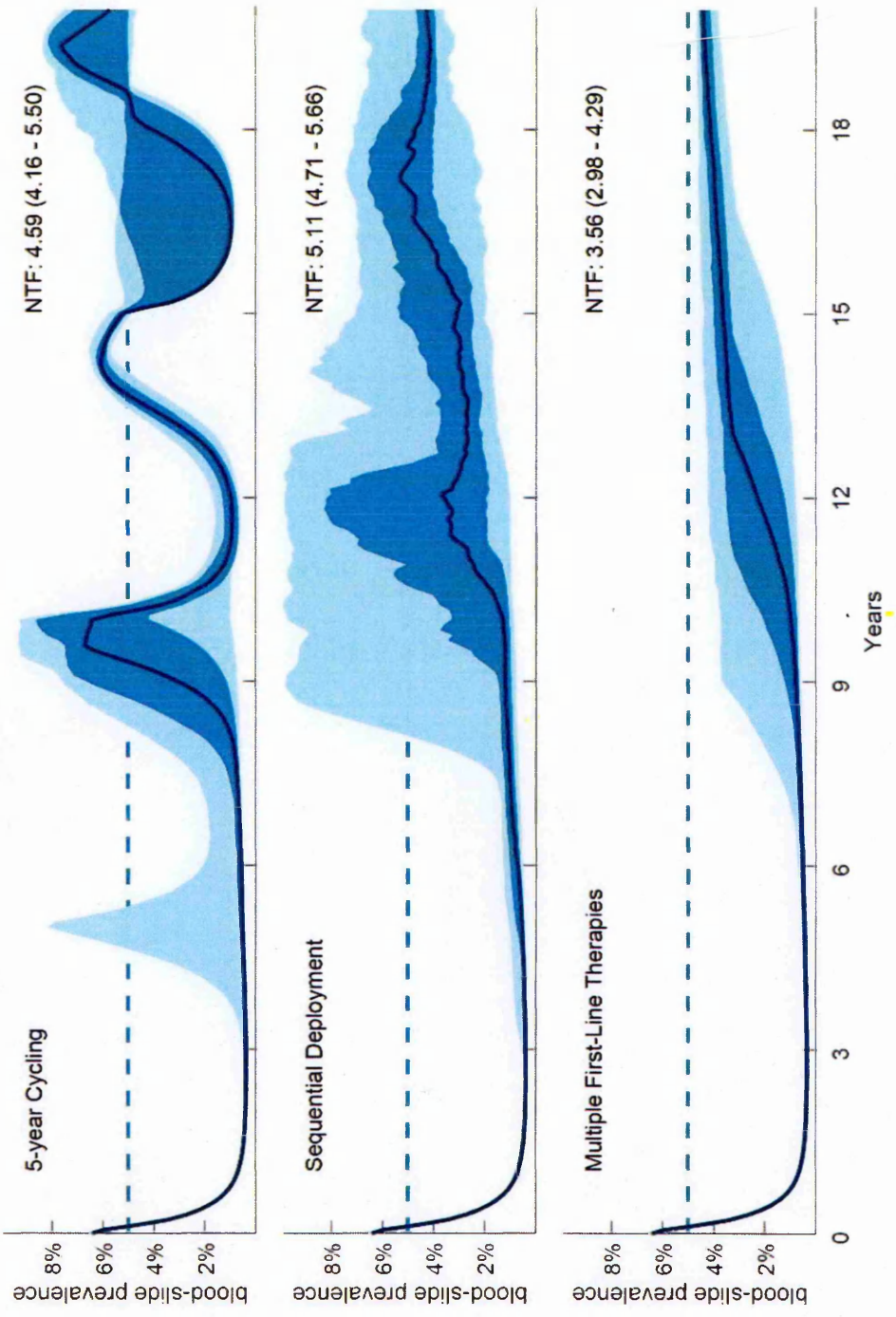

Figure 4.1. Expected paths of drug-resistance evolution and corresponding malaria prevalence under three different treatment regimes. One hundred stochastic simulations were run in a population of one million individuals, in a low transmission setting (EIR=1.3) with 60% treatment coverage and an assumed cost of resistance of 0.5% for all resistant genotypes. The mutation rate is assumed to be highest for intermediate drug concentrations. The black line shows the median prevalence across 100 simulations, and the teal areas show the interquartile and 90% ranges. The media number treatment failures (NTF) with interquartile ranges are shown in each panel ($p < 10^{-6}$ when comparing MFT to the other two strategies). The dashed line shows 5% prevalence. For the cycling/sequential strategies, after the emergence of a novel drug-resistant type, an epidemiological rebound sometimes causes the prevalence to reach higher-than expected levels (here, >6%) for short periods.

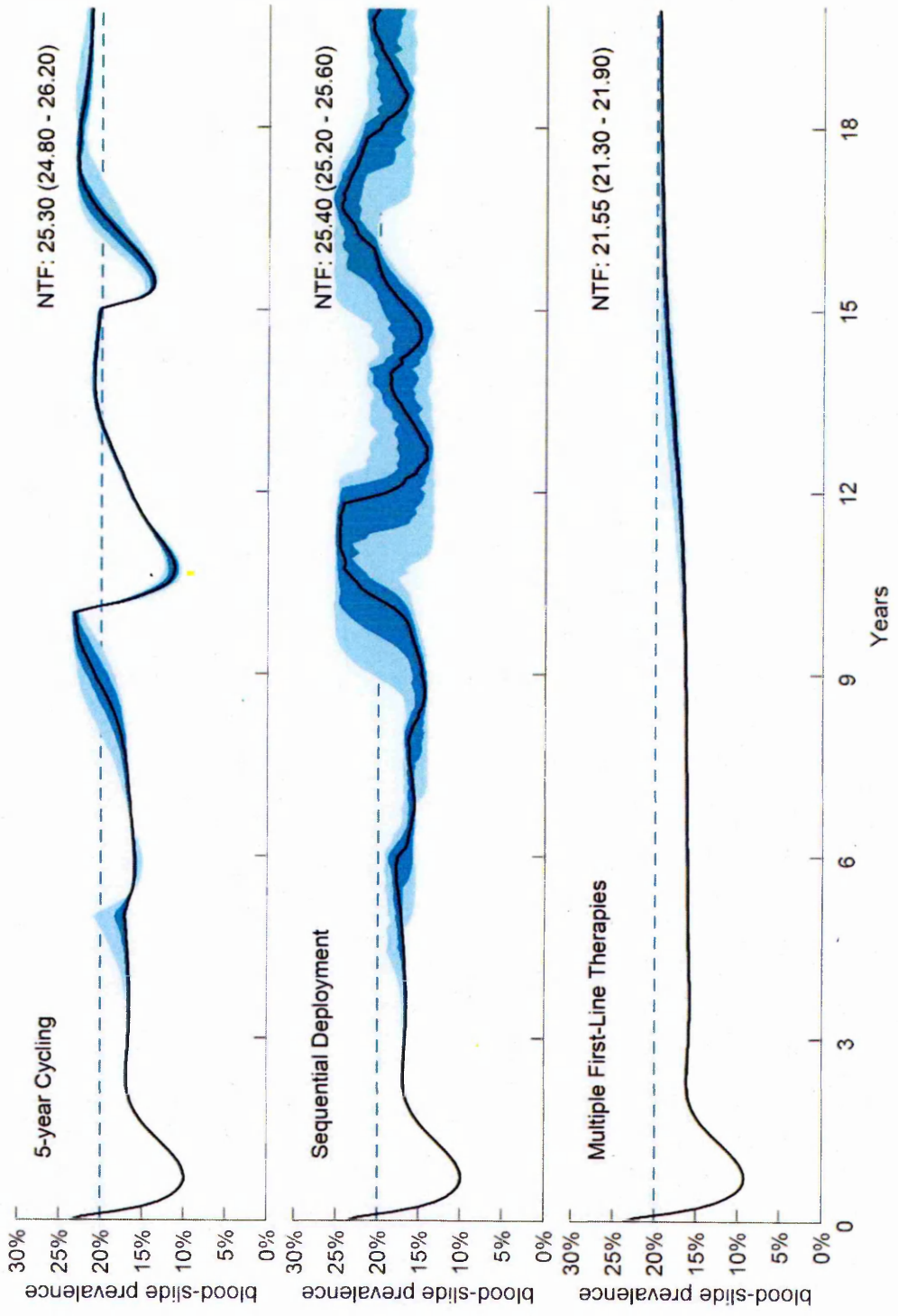

Figure 4.2. As Figure 4.1, 70 stochastic simulations were run in a population of one million individuals, in a high transmission setting (EIR=18) with 60% treatment coverage and an assumed cost of resistance of 0.5% for all resistant genotypes.

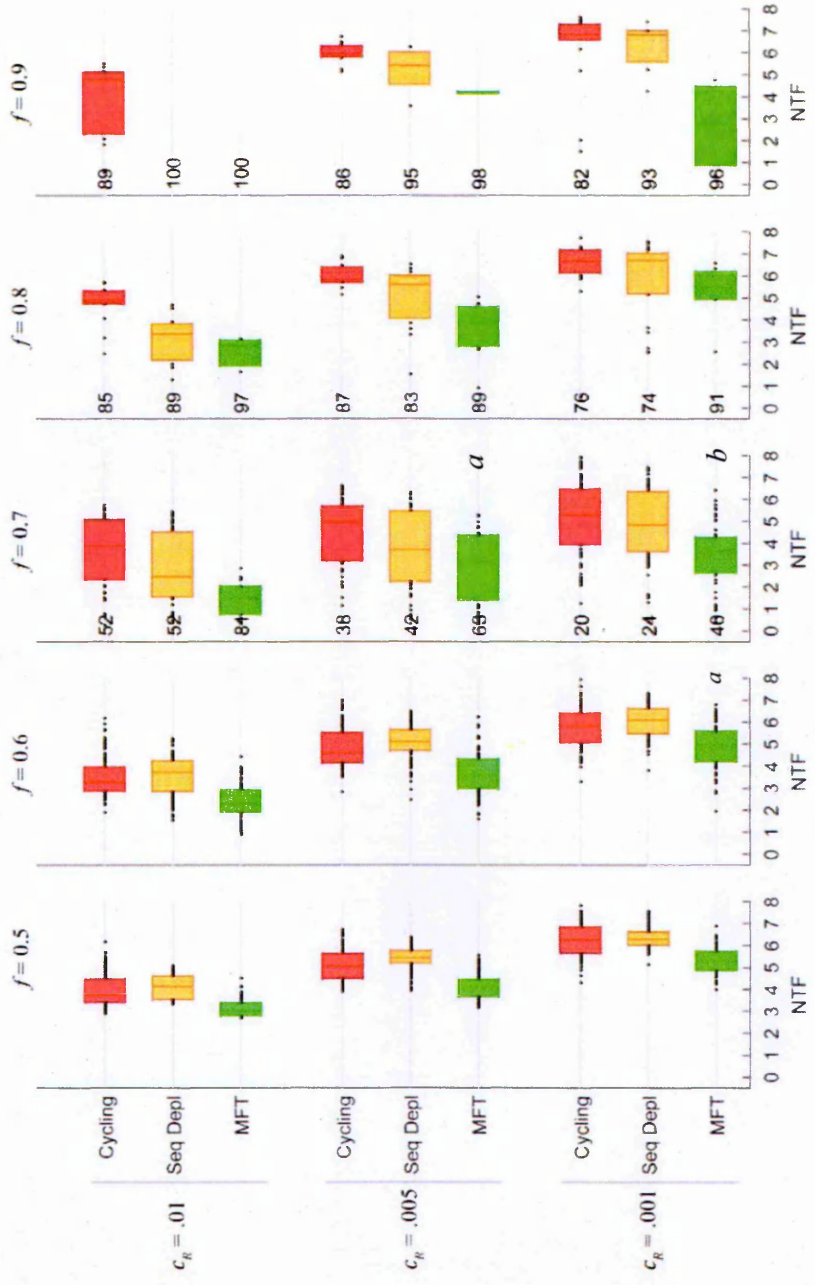

Figure 4.3. Comparisons of MFT, five-year cycling, and sequential deployment. Figure shows the NTF-values – the annual number of combined treatment failures and non-treatments, per 100 individuals – for different strategies, different costs of resistance (c_R), and different treatment coverages (f). Each row shows the NTF results of 100 model simulations with the colored bars spanning the interquartile range. NTF values are lower under multiple first-line therapies; all $p < 10^{-4}$ except for the comparisons marked *a* and *b* where $p < .01$. For $f \geq 0.7$, the NTF distributions had a bimodal shape with NTF < 0.5 corresponding to simulations that achieved extinction or near-extinction; the numbers on the left-hand side of each boxplot show the counts of these (near)-extinctions, and the interquartile ranges are plotted only for simulations that did not result in extinction. Simulations assume that three ACTs with 95% efficacy are available and that the three partner drugs have 4.5-day, 9-day, and 28-day half-lives (corresponding to lumefantrine, amodiaquine, and piperaquine, respectively). Simulations are done in a low transmission setting with EIR=1.3. Drug-resistance mutations have their highest probability of fixation at intermediate drug concentrations. Figure 4.15 shows the results for the case when mutation is proportional to drug concentration.

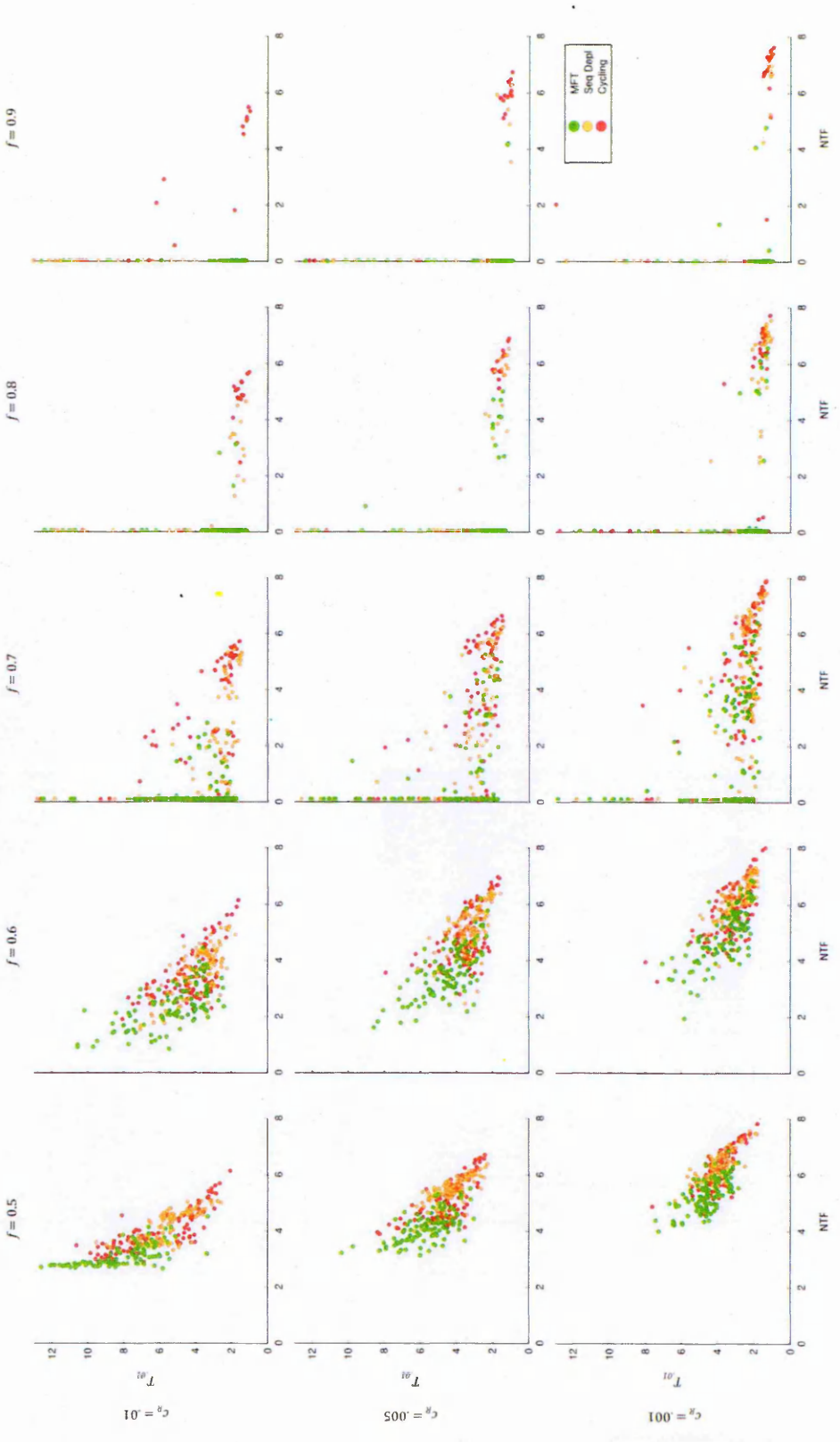

Figure 4.4. As Figure 4.3, figure shows NTF values from the same simulations that are plotted against the time it takes the average resistance level to reach 1% frequency in the population. Note that the variance in time-to-emergence is greater for MFT strategies, resulting in a subset of simulations with long emergence times. Simulations are done in a low transmission setting with EIR=1.3. Drug-resistance mutations have their highest probability of fixation at intermediate drug concentrations.

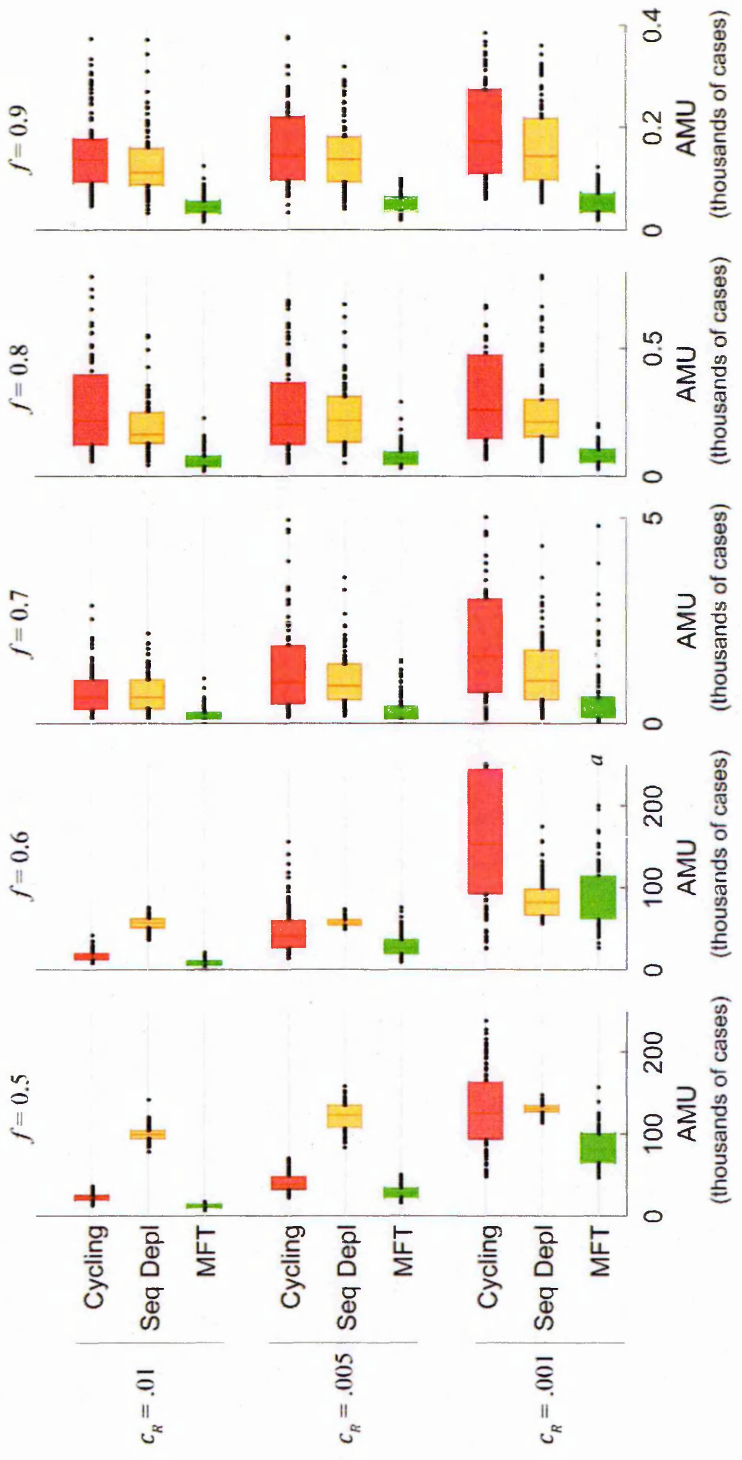

Figure 4.5. Comparisons of artemisinin monotherapy use (AMU) for MFT, five-year cycling, and sequential deployment. AMU-values are shown for different costs of resistance (c_R), and different treatment coverages (f). Each row shows the AMU results of 100 model simulations with the colored bars spanning the interquartile range; AMU values are lower under multiple first-line therapies (all $p <$ .001) except for the two comparisons corresponding to *a*. Simulations assume that three ACTs with 95% efficacy are available and that the three partner drugs have 4.5-day, 9-day, and 28-day half-lives. Simulations are done in a moderate transmission setting (EIR=1.3). Partner-drug resistance mutations have their highest probability of fixation at intermediate drug concentrations. AMU decreases with treatment coverage because prevalence is lower when more individuals are treated. Figure 4.16 shows the results for the case when mutation is proportional to drug concentration.

4.4.2 Further Options for Artemisinin Conservation.

In addition to deploying multiple first-line ACTs, we considered other possibilities that would allow us to preserve the efficacy of artemisinin-based drugs for as long as possible. From the analyses presented here and basic evolutionary theory, it is apparent that alleviating the parasites from artemisinin drug pressure should slow down artemisinin-resistance evolution. Employing a non-ACT alongside two artemisinin-based drugs in an MFT treatment strategy should have this effect. Clearly, the major consideration for such a strategy will be whether the non-ACT component is as effective and safe as an ACT. If this individual-level acceptability criterion is met, an MFT strategy with a single non-ACT therapy[189] could have significant benefits in extending the lifespan of artemisinins. Figure 4.6 shows the lower NTF values and longer UTLs that would be associated with this strategy, the lower NTF being a direct result of a longer time-to-emergence for artemisinin resistance. In these simulations, the treatment coverage is 60%; thus, even in the worst-case scenario of 75% efficacy for a non-ACT therapy, only 4% of individuals in the model experienced a failing treatment as a result of not receiving an ACT. In the six scenarios in Figure 4.6, the median time-to-emergence for a strategy employing a non-ACT was between 43% and 71% longer ($p < .001$; Mood's test) than a strategy using three ACTs. With a mix of two ACTs and one non-ACTs, a third ACT would be preserved in case one of the partner drugs began failing early.

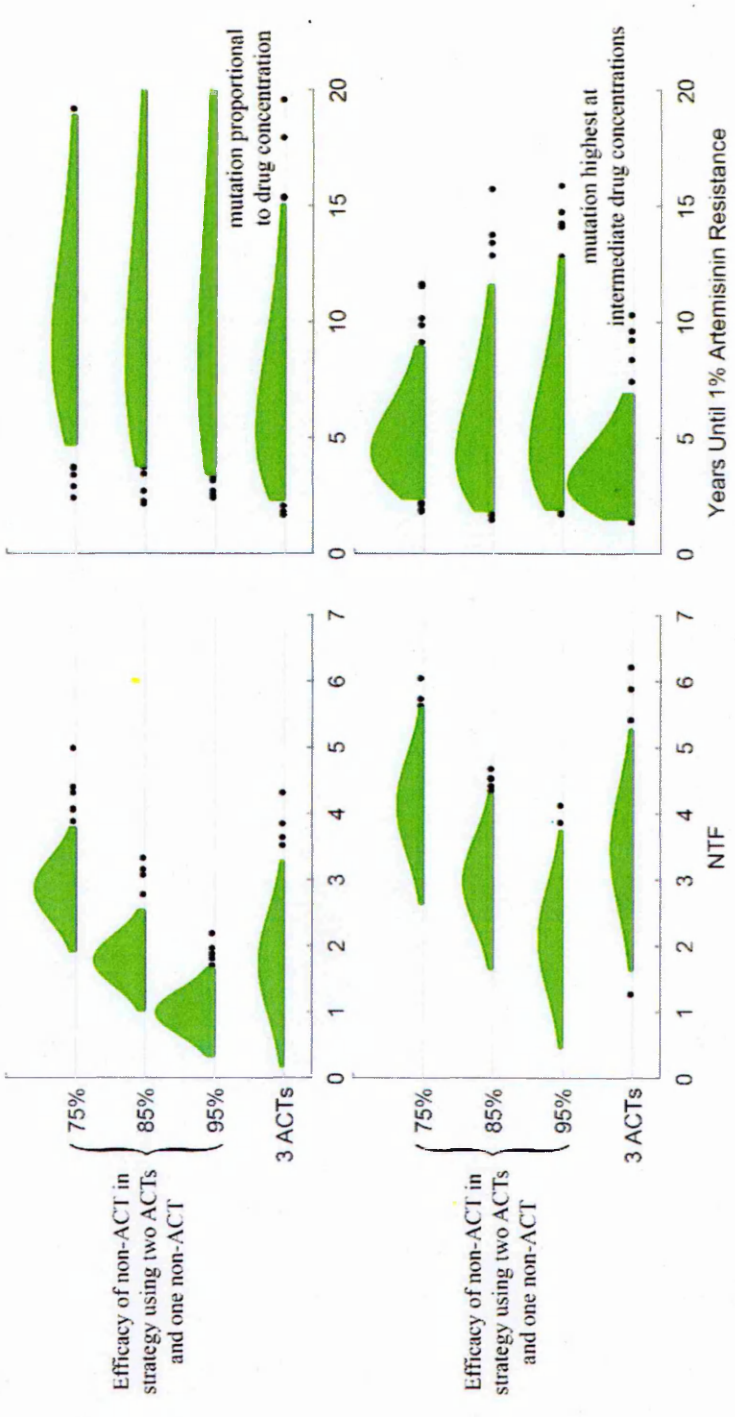

Figure 4.6. Comparison using a non-ACT drug included in MFT strategy. Comparisons between MFT strategies with three ACT components and MFT strategies where one of the components of the treatment strategy is not an artemisinin-based therapy. Results of one hundred simulations for each strategy are summarized as normal distributions for NTF (shown in green out to $\pm 2\sigma$), and as gamma distributions for the time until the frequency of artemisinin resistance reaches 1% (central 90% of distribution shown in green). The top panels use a standard mutation model (k=0.5) where the mutation rate is proportional to the drug concentration. The bottom panels show simulation results when the mutation rate increases at intermediate concentrations (k=4). Simulations assume that three ACTs with 95% efficacy are available and that the three partner drugs have 4.5-day, 9-day, and 28-day half-lives. In the simulations with 2 ACTs, the 4.5-day and 9-day halflife ACTs were used (minimizing selection pressure), and the non-ACT therapy is assumed to be a combination therapy whose components have 7-day and 10-day halflives. Treatment coverage is f=0.6.

4.4.3 Sensitivity Analysis

To perform a sensitivity analysis to certain epidemiological, pharmacological, evolutionary parts of our model, a comprehensive set of simulations was done in order to vary the transmission setting, biting rate heterogeneity, treatment coverage, the relationship between drug concentration and mutation, drug half-life, and the fitness cost of resistance. The ranging values of the parameters are described below.

First we varied the transmission setting by varying the transmission coefficient β (four different values) as well as the coefficient of variation in the biting rate (two different values). The equilibrium behaviors of these eight scenarios are described below. In these test scenarios, we assume that 50% of clinical cases are treated with a drug of 80% efficacy and a 7-day half-life.

Transmission Coefficient (β)	Coefficient of Variation in Biting Rate	Prevalence at Equilibrium	Annual EIR at Equilibrium
0.50	2.0	18.7%	18.0
0.50	1.0	23.1%	20.3
0.25	2.0	9.17%	6.20
0.25	1.0	9.20%	5.43
0.20	2.0	6.56%	4.07
0.20	1.0	4.88%	2.36
0.14	2.0	2.70%	1.33
0.14	1.0	0.01%	<0.01

Table 4.1. Varying transmission intensity in sensitivity analysis.

Because the last scenario in the table above resulted in frequent extinction, this transmission setting was not used in the sensitivity analysis. Only the first seven transmission settings were used. Note that in the simulations, a different EIR will be observed as ACTs are used in our simulated scenarios and the equilibrium prevalence and EIR are lower than in the table reported above. The table above can be thought of as the "pre-ACT era" transmission setting.

The treatment coverage was varied across the five values $f = 0.5$, 0.6, 0.7, 0.8, and 0.9. It is important to remember that 80% coverage or 90% coverage are very high estimates for many malaria-endemic countries. In part, these high-coverage scenarios are being run to compare strategies in the hypothetical situation that coverage and access improve over the next decade.

The cost of resistance was varied across the three values $c_R = 0.001$, 0.005, and 0.010.

To vary the effect of the drug concentration in the probability of drug-resistance evolution we varied the parameter k (see "Drug Resistance Evolution" heading in Section 3.1). Three values are used, $k = 0.5$, 2.0, and 4.0.

The drug half-lives were varied to test four different scenarios: (a) all three partner drugs have a half-life of 4.5 days, (b) all three partner drugs have a half-life of 9 days, (c) all three partner drugs have a half-life of 28 days, (d) the three partner drugs have three different half-lives of 4.5 days (corresponding to lumefantrine), 9 days (corresponding to amodiaquine), and 28 days (corresponding to piperaquine).

In each of the above scenarios, it was assumed that three ACTs were available, and three strategies were evaluated: MFT, 5-Year Cycling, and Sequential Deployment.

Thus, a total of 3780 scenarios are simulated. This requires approximately 4-5 days of computation time on a modern 70-core computer cluster. A total of five complete sensitivity analyses were run (18,900 simulations), and the results are summarized below.

Excluding extinctions, MFT was associated with the lowest NTF values in 86.2% of simulations; extinctions were also more common under MFT. The median reduction in treatment failures achieved by MFT was 10.6% (IQR: 2.9% - 20.0%; $p < 10^{-12}$) when compared to a 5-year cycling strategy and 9.6% (IQR: 3.0% - 18.6%; $p < 10^{-11}$) when compared to a strategy of sequential deployment.

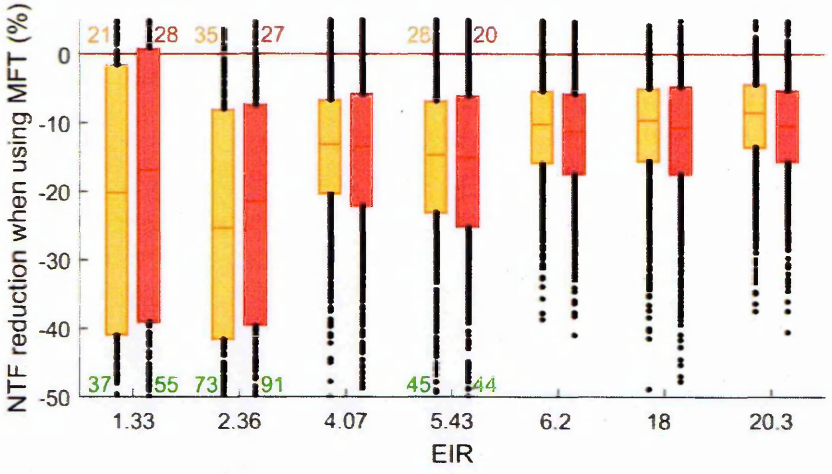

Figure 4.7. This boxplot shows the percent reduction in NTF achieved by using an MFT policy, when compared to sequential deployment (orange) and five-year cycling (red), across all parameter combinations in the sensitivity analysis. The boxes show interquartile ranges, stratified by different transmission intensities. For each parameter combination in the comparison, only scenarios with no extinction (NTF>0.25) are included in the calculation of interquartile ranges. The numbers at the top and bottom of each boxplot show the number of comparisons for which one strategy caused extinction but the comparator strategy did not. The green numbers indicate the number of simulations for which MFT resulted in extinction but the cycling/sequential strategy did not, while the red and orange numbers show the number of simulations when the cycling (red) or sequential (orange) strategies reached extinction but MFT did not. There are fewer extinction under EIR=4.07 than EIR=5.43, because the former is associated with a higher coefficient of variation in the mosquito biting rate. Across the different transmission settings and counting all simulations (including those that did and did not lead to extinction) NTF numbers are lower for MFT than other strategies (all $p < .002$; Mann-Whitney).

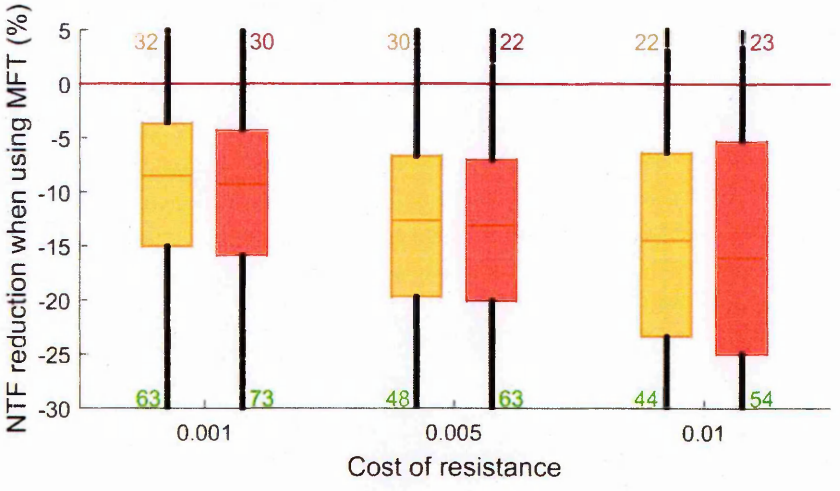

Figure 4.8. This boxplot shows the percent reduction in NTF achieved by using an MFT policy, when compared to sequential deployment (orange) and five-year cycling (red), across all parameter combinations in the sensitivity analysis. The boxes show interquartile ranges, stratified by different costs of resistance. For each parameter combination in the comparison, only scenarios with no extinction (NTF>0.25) are included in the calculation of interquartile ranges. The numbers at the top and bottom of each boxplot show the number of comparisons for which one strategy caused extinction but the comparator strategy did not. The green numbers indicate the number of simulations for which MFT resulted in extinction but the cycling/sequential strategy did not, while the red and orange numbers show the number of simulations when the cycling (red) or sequential (orange) strategies reached extinction but MFT did not. For the three different costs of resistance, and using all simulations (including those that did and did not lead to extinction), NTF numbers are lower for MFT than other strategies (all $p < 10\text{-}6$; Mann-Whitney).

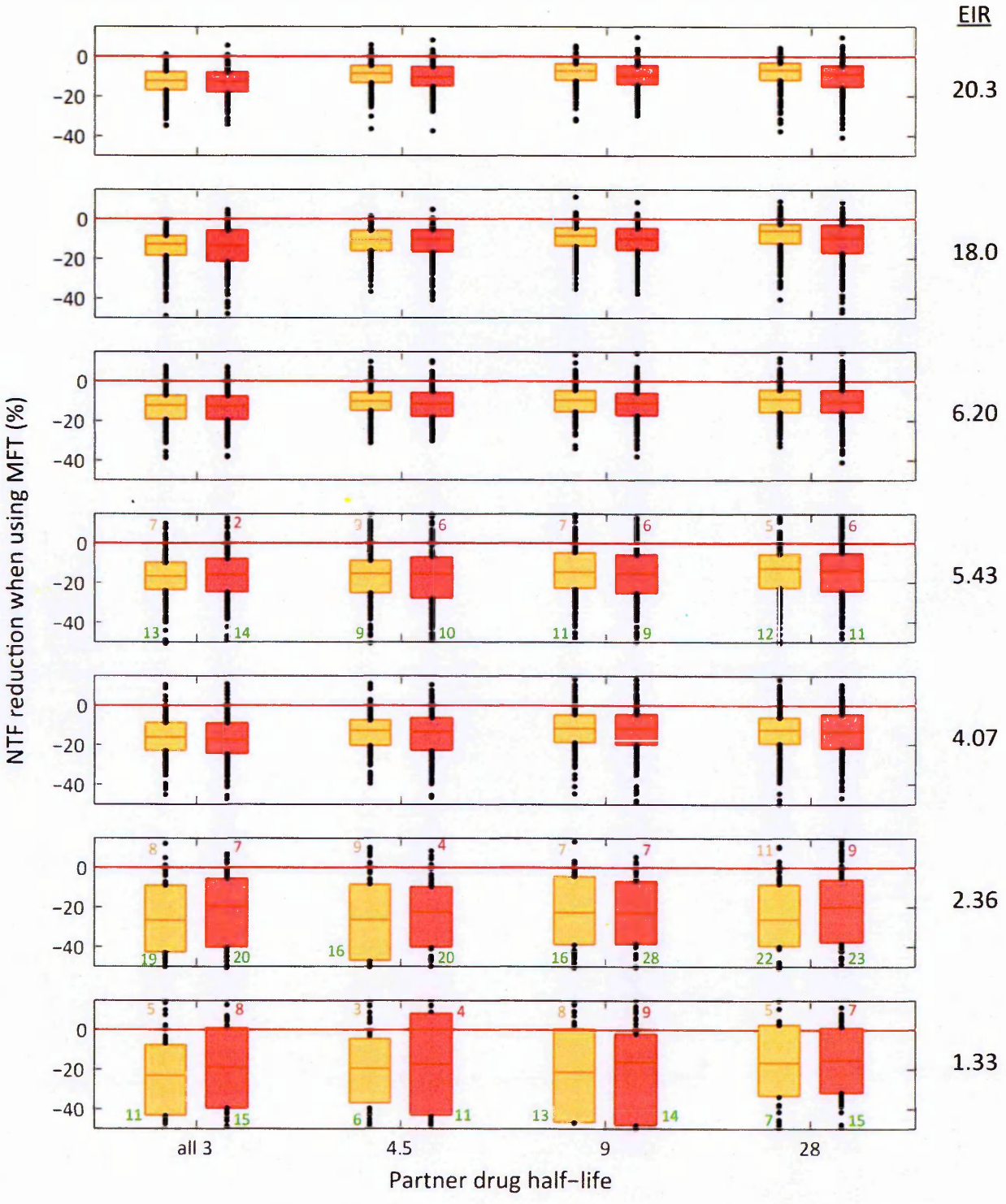

Figure 4.9. As Figure 4.7 and Figure 4.8, stratified by EIR and partner drug half-life. For the higher transmission scenarios (top five rows), NTF numbers are lower for MFT than other strategies ($p < 10^{-4}$; Mann-Whitney, for each boxplot). For the bottom two rows, the main qualitative feature of these comparisons is the number of total extinctions in the simulations (approximately 50%) and not a comparison of medians or ranks. MFT caused more extinctions than Cycling or Sequential Deployment in all of these comparisons; for simulations that did not result in extinction the NTF values for MFT were lower ($p < .002$; Mann-Whitney, for each boxplot).

4.4.4 Comparison to Results in Antao-Hastings (2012)

In a 2012 paper in Malaria Journal, Antao and Hastings [66] performed comparisons between MFT and Sequential Deployment strategies. For certain parameter combinations ($0.4 \leq f \leq 0.6$; MOI = 2 or 4; $c_R = 0.10$), they observed that MFT strategies resulted in a quicker time to the 10%-treatment-failure milestone and were thus associated with shorter useful therapeutic lives (UTL).

In this section, we attempt to recreate the conditions that led to these outcomes in the Antao-Hastings analysis. However, several important caveats need to be stated and some differences between the models need to be underlined. The differences between the model constructions are substantial, and the comparison presented in this section is approximate.

(a) The Antao-Hastings model (called ogaraK) does not explicitly model a population of humans. It only tracks gene frequencies of malaria parasites (as in a traditional population genetics framework). Therefore, some key aspects of malaria epidemiology are missing in this model and are not able to be compared to our model. For example, malaria prevalence cannot be tracked in ogaraK, and as resistance evolves in ogaraK it is not known if prevalence increases or by how much; hence, we cannot compare a prevalence trajectory from our model and the Antao-Hastings model. Likewise, ogaraK does not track clinical/symptomatic cases, age-structure of malaria cases, or MOI distribution, so these general epidemiological measures of malaria cannot be compared.

(b) UTLs can be compared between the two models, but NTF values cannot be compared, as a purely population-genetic model cannot track the total number of treatment failures in a single model simulation. We will present the NTF and UTL comparisons from our model below, but it is important to remember that the total number of treatment failures is the more appropriate health outcome measure for policy comparison, as this represents the number of individuals that will receive a failing/ineffective therapy during a fixed time period (in our model, 20 years).

(c) OgaraK uses a fixed "generation time" of approximately 50 days, meaning that the model assumes that it takes about 50 days for one malaria infection to generate a second malaria infection. The generation time in our model is variable and dependent on symptoms, age, parasitaemia, biting rate, and current prevalence. The relationship between prevalence and generation time is especially important because at low prevalence the generation time will be longer, resulting in slower evolution in general; at high prevalence, mosquito bites are more common and the generation time is shorter, resulting in a faster process of positive selection or negative selection if either of these is occurring.

(d) OgaraK fixes its MOI distribution. The MOI distribution in our model is dependent on prevalence. At high prevalence, individuals get bitten more often by infectious mosquitoes and the number of clonal parasite populations carried by each individual will generally be higher. The ogaraK simulations were run with MOI set to either 2 or 4 for all individuals. Because we cannot calibrate our model so that each host has exactly 2 or 4 clonal parasite populations, we chose prevalence levels where the mean MOI was equal to 2 or 4.

(e) There are other model differences that will affect the results. Our simulation has a model of immunity, within-host parasitaemia, immunity-mediated symptoms, immunity-mediated parasitaemia, and a transmission cycle that depends on parasite density levels, pharmacokinetics, pharmacodynamics, and biting rate heterogeneity. All of these features will affect the epidemiology and evolution in the simulation to some degree.

First, we attempted to calibrate the transmission setting in our model to mimic the MOI levels in the Antao-Hastings paper. We used these two transmission settings:

Transmission Coefficient (β)	**Coefficient of Variation in Biting Rate**	**Prevalence at Equilibrium**	**Annual EIR at Equilibrium**	**Mean of MOI distribution**
1.50	2.0	44.0%	94	2.12
8.00	2.0	83.8%	791	4.01

Table 4.2. Transmission settings used to compare with Antao-Hasting model.

However, after running these at $f = 0.6$ and $c_R = 0.10$, we could not compare results because, in our model, a 60% coverage and a 10% cost of resistance do not generate sufficient selection pressure for rapid resistance evolution (note that both our model and the Antao-Hastings model use a multiplicative fitness model for cost of resistance in multi-drug resistant genotypes). Very little resistance evolution was seen in about 500 model runs, and the useful therapeutic lives of both strategies (MFT and Sequential) were equal to 20 years for a 20-year model simulation. This was not a consequence of the mutation rate or of the introduction/non-introduction of resistant mutants at the beginning of the simulation (we tested both hypotheses). This was simply a consequence of the resistant types experiencing a weak selective environment, which resulted in very slow resistance evolution.

Therefore, we set the cost of resistance to $c_R = 0.025$ in the MOI = 2 scenario, and we set the cost of resistance to $c_R = 0.010$ in the MOI = 4 scenario, in order to get resistance evolution times that were close to those seen in Figures 1 and 3 of the Antao-Hastings paper. Below we present the comparisons between an MFT strategy and a Sequential Deployment strategy under these conditions. For sequential deployment, normally the drugs are deployed as AL first, then AS-AQ, then DHA-PPQ, so that shorter half-life ACTs are used first to minimize drug pressure. For these comparisons, we also tested the inverse order ("Seq Depl Inv"), as the UTLs were quite long in most cases and using the long-half life drug first sometimes minimized prevalence and NTF.

For MOI = 2, the comparisons between MFT and Sequential Deployment were:

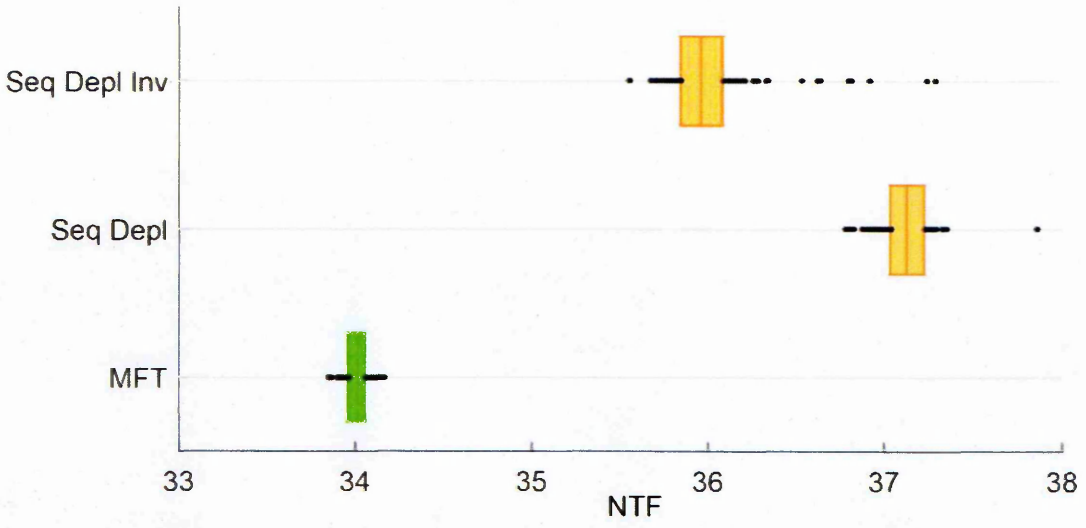

Figure 4.10. Comparison of MFT and Sequential Deployment (one hundred simulations for each strategy) under the Antao-Hastings scenario of MOI = 2. Cost of resistance in this figure is $c_R = 0.025$. Treatment coverage is $f = 0.6$. Drug-resistance mutations are more likely at intermediate concentrations ($k = 4$). All $p < 10^{-15}$ when comparing MFT to other strategies.

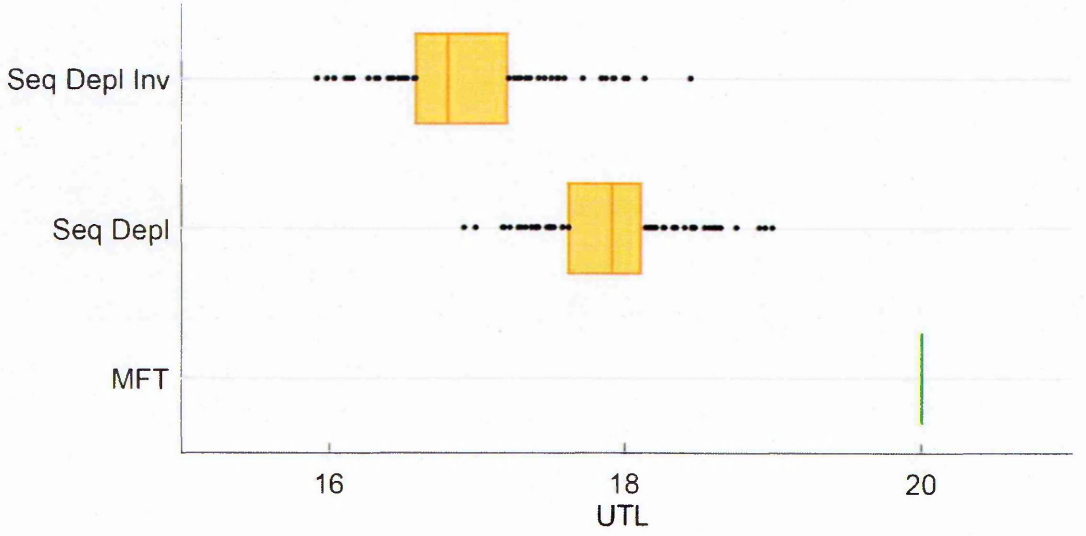

Figure 4.11. Useful therapeutic lives (UTLs) of drug strategies from Figure 4.10. All $p < 10^{-15}$ when comparing MFT to other strategies.

For MOI = 4, the comparisons between MFT and Sequential Deployment were:

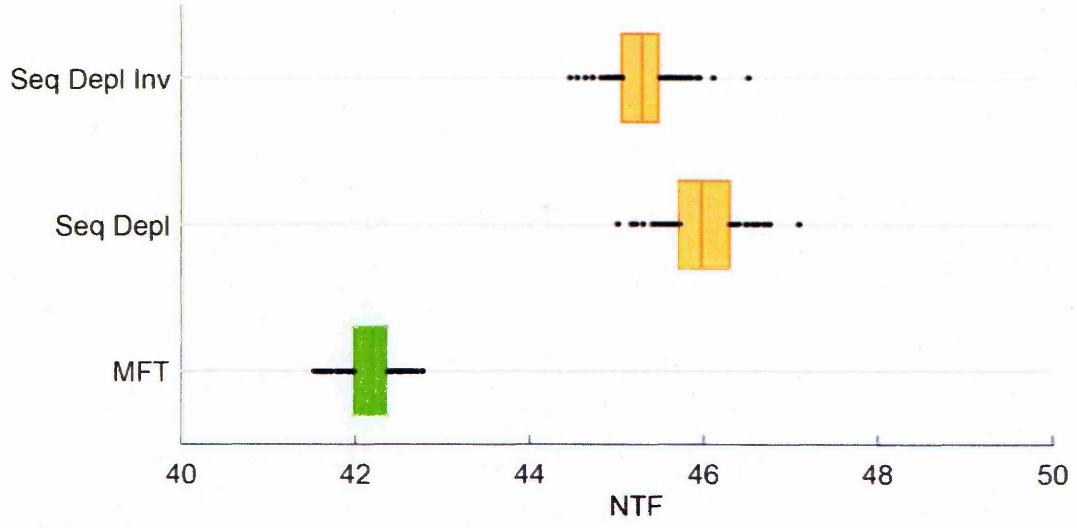

Figure 4.12. Comparison of MFT and Sequential Deployment (one hundred simulations for each strategy) under the Antao-Hastings scenario of MOI = 4. Cost of resistance in this figure is cR = 0.010. Treatment coverage is f = 0.6. Drug-resistance mutations are more likely at intermediate concentrations (k = 4). All p < 10-15 when comparing MFT to other strategies.

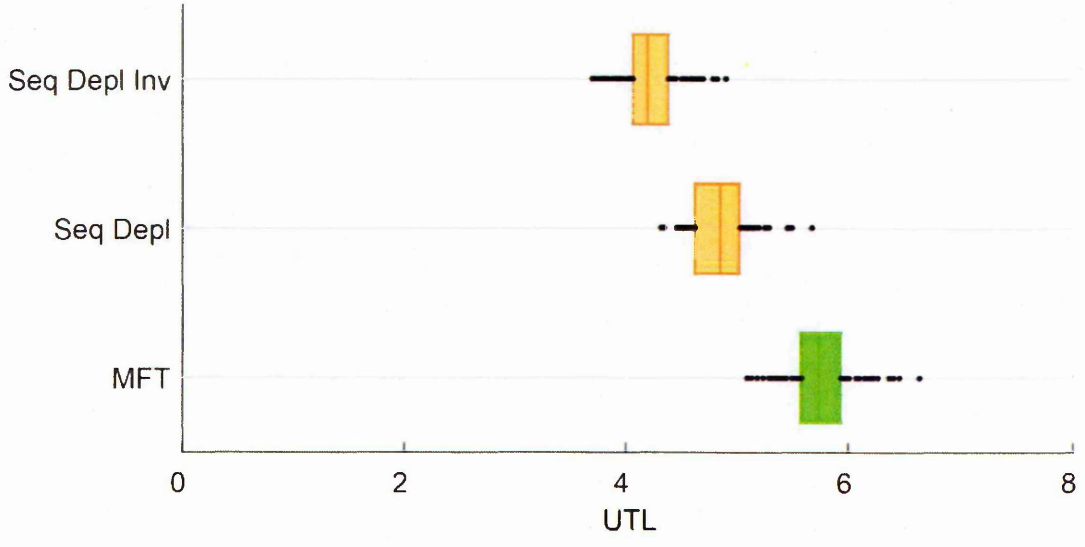

Figure 4.13. Useful therapeutic lives (UTLs) of drug strategies from Figure 4.12. All $p < 10^{-15}$ when comparing MFT to other strategies. Drug resistance evolution occurs more quickly in this scenarios than for MOI = 2 because the costs of resistance are different for the two figures. No resistance evolution was observed in the MOI = 4 scenario when $c_R = 0.025$.

4.4.5 Age-targeting Distribution

We investigated the possibility of targeting different age groups with different ACTs. We found no simple method of optimizing either of these strategies. A specific challenge with an age-based treatment strategy is the changing age-profile of symptomatic infections as transmission intensity decreases over time. Previous studies[52,77,190] have described selection pressure for drug resistance increasing with lower transmission. However, our age-structured model shows that this effect has a strong interaction with age, with younger age groups exerting less selective pressure as transmission falls and older age groups exerting more selection pressure as transmission falls (Figure 3.7 and Figure 3.8).

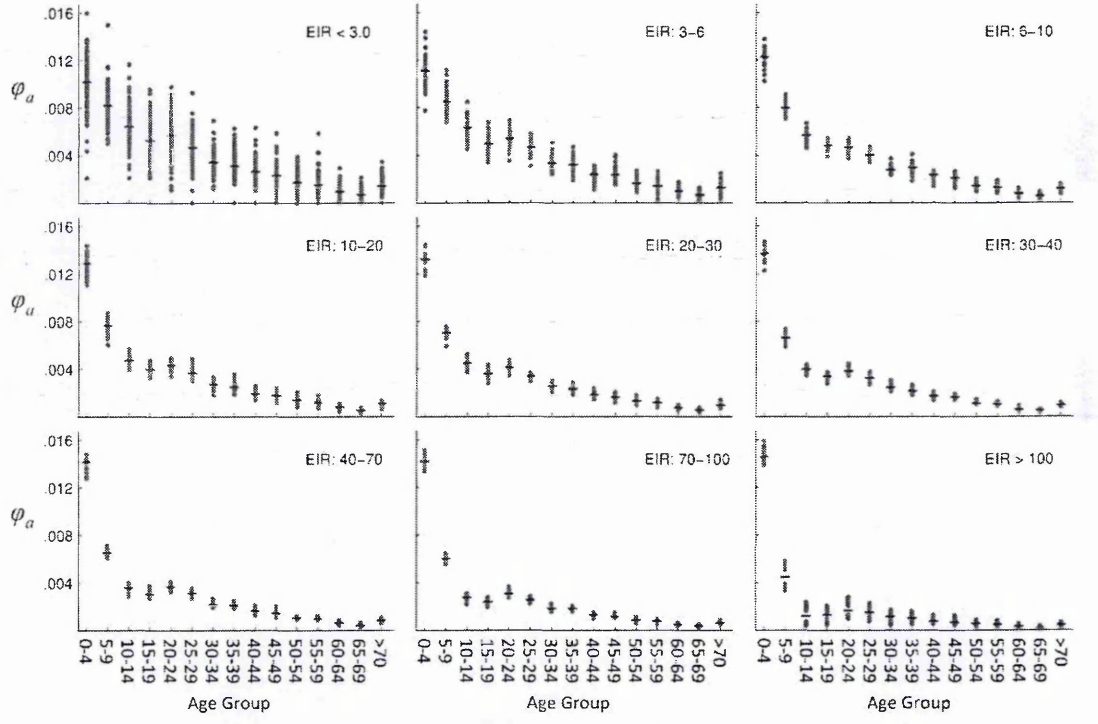

Figure 4.14. Age-specific relationship between EIR and the fraction of infected hosts that are symptomatic. The gray dots in the figure show what fraction φ_a of all malaria infections are symptomatic infections in a specific age group (red lines are medians). Assuming that infections are treated equally among age groups, the quantity φ_a is a proxy for the evolutionary pressure placed on malaria parasites via treatment of symptomatic cases. For example, when EIR is between 10 and 20, a median of 1.3% of all malaria infections will occur as symptomatic cases in 0-4 year-olds. In adults, φ_a decreases with EIR because immunity in adults increases with EIR increasing the likelihood of asymptomatic infections. In children aged 0 to 4, φ_a increases with EIR because and frequent biting, frequent clinical episodes, and none or low acquired immunity. Simulations were run with treatment coverage f=0.5. The fraction φ of all symptomatic cases among all cases decreases from 5.8% when EIR < 3.0 to 3.0% for EIR > 100.

4.4.6 Varying the Parameter *K* Which Describes the Relationship between Drug Concentration and Mutation Probability

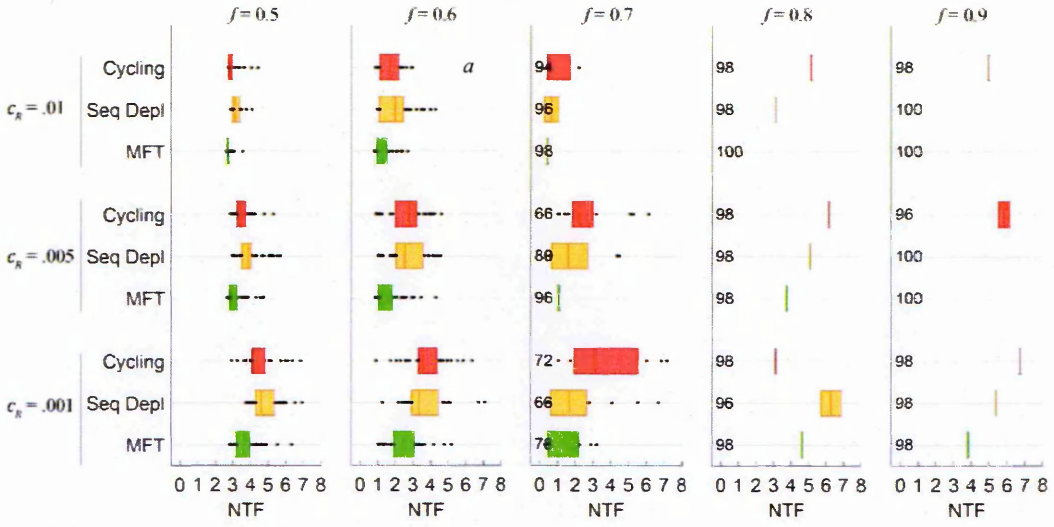

Figure 4.15. As Figure 4.3, but with k = 0.5; i.e. the probability of a drug-resistance mutation is proportional to drug concentration. Fifty simulations are shown for each strategy, drug coverage (f), and cost of resistance (c_R) combination. NTF values exhibited a bimodal distribution corresponding to simulation runs that did or did not result in extinction. Box plots show NTF interquartile ranges for simulations with no extinctions. The numbers on the left-hand side of each plot show the percentage of simulations that resulted in extinction. Mutations accumulate more slowly for k=0.5 (this figure) than for k=4.0 (Figure 4.3), and for this reason extinction is more likely for k=0.5 when treatment coverage is very high. For f = 0.5 and f = 0.6, NTF values were lower under MFT (p=0.02; except for comparison *a*).

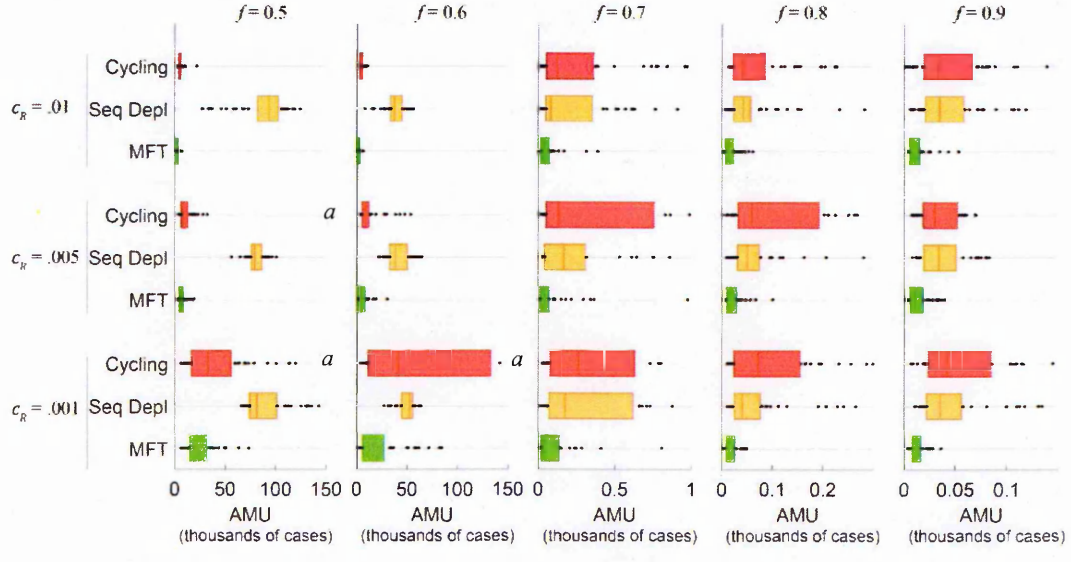

Figure 4.16. As Figure 4.5, but with k = 0.5; i.e. the probability of a drug-resistance mutation is proportional to drug concentration. Fifty simulations are shown for each strategy, drug coverage (f), and cost of resistance (c_R) combination. AMU values did not exhibit a bimodal distribution, and interquartile AMU ranges are shown as boxplots for all fifty simulations. For $f \geq 0.7$, AMU values were lower under MFT ($p < 0.003$). For $f \leq 0.6$, AMU values were lower under MFT ($p < 0.01$, except for those labeled *a*); note that in these three cases it was only the 25th percentiles were not statistically different.

4.4.7 Varying the Transmission Setting

Under different transmission settings, ranging from moderate to high, the results from Figure 4.17 and Figure 4.18 show that MFT strategies are associated with lower number of treatment failures compare to other cycling strategies.

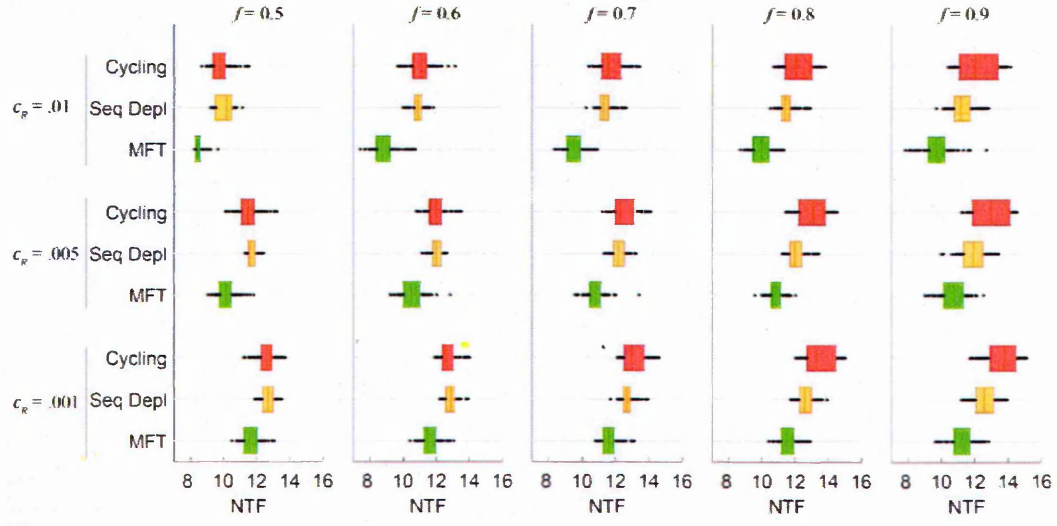

Figure 4.17. As Figure 4.3 but in a moderate transmission setting corresponding to the fifth scenario listed in the Table 4.1. Annual EIR is 4.07. All $p < 10^{-10}$ when comparing MFT to other strategies. Each boxplot corresponds to 100 simulations.

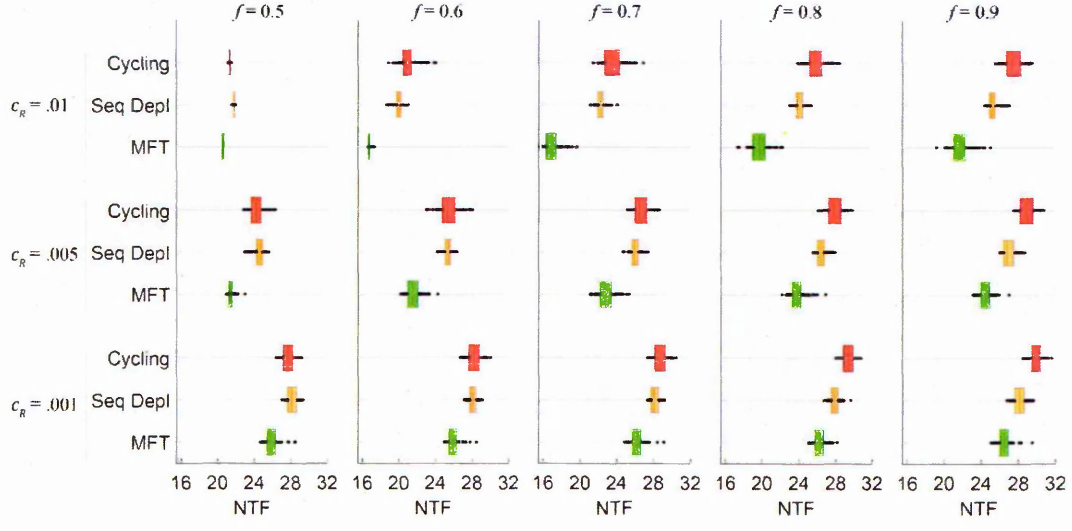

Figure 4.18. As Figure 4.3 of the main text but in a high transmission setting corresponding to the first scenario listed in Table 4.1. Annual EIR is 18.0. All $p < 10^{-11}$ when comparing MFT to other strategies. Each boxplot corresponds to 100 simulations.

4.4.8 Changing Distribution Based On Drug Half-Life

We also experimented changing usage frequencies for ACTs according to the partner drug half-life. The results show that adjusting the distribution strategy according to half-life also had no noticeable effect on long-term treatment outcomes (Figure 4.19 and Figure 4.20).

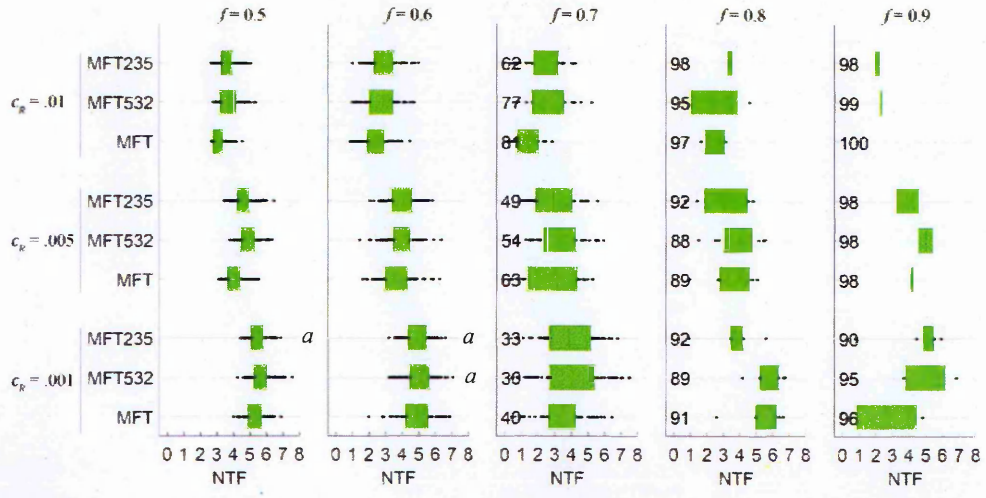

Figure 4.19. As Figure 4.3, but two new strategies are added: MFT235 and MFT532. In MFT235 the proportion of patients that are treated with AL, ASAQ, and DHA-PPQ are 20%, 30%, and 50%, respectively. In MFT532 the proportion of patients that are treated with AL, ASAQ, and DHA-PPQ are 50%, 30%, and 20%, respectively. These simulations were run in a low-transmission scenario, and it does not appear that altering the distribution of therapies according to half-life has a consistent effect on patterns of resistance evolution. One hundred simulations are shown for each scenario. For $f = 0.5$ and $f = 0.6$, MFT has a lower NTF distribution ($p < .004$, except for the comparisons labeled *a*), but the magnitudes of the differences are small. For $f \geq 0.7$, the number of extinctions is quite high and a statistical comparison of NTF ranges is not done. Mutation rate is highest at intermediate drug concentrations ($k = 4$).

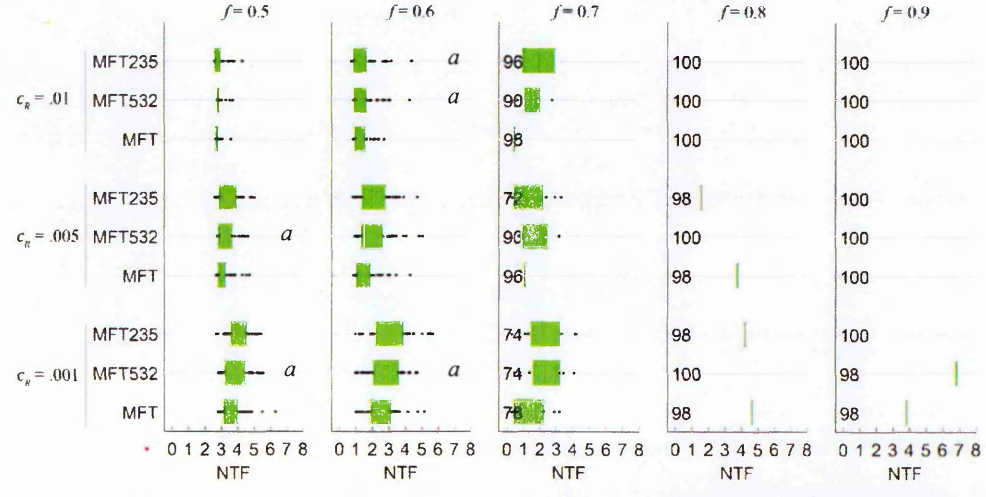

Figure 4.20. As Figure 4.19, but the mutation rate is proportional to drug concentration ($k = 0.5$). Fifty simulations are shown for each scenario, but note the small number of simulations plotted for $f \geq 0.7$ as the majority of simulations in these scenarios reached extinction. For f = 0.5 and f = 0.6, MFT has a lower NTF distribution ($p < .01$, except for the comparisons labeled *a*), but the magnitudes of the differences are small.

4.4.9 Variation in the Surveillance Window That Determines The 10% Treatment Threshold

Normally, we simulate a sequential deployment strategy by assuming that the treatment failure rate is computed by analyzing the successful and failing treatments over the past 60 days ("ws60"). Here, we look at the differences if the past 120 days ("ws120") or past 180 ("ws180") days are used.

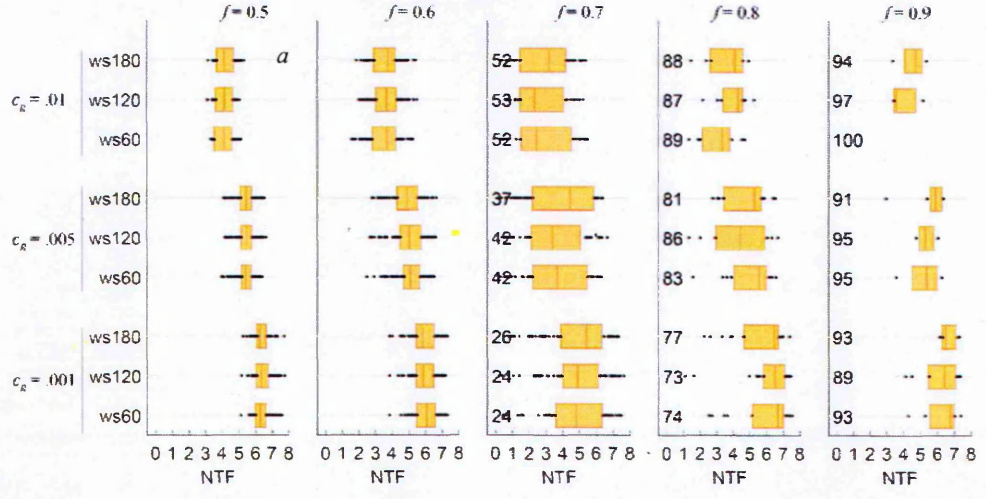

Figure 4.21. Epidemiological scenario from Figure 4.3. Sensitivity analysis for the sequential deployment strategy aimed at investigating if the method of computing the 10% treatment-failure threshold will have a large effect on the strategy's long-term outcomes. Here, we look at the differences if the past 120 days or past 180 days are used. For $0.5 \leq f \leq 0.7$, there are no statistical differences when "ws60" is compared to either "ws120" or "ws180" (all $p \geq 0.05$) except for the comparison (*a*) where the 25th quantiles of these distributions are statistically different at $p = 0.022$. For $f \geq 0.8$, the majority of these simulations resulted in extinction (numbers plotted to the left hand side of these panels) and statistical comparison among these distributions is not meaningful. Each boxplot corresponds to 100 model simulations.

4.4.10 Robustness of the Biting Model

Here, the frequency with which a host is bitten by mosquitoes is associated with weight in kilograms. This relationship is motivated by the findings of Port et al [116] and the analysis presented in Smith et al [90]. Weight is taken to be directly proportional to likelihood of biting and age-for-weight measures are taken from WHO [191]. Figure 4.22 shows the comparisons between strategies when applied the age-weighted biting probability.

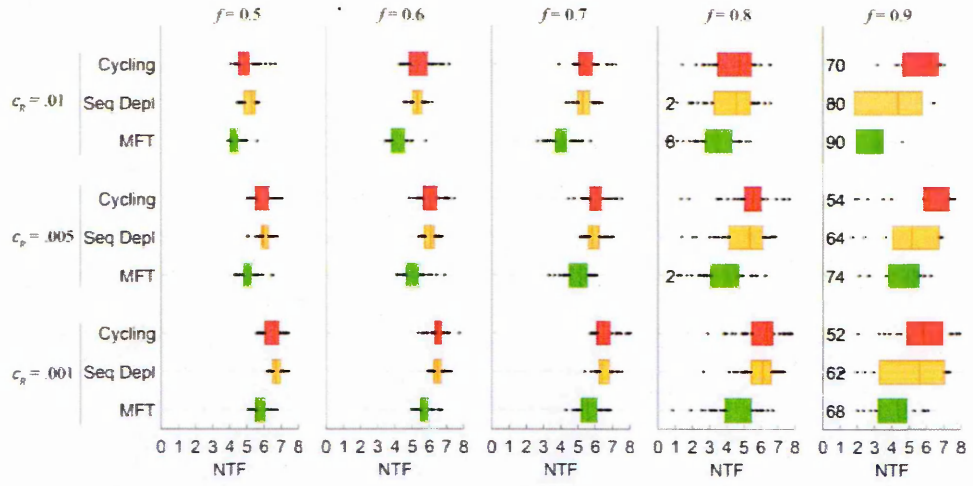

Figure 4.22. Epidemiological scenario from Figure 4.3. Each boxplot corresponds to 50 simulations, and for $f \leq 0.8$ all $p < 10^{-3}$ when comparing MFT to other strategies except (*a*) and (*b*) where the 25th percentiles of these 'Seq Depl' NTF-distributions are not statistically different from MFT. For $f = 0.9$, statistical comparisons among interquartile ranges were not done as the majority behavior in these simulations was extinction.

Here, the probability of an infectious bite causing an infection is proportional to a host's relative level of immunity (which normally depends on age). The data in Hoffman et al [35] suggest that there may be a five-fold or six-fold difference in this probability between children and adults (not accounting for size, weight, or immunity), and in the comparisons presented in the figure 4.23 we let this infection probability vary from 0.04 to 0.16 according to Prob = 0.04 + 0.12×(1 – ImmuneLevel). The moderate transmission scenario from Figure 4.17 was chosen for this comparison so that there would be more variation in host immunity in the population.

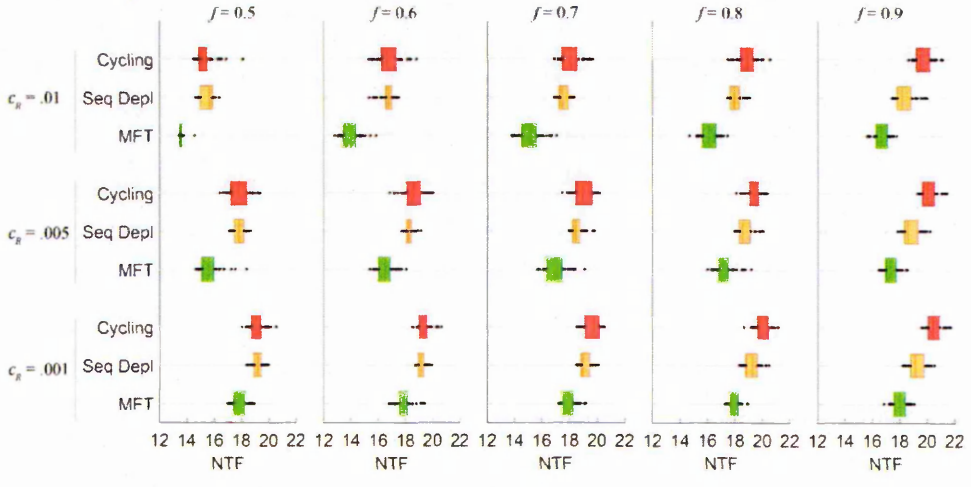

Figure 4.23. Epidemiological scenario from Figure 4.17. Each boxplot corresponds to 50 simulations, and all $p < 10^{-5}$ when comparing MFT to other strategies.

4.4.11 Smaller Population Size

As can be seen from Figure 4.24, reducing population size to 500,000 does not have any unexpected effects on the benefit of MFT to other cycling strategies.

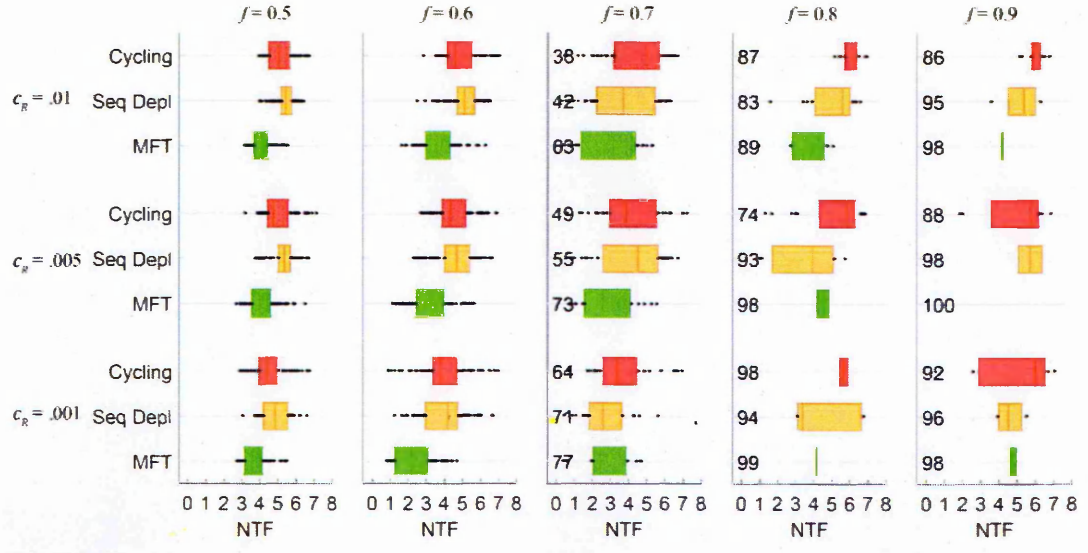

Figure 4.24. As Figure 4.3 (with cost of resistance fixed at $c_R = 0.005$), and population size is varied here to see if there are any unexpected effects at small population size. The major observed effect is more frequent extinctions observed at small population sizes, which is expected. Each boxplot corresponds to 100 simulations, and the numbers at the left of each panel show what percentage of those simulations reached extinction. For $f = 0.5$ and $f = 0.6$, all $p < 10^{-6}$ when comparing MFT to other strategies. For $f \geq 0.7$ the predominant behavior is extinction, and in all cases MFT is associated with more frequent extinction events than either cycling strategy.

4.5 Conclusions

The main conclusions reached in this chapter were that the deployment of multiple first-line artemisinin combination therapies has better population-level outcomes than cycling ACTs through the population one by one. An MFT strategy is associated with delayed resistance emergence, slower resistance evolution, and as a result, a smaller number of negative outcomes for patients which in this chapter are described as "treatment failures." This result has proven to be robust to a variety of epidemiological, pharamacological, and entomological scenarios, and it is also robust to model structure as past analyses on antimalarial drug resistance and antibiotic resistance have come to the same conclusion. It seems that recommending the deployment of MFT at the level of national malaria control programs would be beneficial both for those counties and their neighbours. However, implementation challenges loom around the

corner. In Chapter 7, I discuss the urgency of a global malaria policy aimed at stemming the spread of artemisinin resistance, the future challenges of MFT implementation, and certain model caveats that should keep us on guard for situations where model-based predictions may not be in line with real epidemiological scenarios,

Chapter 5

Introducing New Biological Features

In general, developing a mathematical model, especially an individual-based model, involves a trade-off between simplicity and realism (or accuracy) of the model. Occam's razor principle is often used as a heuristic technique to develop theoretical models; it states that we should prefer a simpler model over a complex one when those models have similar predictive power [192]. In other words, adding complexity can improve the realism of a model, however, it can make the model more difficult to understand and analyze, especially for model-fitting and validation. Furthermore, increasing the complexity can also pose new computational problems. In contrast, Thomas Kuhn argued that during scientific progression, scientists tend to enlarge the central paradigm by adding more complexity to their explanations before a paradigm shift offers a radical simplification or a new theory [193]. I would not be bold enough to say that we are near a paradigm shift for malaria epidemiology, but in modifying my individual-based simulation I will consider each additional change carefully, looking both at its potential to improve the model's realism and to improve our understanding of malaria.

With these two principles in mind, the version of the model in Chapter 2 (version 3.0.2, as it will be called when it is released on GitHub in August 2015) has balance in the complexity by simplifying components of the model to a certain level in order to maintain not only the computational performance but biological meaning in analysis. For instance, the resistant genotype representation is modelled as just a single value for each resistance locus (sensitive or resistant), and we do not explicitly keep track of gametocyteamia but instead use a formula describing the relationship between asexual parasite density and gametocyteamia.

As the analysis moves forward, in order to evaluate MFT strategies in many more complex situations, new biological features will be required and implemented. Based on the fact that drug resistance can be associated with multiple alleles at different loci [76,194] and different alleles

at a single locus can be associates with different degrees of resistance [13,195], , a new genotype presentation is introduced in this chapter to fulfill this requirement (Section 5.1). In addition, each genotype will be associated with a particular drug EC50 that allows partial resistance in the model (Section 5.2).

Not all antimalarial drugs are gametocytocidal, and patients are observed to be gametocyte carriers for up to 28 days after radical cure with an ACT [196,197]. Hence, some modifications in the infectivity function and the asexual parasite density value at which parasites are considered "removed" from the individual are introduced (Section 5.3).

Finally, in this new model version I also allow for variation in the initial clinical parasite density (previously set to 10^{11} parasites per individual) as it is known that different individuals exhibit different parasite burdens at peak parasitaemia (Section 5.4).

5.1 New Genotype Representation

Instead of using bit strings to represent genotypes, an integer vector is used to express the genome structure of a parasite. Each position in the vector represents one locus and a particular integer value codes for a specific allele. The ancestral allele (i.e. the drug-sensitive allele) is coded with value 0.

Examples of genotypes with 3 loci, where each locus has 3 different alleles (values 0, 1, and 2 are shown below, but any positive integer value is possible):

- Ancestral sensitive genotype: [0,0,0]
- Single mutation at 1 locus: [0,0,1], [0,1,0], [1,0,0]
- Multiple mutations at 1 locus: [0,0,2], [0,2,0], [2,0,0]
- Multiple mutations at multiple loci: [0,1,1], [0,2,1], [0,2,2], ...

To implement the resistance evolution feature, two new classes Allele and Locus are created to store all necessary information and their class diagrams are shown in the Figure 5.1. This flexible allele class will allow us to model multiple copies of the *pdmdr1* gene without requiring

an explicit representation of the genome. Each Locus object stores all predefined alleles in an allele vector, their positions in the genotype expression and the cost of resistance.

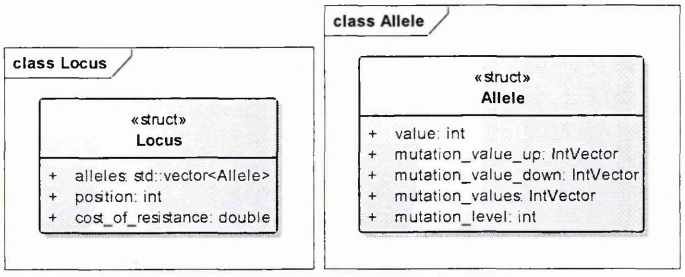

Figure 5.1. Class diagrams of Allele and Locus class.

The evolution pathway of an allele is stored in an integer vector and these numbers represent the new values that a particular allele can mutate to. The mutations only occur under drug pressure, and the mutation is allowed to occur when it reduces drug efficacy. The implementation of the mutation process is described in Figure 5.2.

```
For each mono drug i that is circulating in an individual
    If mutation under drug i pressure occurs
        Mutation_locus <- select randomly locus from affecting loci of drug i;
        New_mutation_allele <-select randomly new mutation allele (both up and down)
        If drug i has lower efficacy to the new genotype
            Allow mutation by replacing the old genotype by the new genotype
        Else
            Discard mutation
        End if
    End if
End for
```

Figure 5.2. Pseudo code describes the drug resistance mutation process

The value stored in the mutation level of an allele object determines how far that allele is to the ancestral allele, i.e. 0 means ancestral, or 2 means 2 mutations away; this value is also used to calculate the cost of resistance for a particular genotype (Figure 5.3).

```
relative_fitness_multiple_infection_ = 1;
for (int i = 0; i < number of loci in gene expression; i++) {
   relative_fitness_multiple_infection_ *= (1 - de novo cost_of_resistance of locus i) ^
                                           mutation_level of allele at position i;
}
```

Figure 5.3. Pseudo code to calculate the cost of resistance for a genotype

Total number of genotypes that can be used in the simulation is calculated by the equation 20.

$$\prod_{i=1}^{n} number\ of\ alleles\ at\ locus\ i \tag{20}$$

A database of all genotypes is generated at the beginning of the simulation, and each generated genotype is assigned its own ID. During the ID assignment, the genotype string is generated according to the following pseudocode:

```
int temp = id;
for (int i = 0; i < number of loci; i++) {
    allele at locus i = temp div weight[i];
    temp = temp mod weight[i];
}
```

Figure 5.4. Pseudo code to generate genotype string from a given ID.

The weight vector is calculated from the equation 21.

$$weight_i = \begin{cases} 1, & i = n \\ \prod_{j=i+1}^{n} number\ of\ available\ alleles\ at\ locus\ j, & i < n \end{cases} \tag{21}$$

where n is the number of predefined loci in the simulation.

In reverse, to get an ID of a particular gene string, equation 22 is used.

$$ID = \sum_{i=1}^{n} weight_i \times allele_i \tag{22}$$

5.2 Partial Resistance

In the previous version of the model (Chapter 3), the drug had no efficacy on a resistant parasite type. To implement the partial resistance feature in this new version, each genotype is associated with an EC50 for each drug used in the simulation. By adjusting the EC50, the efficacy of a drug to a specific parasite strain can vary between 0% and 100%.

An EC50 matrix is used to define the relationship between a genotype and EC50 of a single drug. Each row of the matrix represents one genotype and the row number is the ID of the genotype. The columns of the matrix represent single drugs that are used in the model and the column number is the id of the drug.

An example of an EC50 matrix with three mono drugs is shown in the Table 5.1.

Genotype ID	Drug1 EC50 (efficacy)	Drug2 EC50 (efficacy)	Drug3 EC50 (efficacy)
0 - [0,0,0]	0.65 (80%)	0.65 (80%)	0.65 (80%)
1 - [0,0,1]	0.65 (80%)	0.65 (80%)	1.3 (30%)
2 - [0,1,0]	0.65 (80%)	1.3 (30%)	0.65 (80%)
3 - [0,1,1]	0.65 (80%)	1.3 (30%)	1.3 (30%)
4 - [1,0,0]	1.3 (30%)	0.65 (80%)	0.65 (80%)
5 - [1,0,1]	1.3 (30%)	0.65 (80%)	1.3 (30%)
6 - [1,1,0]	1.3 (30%)	1.3 (30%)	0.65 (80%)
7 - [1,1,1]	1.3 (30%)	1.3 (30%)	1.3 (30%)

Table 5.1. Example of EC50 matrix for 3 mono drugs (with 7 days half-life), the mutation position is associated with the drug ID, i.e. mutation at locus 1 cause resistance to drug 1, and each locus have 2 alleles (naïve is 0 and mutation is 1).

5.3 Change in Infectivity Function and *parasite_zero_level* to 100 Total Parasites (2 x 10^{-5}/µl)

In the previous model version, the infectivity to mosquito of an individual was calculated based on the current asexual parasite density using the formula in Ross et.al. [91] (described in Section 3.2). When the parasite density declines, the infectivity to mosquitoes will also decrease; however, when the parasite is cleared by a successful treatment, the infectivity is immediately set to zero. In the new version, after the parasite density drops to zero, the infectivity to mosquitoes will remain stable at a very low level (1%) for a couple of weeks (14 days) before dropping down to zero. The rationale for this is that the proportion of gametocyte carriers at day 28, after radical cure, was observed to range from 0.3% to 3% [197]. It is impossible to compare these numbers directly as the former describes successful transmission to mosquitoes, but the latter describes the observation of gametocytes on blood slides.

To fulfill these requirements, two adjustments have been made. Firstly, the infectivity curve is shifted up by 1%, so that the minimum infectivity at all time during an infection is 1%. Secondly, the parasite density level at which the parasite will be cleared from blood is set to 100 total parasites (or $2x10^{-5}$ parasites/μl). Figure 5.5 shows the change in infectivity of an individual from the previous version to the current version. These changes are very small, but they are made to improve the realism of the model.

5.4 Variation in Maximum Parasitaemia

For each individual who progresses to symptoms, the model will now assign a random parasite density level drawn from a uniform distribution (logscale) between 2,000 to 200,000 parasites/μl (i.e. the actual draw is from $U[3.3, 5.3]$). This range was chosen to have the similar range with the initial parasite density of the recruited patients to clinical trials [198–200].

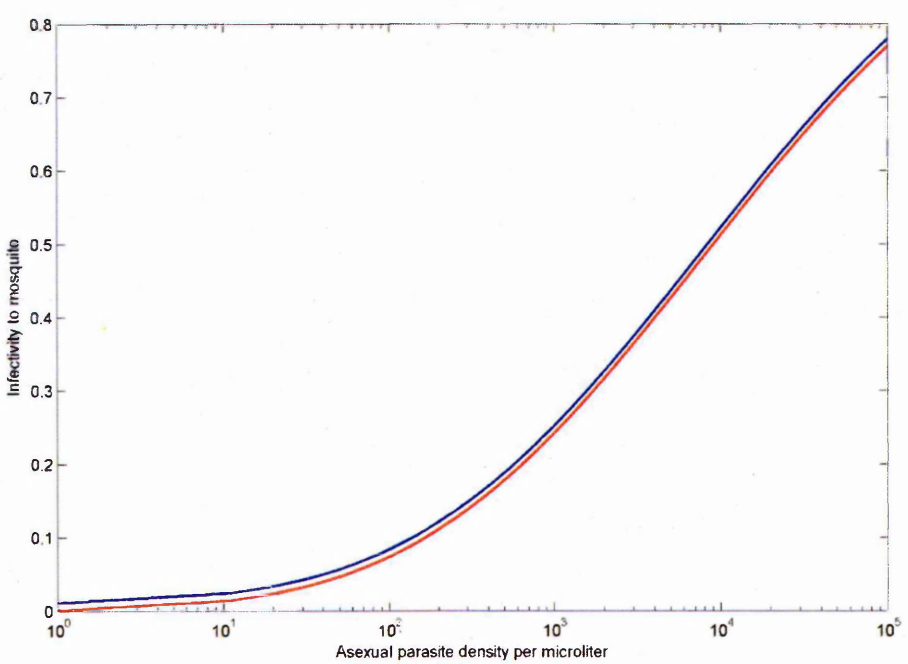

Figure 5.5. Change in infectivity function. Red line shows the curve for the old version and the blue one represents the curve for the new version.

5.5 Validation

A low transmission scenario is chosen to compare with the results from Chapter 4. Here we simulate with the same three ACTs used in the previous chapter, however with the new partial resistance feature, the cure rate of an ACT for patients with single resistant strain is around 75% (artemisinin resistance) or 80% (partner drug resistance). The efficacy wanes to 30% for a double-resistant parasite as shown in Table 5.2.

Genotype ID	ASMQ	AL	DHA-PPQ
0 - [0,0,0,0]	95%	95%	95%
1 - [0,0,0,1]	80%	95%	95%
2 - [0,0,1,0]	95%	80%	95%
3 - [0,0,1,1]	80%	80%	95%
4 - [0,1,0,0]	95%	95%	80%
5 - [0,1,0,1]	80%	95%	80%
6 - [0,1,1,0]	95%	80%	80%
7 - [0,1,1,1]	80%	80%	80%
8 – [1,0,0,0]	75%	75%	75%
9 – [1,0,0,1]	30%	75%	75%
10 – [1,0,1,0]	75%	30%	75%
11 – [1,0,1,1]	30%	30%	75%
12 – [1,1,0,0]	75%	75%	30%
13 – [1,1,0,1]	30%	75%	30%
14 – [1,1,1,0]	75%	30%	30%
15 – [1,1,1,1]	30%	30%	30%

Table 5.2. Efficacies of 3 ACTs on the different genotypes

Here, the MFT strategy still has a lower number treatment failures compared to other strategies. However, the MFT results have a lower effect compared to the previous model version; this was due to the effect of the partial resistance as drugs still have 30% efficacy when being used by patients infected with a double-resistant strain; thus drug resistance evolves more slowly for a single-drug strategy than was observed in chapter 4.

Figure 5.6 can be compared to Figure 4.1. The main difference between these two figures is that the 5-year cycling strategy shown in Figure 5.6 appears to be largely a successful strategy as opposed to the simulations shown in Figure 4.1, where both 5-year cycling and sequential deployment fare very poorly when compared to MFT. The reason for this difference is essentially that drug resistance is not as bad in the new model (v3.1, Chapters 5 and 6) as it was in the old model (v3.0.2, Chapters 3 and 4). In the new model, drug-resistant parasites still have a chance to be cleared by ACTs, and thus, even though the 5-year cycling strategy generates more drug resistance than the MFT strategy, the consequences (higher prevalence, more treatment failures) are minor as 75%-80% of the single-resistants and 30% of the double-resistants are still able to be cleared by the currently used therapies.

Due to the changes introduced in this chapter, the dynamics of the system have changed, and I did not notice the extent of these differences until after all of the simulations had run (a time-consuming process). For example, in the base scenario in Figure 4.1, the EIR is 1.4, but in Figure 5.6 the EIR is 1.7. When publishing these results, I will try to match the EIRs exactly so that the results can be comparable to the results published in my first paper in Lancet Global Health.

The sequential deployment strategy is the worst of the three in Figure 5.6; approximately 25% of simulations of sequential deployment reached prevalence levels above 4% by year 12. Remember that the sequential deployment strategy has a 1-year delay built in between policy changes, and it is likely that these accumulated delays over the first decade allowed drug resistance to establish. Again, however, note that MFT's relative advantage over sequential

deployment in this scenario is smaller than the advantage shown in Figure 4.1 where drug resistance is modeled as "100% fully resistant".

One key parameter that has not been discussed so far is the mutation rate. In treatment strategy modeling comparisons for drug-resistance management, if the mutation rate is set too low, all treatment strategies will appear to be equal as drug resistance will be very unlikely to emerge during each 20-year simulation run. Likewise, if the mutation rate is set too high, all strategies will appear equal as the multidrug resistance will appear very early in the simulation, and widespread multidrug resistance also ensures that the three strategies will be equal in the numbers of treatment failures that patients experience. Note in Figure 5.7 below – where the mutation rate is ten times higher than in Figure 5.6 to demonstrate this principle – drug resistance does emerge earlier in the 5-year cycling scenario and the final distribution of NTF values for 5-year cycling is noticeably lower than that observed under MFT.

Figure 5.8 shows comparisons among MFT, 5-year cycling, and sequential deployment, under the standard mutation rate used in Figure 5.6. Note that the principle described in Chapter 4 – namely that MFT creates the most variable environment, and thus the most difficult environment in which to evolve drug resistance – still holds. However, when the modeling assumes that drug resistance is partial, drug resistance will not always lead to treatment failure. Hence, when comparing the three strategies using a public-health measure like NTF, the relative advantage of MFT is smaller than that which we observed in Chapter 4. Essentially, drug resistance does not have the same detrimental public health outcomes in this scenario, and delaying drug resistance has a small public health benefit.

The analyses in Chapter 6 use this newer and more realistic version of my individual-based model. Chapter 6 will also show that there are additional parameters (compliance and the length of an ACT course) and additional types of strategies (e.g. multiple ACTs per patient) that need to be considered when trying to find best and most appropriate public health solution to antimalarial drug resistance.

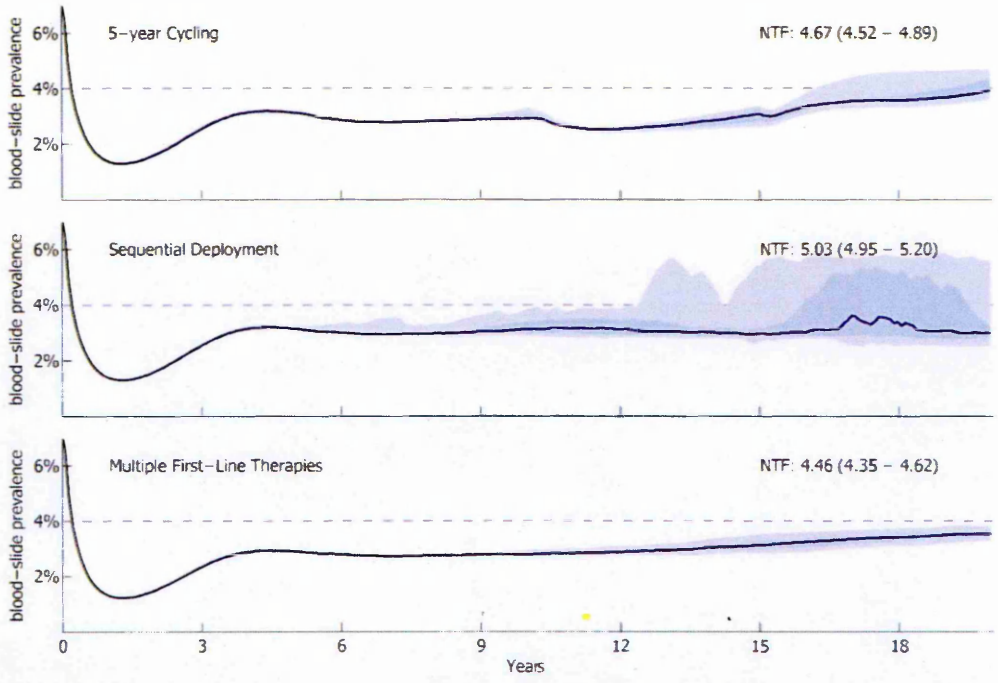

Figure 5.6. Expected paths of drug-resistance evolution and corresponding malaria prevalence under three different treatment regimes. 100 stochastic simulations were run in a population of one million individuals, in a low transmission setting (EIR around 1.7) with 60% treatment coverage and an assumed cost of resistance of 0.5% for all resistant genotypes. The mutation rate is assumed to be highest for intermediate drug concentrations. The black line shows the median prevalence across 100 simulations, and the violet areas show the interquartile and 90% ranges. The median number treatment failures (NTF) with interquartile ranges are shown in each panel. The dashed line shows 4% prevalence.

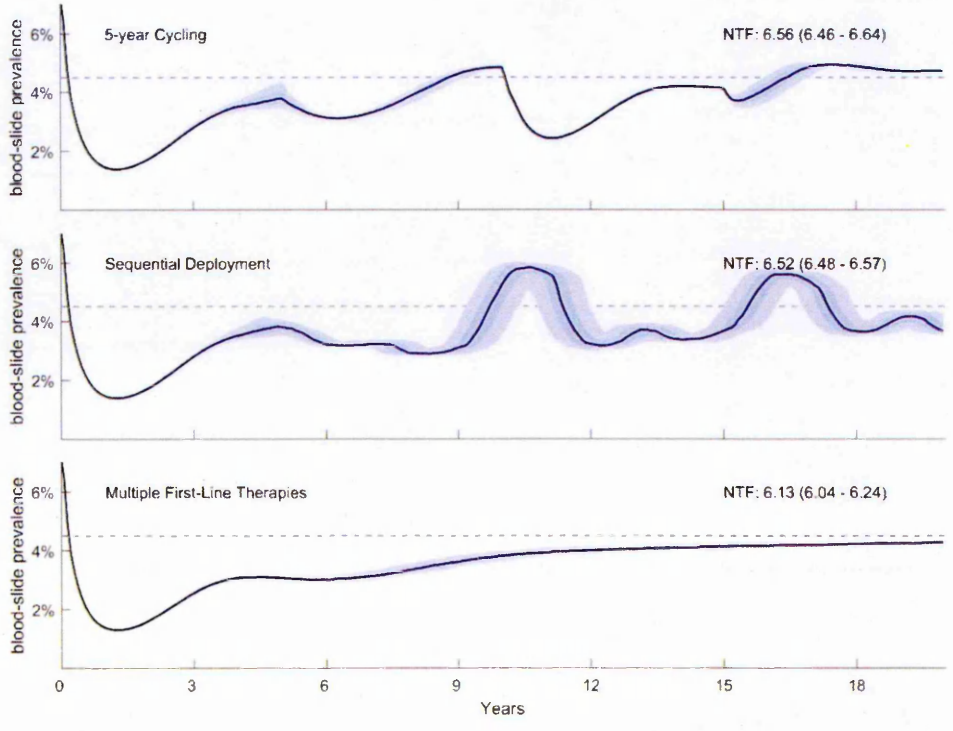

Figure 5.7. As Figure 5.6, but the mutation rate is ten times higher.

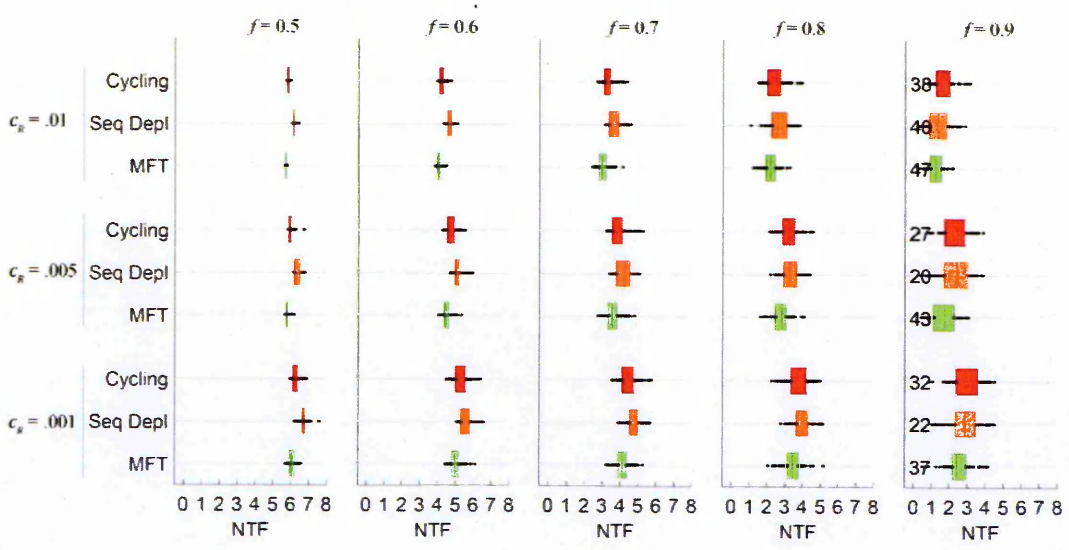

Figure 5.8. As Figure 4.3, but with new model features as described in this chapter.

Chapter 6

Comparison of Standard 3-Day Artemisinin Combination Therapies with Shorter and Longer Dosing Schedules

6.1 Introduction

Global malaria cases have declined by more than 40% over the past decade. This is because the improvements to health care access, wider distribution of ITNs, and the effectiveness of the artemisinin combination therapies (ACTs). However, artemisinin-resistant malaria has emerged on the Thai-Cambodian border and recently has spread as far as the border between Myanmar and India[175]. This situation reminds us of the previous emergence of resistance to chloroquine, sulfadoxine–pyrimethamine, and mefloquine all of which originated from South East Asia and spread globally. Artemisinin resistance is an extreme threat to the global health community's plans for malaria control and elimination since artemisinin is currently the most powerful antimalarial drug available, with other potential drugs still in various phases of development or clinical trials. When artemisinin resistance spreads to sub-Saharan Africa, the situation may turn quite severe as Africa has the highest malaria disease burden and less adequate systems for monitoring and containing resistance.

To contain artemisinin resistance, many strategies have been proposed. At the population level, deployment of multiple first-line therapies (MFT), as discussed in this thesis and in past publications, has offered a potential solution to tackle the problem of artemisinin resistance. However, the global health community is not close to implementing MFT in real–world epidemiological settings.

Another population-level strategy to combat artemisinin resistance and accelerate malaria elimination is mass drug administration (MDA). MDA trials have been initiated to test elimination strategies in the context of artemisinin resistance (i.e. in Southeast Asia). Although

an MDA strategy is believed to have a lot of promise, MDA implementation encounters significant challenges due to an inability to locate all residents of an area, refusal by individuals to be repeatedly treated with antimalarials, a lack of human resources in public health agencies to perform outreach and monitoring in an MDA strategy, and the obvious risk of malaria resurgence in the months after an MDA has been completed.

At the individual-level, one possible option to combat artemisinin-resistant parasites is to lengthen the course of ACT treatment. There are many reasons that lengthening the dose should be a good strategy. First of all, the prevalence of day-3 positives after ACT treatment is associated with novel mutations in the K13-propeller gene[19], and therefore lengthening the course of ACT therapy (for more than 3 days) should improve the efficacy of the treatment by allowing artemisinin continue to killing partially-resistant parasites for a longer period. Secondly, results from modelling, which are based on data from Pailin, Cambodia, show that the efficacy of ACTs has been reduced due to the significant reduction in the efficacy of artesunate on ring-stage parasites[201]. With a lengthening of the ACT course, artemisinin would be able to kill the resistant ring-state parasites when they develop into schizonts, thus improving efficacy.

This type of treatment strategy – a lengthened course of ACT – has been used at the Shoklo Malaria Research Unit on the Myanmar–Thailand border, to treat uncomplicated hyperparasitaemic patients in order to improve treatment efficacy, as patients there may be infected with artemisinin-resistant parasites. The patients receive seven days of treatment with high-dose artesunate (4mg/kg) on days 0 to 3, followed by an ACT (3 to 5 day course) starting on day 4; in addition, this treatment is combined with single dose of primaquine on day 0. The options for ACT here are 3 days AS-MQ, 5 days of DHA-PPQ, or 5 days of Coartem (AL).

From my experience in Chapter 4, the NTF comparisons between strategies show that small differences usually result in statistically significant results. Due to the volume of analyses

performed in this chapter, I do not perform statistical tests for the results in this chapter to avoid cluttering the diagrams and figure captions.

6.2 Rationale for lengthen dosing schedule

Although ACTs may achieve a cure rate of 95%, according to detection by microscopy on day 28, the true number of patients that are cleared of parasites is unknown. Since malaria clinical trials only perform PCR testing for participants who still have parasites detectable by microscopy on day 28, the microscopy-negative patients are not investigated further and it is unknown how many of these are PCR-positive for malaria parasites. Results from a study known as the "Targeted Malaria Elimination" (TME) study, currently being implemented in Southeast Asia, show that a blood-slide prevalence of about 1% corresponds to a PCR-positive prevalence of around 10-15% (unpublished data). These undetectable but parasite-positive patients may act as a source of re-infection in the community, and they may have a very detrimental role in malaria elimination campaigns. If we can lengthen dosing schedules, it would reduce the undetected malaria carriers and therefore reduce transmission and the spread of drug resistance.

Using the modified model as described in Chapter 5, I evaluated the efficacy of different course durations for ACTs in 10,000 simulated patients. Although the 3-day course has a high efficacy, between 95% and 97%, the percentage of patients who still carry parasites on day 3 (undetectable by microscopy, but present) was still high, between 20% and 30% in these model simulations. Figure 6.2 shows the effects of different course durations, ranging from one to six days, for Artemether-Lumefantrine. This figure was designed to show the distribution of parasite densities as a heat map (on a log scale) in 10,000 patients, so that we can visualize what percentage of patients are above certain critical parasite densities. The three orange bars in this plot demarcate the quartiles of the distribution, so that the central part of the distribution can be easily seen. As expected, 1-day and 2-day courses – representing situations in which patients fail to complete a course of ACT – result in high numbers of patients with PCR-detectable

parasitaemia on day 28. The top quartile of patients with 1-day or 2-day treatment courses had day-28 parasite levels above 7 parasites/microliter; even though some of these patients may meet the WHO definition of adequate clinical and parasitological response (due to lack of detection by microscopy) it is clear that this is a worrisome situation epidemiologically since it is very likely that these patients can continue transmitting. The same outcome is observed for dihydroartemisinin-piperaquine (DHA-PPQ) and artesunate-amodiaquine (ASAQ) in Figure 6.3 and Figure 6.4, where the top quartile of patients treated for 1 or 2 days will have parasitaemia levels above 6/μl on day 28.

Contrasting 1-day and 2-day treatment courses to 5-day and 6-day courses shows a large difference. For 5- and 6-day courses, for AL, ASAQ and DHA-PPQ, 98% of patients of patients have day-28 parasitaemias lower than 2/μl and 99% have day-28 parasitaemias lower than 45/μl. This suggests that, by any measure, the difference between a short course and a long course accounts for 23 or 24 percentage points in efficacy. In the next two sections I look at the individual and population-level effects of longer courses of artemisinin combination therapy.

Figure 6.1 shows the effect of lengthening the dosing schedule. Initial parasite density in hosts ranged from 2,000 to 200,000 parasites per microliter (chosen uniformly on a log10 scale). These graphs shows that while the efficacy of treatment only increases from 95% to around 99% (microscopy detection), the percentage of patients that are still carrying parasites at day 28 is reduced significantly from 40% to approximately 15% (PCR detection) as the number of dosing days increases from three to six.

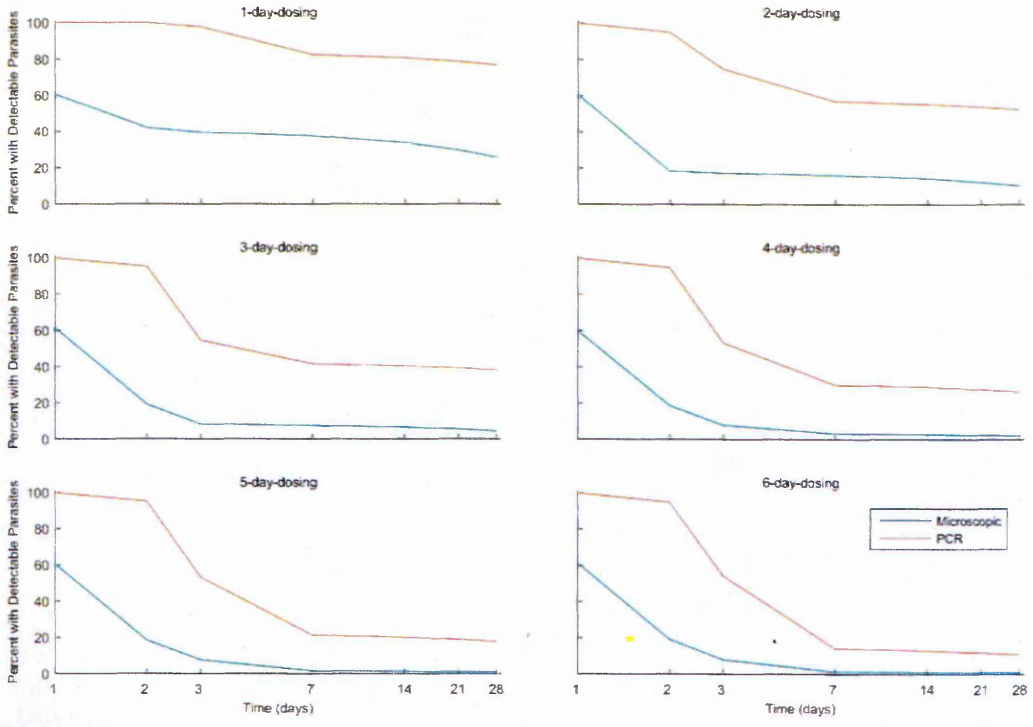

Figure 6.1. The effect of different dosing days on treatment efficacy as measured by microscopy and PCR. 10,000 clinical cases with different initial parasitaemia (ranging from 2000 to 200000 parasites per microliter) were treated with Artemether Lumefantrine.

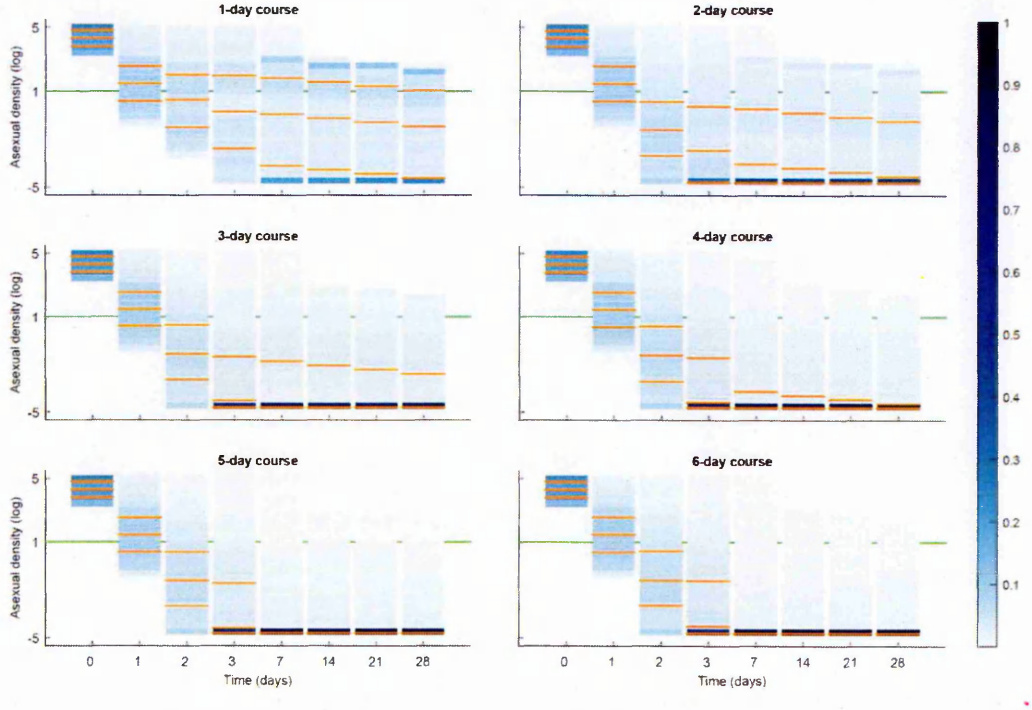

Figure 6.2. The asexual parasite density over 28 days when lengthening dosing from 1 to 6 days. The green line shows the detection level of microscopy. The intensity of the blue color represents the distribution of the individuals that carry a specific asexual parasite density. 10000 clinical cases with different initial parasitaemia (ranging from 2000 to 200000 parasite per microliter) were treated with Artemether Lumefantrine.

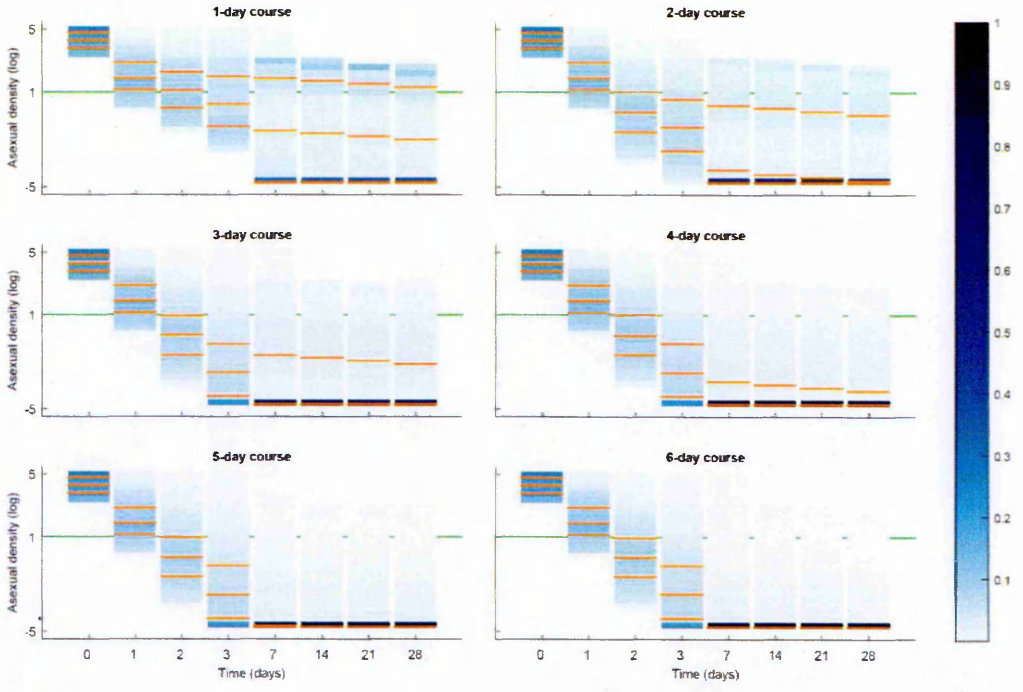

Figure 6.3. As Figure 6.2, but ASAQ is used instead of AL. Here ASAQ has less of an effect than AL at day 3 because we assumed AQ, with longer half-life, has a lower power killing rate than lumefantrine. This allows us to maintain the same efficacy of both DHA-AQ and AL (around 95% at day 28, 3-day dosing).

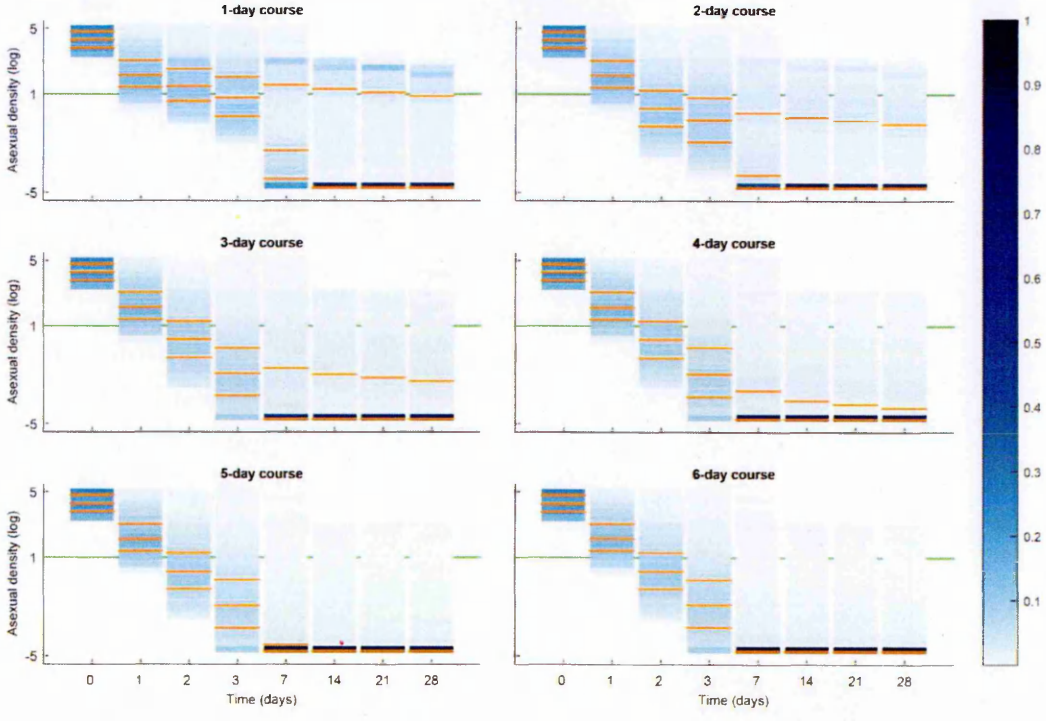

Figure 6.4. As Figure 6.2, but DHA-PPQ is used instead of AL. Here the DHA-PPQ has less of an effect than AL at day 3 because we assumed PPQ, with longer half-life, has a lower killing rate than lumefantrine. This allows us to maintain the same efficacy of both DHA-PPQ and AL (around 95% at day 28, 3-day dosing).

6.3 Results - Changing the Length of a Single ACT Course

6.3.1 Effect of Lengthen Dosing on Population-Level Treatment Strategies

In this section, I present the population-level results of changing the duration of a single course of ACT. In keeping with the framework and analyses presented in Chapter 4, I will evaluate the number of treatment failures (population wide) during a 20-year time span, and I will perform the comparisons for both cycling and MFT strategies. Initial comparisons are done in a low transmission setting with an EIR of approximately 1.7 at equilibrium when 50% of clinical cases are treated with a drug of 80% efficacy and a 7-day half-life.

Figure 6.5 shows the basic pattern of population-level changes as we vary the number of dosing days in an MFT strategy. As in other chapters, the quantity of interest here is the number of treatment failures (NTF) and a treatment failure is counted as such if on day 28 a patient still has microscopy-detectable parasitaemia. As in other chapters, a non-treatment is counted as a treatment failure. As expected, the number of treatment failures drops as the number of dosing days is increased. This is a straightforward result of the direct effect that a longer course has on reducing the probability that a patient still harbors high levels of parasitaemia after the treatment course is finished (as shown in Figure 6.2 to Figure 6.4). Note that the expected epidemiological indirect effect should also be observed here. That is, reducing the number of treatment failures reduces the amount of onward transmission, and this reduces the absolute numbers of cases and treatment failures in the future. For this reason, a larger absolute effect is seen at higher coverage ($f = 0.8, f = 0.9$), as we are close to the steep part of the R_0-prevalence curve in this scenario, and the indirect effects of reduced transmission are easier to see.

Similar effects are seen for Cycling and Sequential Deployment strategies (Figure 6.6 and Figure 6.7) assuring us that the dose lengthening has a population-level effect that is independent of the treatment strategies that were defined in Chapter 4. It is worth noting that longer courses are more likely to bring individual patients' parasite counts to zero, and thus are

more likely to end in malaria elimination in the model simulation. When looking at the high coverage scenario in which 90% of patients receive treatment, under all treatment scenarios, we see a potential doubling of the probability of extinction by increasing the length of an ACT course from the currently recommended 3 days to 5 or 6 days.

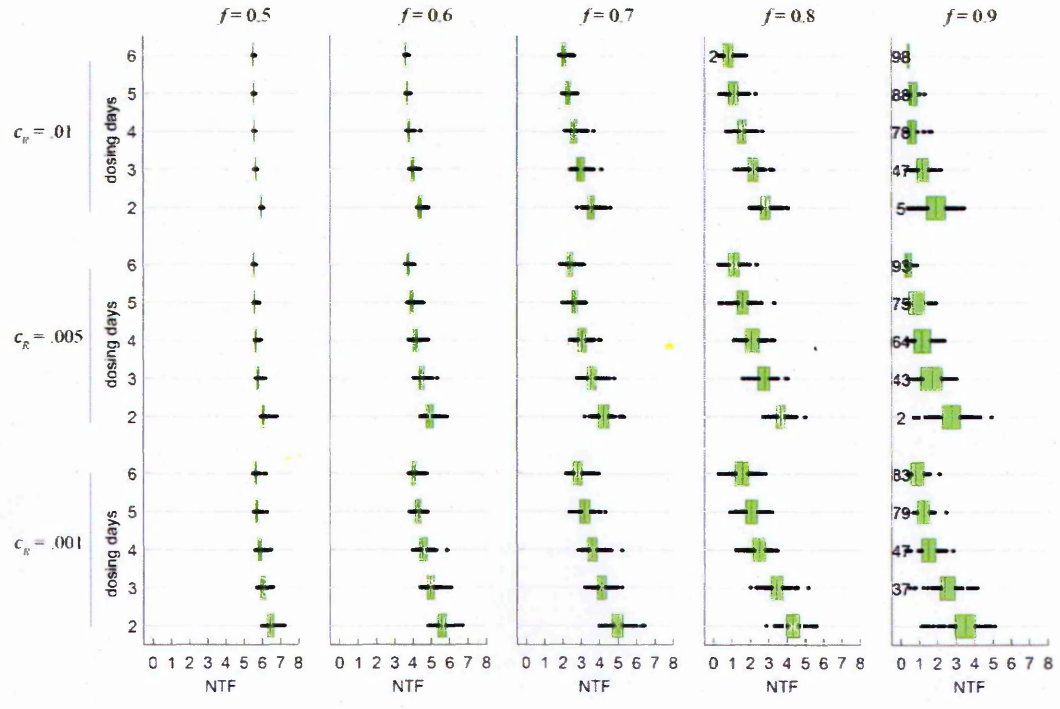

Figure 6.5. The effect of lengthen dosing days for MFT Strategy. The chart shows the NTF-values – the annual number of combined treatment failures and non-treatments, per 100 individuals – for different dosing days (ranging from 2 to 6-day dosing), different costs of resistance (c_R), and different treatment coverages (f). Each row shows the NTF results of 100 model simulations with the colored bars spanning the interquartile range. For $f \geq 0.9$, the NTF distributions had a bimodal shape with NTF < 0.5 corresponding to simulations that achieved extinction or near-extinction; the numbers on the left-hand side of each boxplot show the counts of these (near)-extinctions, and the interquartile ranges are plotted only for simulations that did not result in extinction. Simulations assume that three ACTs with 95% efficacy are available and that the three partner drugs have 4.5-day, 9-day, and 28-day half-lives (corresponding to lumefantrine, amodiaquine, and piperaquine, respectively). Population size is 1,000,000.

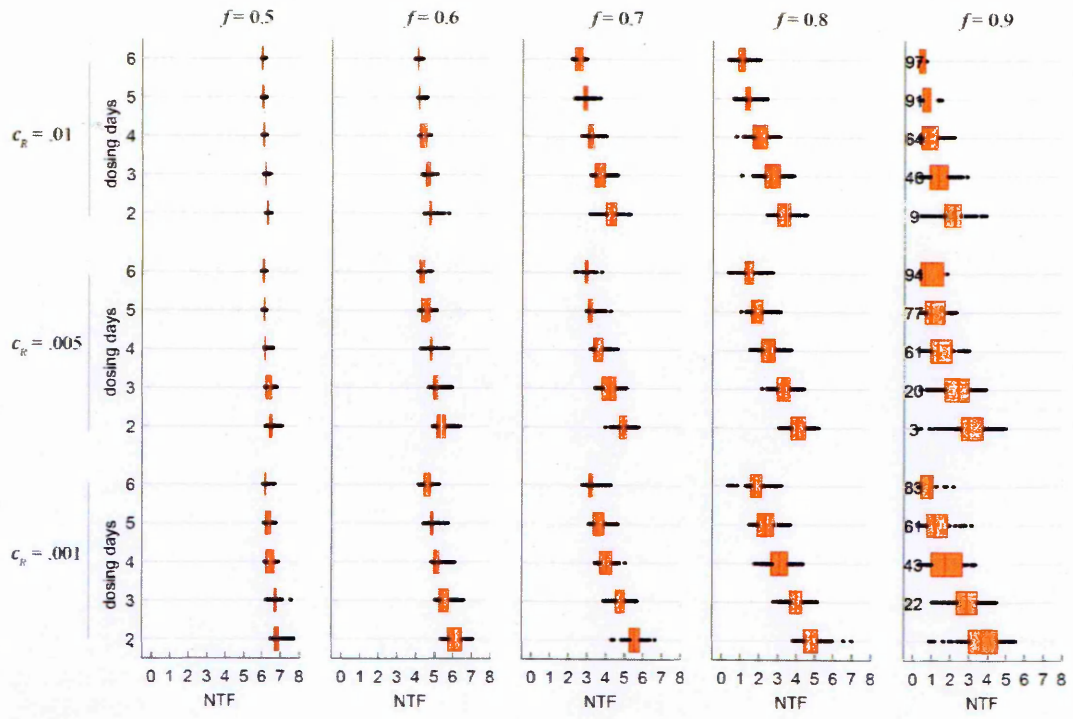

Figure 6.6. As Figure 6.5, the strategy is Sequential Deployment Strategy.

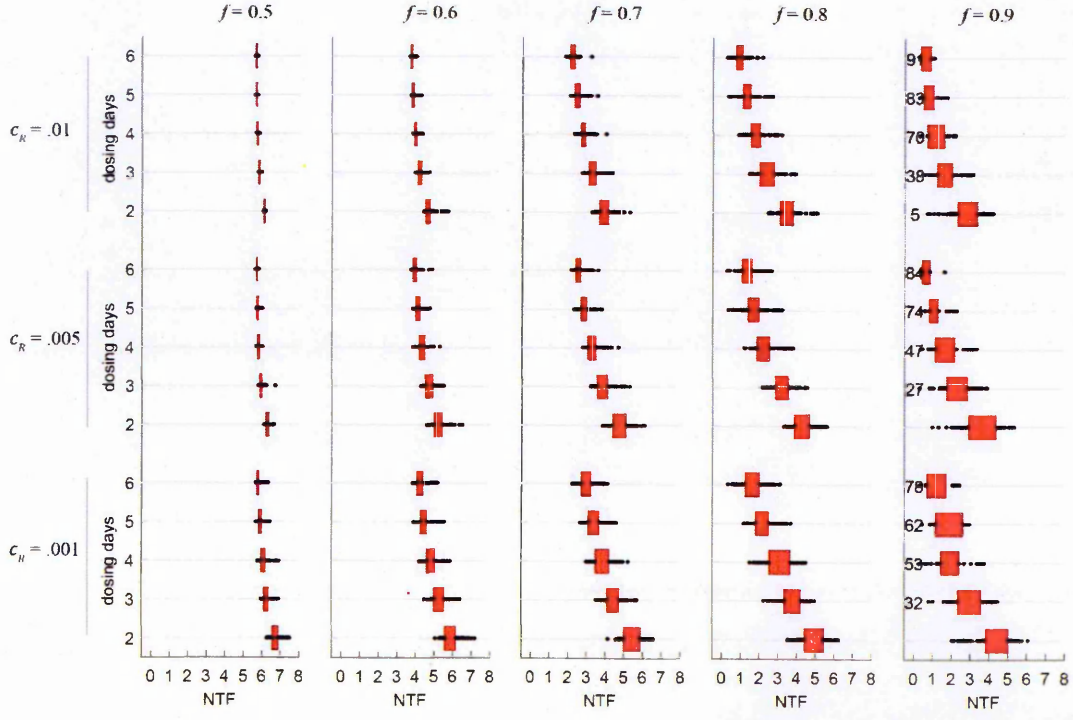

Figure 6.7. As Figure 6.5, the strategy is 5-year Cycling Strategy.

6.3.2 Comparing Different Treatment Strategies with Different ACT Course Durations

As an additional analysis, we would like to verify here that the length of an ACT course does not have an effect on the results of Chapter 4: that MFT is associated with fewer treatment failures in the long term than either cycling strategy. The results from Section 6.3.1are re-grouped by the number of dosing days to perform the comparison between MFT and other cycling strategies.

Figure 6.8 to Figure 6.12 show that under the same transmission and dosing setting, MFT strategies have the lowest number of treatment failures than other cycling strategies. When resistance does evolve ($0.5 \leq f \leq 0.9$ for 2-day dosing and $0.5 \leq f \leq 0.8$ for dosing longer than two days), MFT strategies have median NTF values that are between 2% and 23% lower than either sequential or cycling strategy. The one scenario that does not conform to this pattern is the 6-day dosing 80%–coverage scenario with a cost of resistance equal to 0.001; here, the simulations performed under MFT have a median NTF value that is 5% higher than the cycling strategy. The two distributions are very similar in this case ($p = 0.56$; Kolmogorov-Smirnov test), so this particular simulation set may simply be an aberration, given that the NTF of cycling strategies is usually higher than the NTF of MFT strategies. Finally, elimination was observed more often under MFT strategies as these strategies preserve full drug efficacy for longer than either cycling strategy.

In these simulations, the NTF-benefits of MFT over the two cycling strategies are lower than those presented in Chapter 4 where median NTF values of MFT were 16% to 40% lower than those for cycling strategies. This is likely due to the effect of the partial resistance feature that was introduced in Chapter 5. In the simulations presented in this chapter, ACTs still have up to 30% efficacy to the fully resistant strain, and between 75% and 80% efficacy for other resistant strains. This makes drug resistance evolve more slowly and it lessens the differences among the treatment strategies.

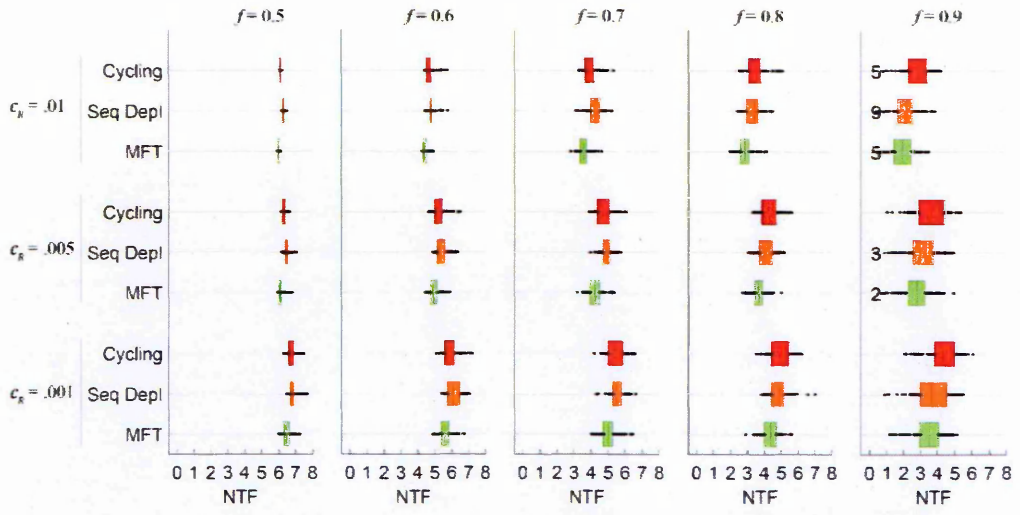

Figure 6.8. Comparisons of MFT, five-year cycling, and sequential deployment. The chart shows the NTF-values – the annual number of combined treatment failures and non-treatments, per 100 individuals – for different strategies, different costs of resistance (c_R), and different treatment coverages (f). Each row shows the NTF results of 100 model simulations with the colored bars spanning the interquartile range. For f = 0.9, the NTF distributions had a bimodal shape with NTF < 0.5 corresponding to simulations that achieved extinction or near-extinction; the numbers on the left-hand side of each boxplot show the counts of these (near)-extinctions, and the interquartile ranges are plotted only for simulations that did not result in extinction. Simulations assume that three ACTs with 95% efficacy are available and that the three partner drugs have 4.5-day, 9-day, and 28-day half-lives (corresponding to lumefantrine, amodiaquine, and piperaquine, respectively). Population size is 1,000,000 and all therapies are 2-day dossing.

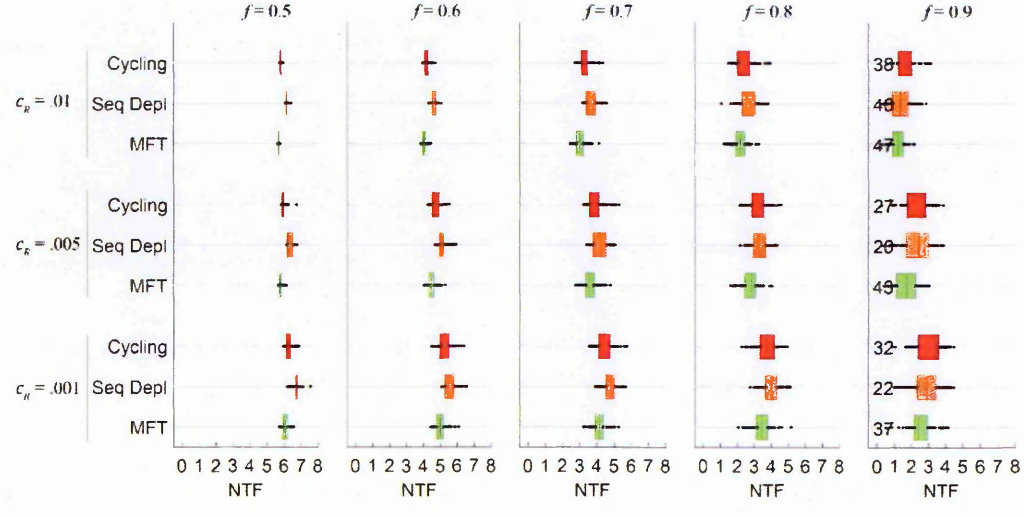

Figure 6.9. As Figure 6.8, all therapies are 3-day dosing.

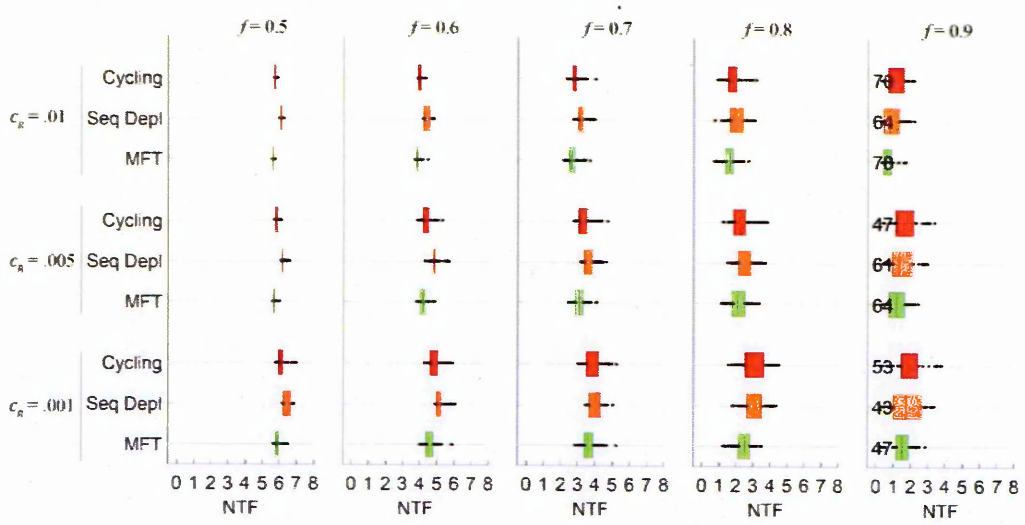

Figure 6.10. As Figure 6.8, all therapies are 4-day dosing.

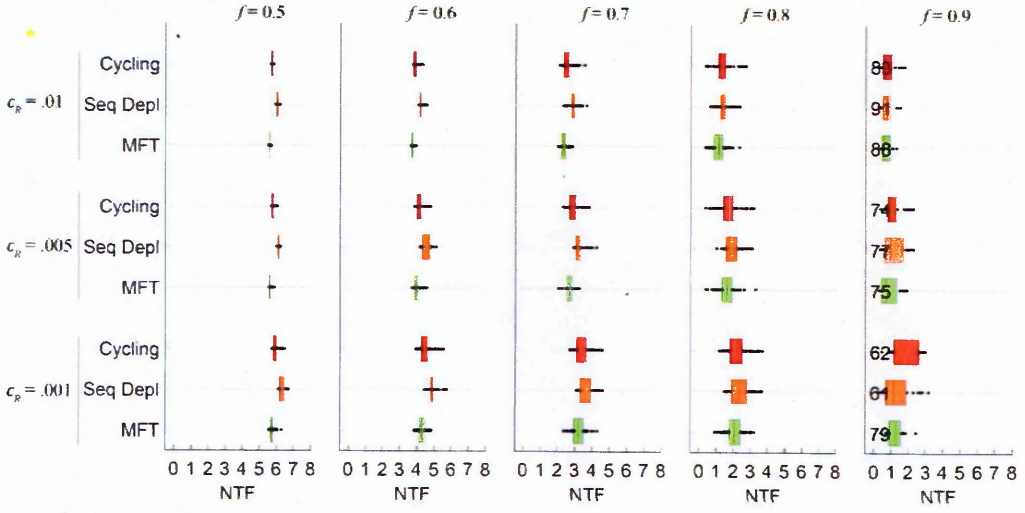

Figure 6.11. As Figure 6.8, all therapies are 5-day dosing.

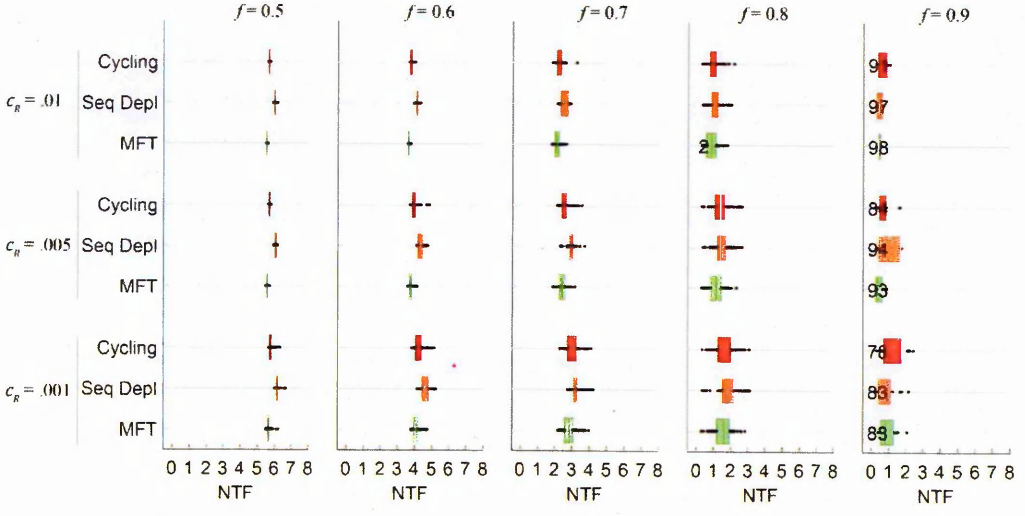

Figure 6.12. As Figure 6.8, all therapies are 6-day dosing.

6.4 Treatment Strategy Employing Multiple ACT Courses (MAC)

In this section, I will look at whether there is any benefit to one patient being treated with multiple ACTs sequentially during a single infection; for instance, the patient would take AL for 3 days which would be followed by a course of DHA-PPQ, either on days 4, 5, and 6, or with a delay on days 7, 8, and 9. This strategy was suggested recently by Sutherland et al, considering the current context of emerging artemisinin resistance and whether applying sequential 3-day courses of two different ACTs would improve the treatment efficacy[202].

In modeling these scenarios, we label them with the acronym MAC for "multiple ACT courses" and in most scenarios we will be modeling the two ACTs artemether-lumefantrine and DHA-piperaquine. I will introduce multiple variations of MAC treatments with the total number of dosing days being either four or six; these treatments will correspond to 2-day/3-day dosing with one ACT followed by 2-day/3-day dosing with a second ACT. A strategy I call "MAC41" will have four total days of dosing, and the "1" in the name means that this is version 1 of this strategy. In MAC41, patients are treated with AL for 2 days which is immediately followed by a 2-day course of DHA-PPQ. In a "MAC61" strategy, patients are treated with AL for 3 days which is immediately followed by a 3-day course of DHA-PPQ. Clinicians have recommended (personal communication: Francois Nosten, Nicholas White) that in order to reduce side effects of a long course of ACTs, it may be helpful to give the patient a break of a few days. Hence, I also evaluate two strategies I call MAC42 and MAC62 which include a 2- or 3-day break (equal to the length of first ACT course) before receiving the second ACT course. In other words, in MAC42 the patient receives AL on days 1 and 2, nothing on days 3 and 4, and DHA-PPQ on days 5 and 6.

In an additional scenario, I show how three different ACTs (described in Chapter 4) can be used in a MAC strategy, by allowing a patient to receive randomly two different ACTs (drawn randomly from 3 ACTs) and having them prescribed in a random order or either order, and this

new strategy is called Randomized Multiple ACT Course (MACR). I denote these strategies with MACR41, MACR42, MACR61, and MACR62 meaning that they are random, that there is four or six total days of dosing, and the two versions ("1" and "2") are as before (with and without a break, respectively, between doses of the two ACTs). The random MAC strategy with 3 different ACTs is identical to an MFT strategy with 6 different MAC therapies – formed by three combinations of two ACTs – which will allow us to evaluate the benefits of using or not using MFT with MAC strategies.

Also, note that in the first five chapters of this thesis, additional combination therapies were ignored. In other words, in deciding how best to deploy AL, ASAQ, and DHA-PPQ, we did not consider a hypothetical quadruple combination of Artemisinin coformulated with all three partner drugs. The reason we did not consider this is that a coformulated quadruple therapy would need to undergo safety and efficacy testing before it was approved by WHO and ministries of health in malaria-endemic countries. This would have been an ideal strategy to evaluate as past analyses – such as Bonhoeffer et al (1997) and the early work done in evaluating the models in Boni et al (2008) (personal communication: Maciej Boni) – have shown that combination therapy is generally a very favorable way of delaying/preventing resistance evolution. Very broadly, these results claimed that combination therapy should be as good or slightly better than MFT and better than cycling strategies, with the caveat that combination therapy carries the extra risk of driving the evolution of the multi-drug resistant if this completely resistant genotype were to emerge.

With the MAC strategies introduced in this chapter, we can evaluate a drug distribution strategy that mimics a combination therapy. Because the two ACTs in a MAC strategy are given very close together, this gives the parasite population a very small number of generations in which multiple drug-resistance alleles would need to emerge to fend off all the different therapeutic agents circulating in the blood. This is the same principle of 'resistance prevention' that is used to justify combination therapies (for all diseases) and indeed it is also the principle at work in making MFT strategies more optimal than cycling strategies. Thus, since MAC strategies are

the closest imitation of "combination-ACT-therapy" (i.e. a combination of multiple ACTs) we expect that these strategies will be as good as or better than MFT at preventing resistance evolution.

6.5 Results – Evaluation of MAC Strategies

My results show that MAC and MACR strategies have lower NTF values compared to MFT. Note that MFT and MACR use three ACTs while a normal MAC strategy only uses two ACTs.

Figure 6.13 shows the comparison among MFT strategies, MAC strategies, and MACR strategies. Initial comparisons are done in the same low-transmission setting as in Section 6.3; again, note that in some high-coverage settings treatment drives the parasite population an elimination. For intermediate coverage levels ($0.5 \leq f \leq 0.7$), MAC strategies have median NTF values that are between 6% and 49% lower than MFT strategies under the same number of total dosing days. In addition, elimination was observed more often under MAC strategies, possibly due to the fact that these strategies are better at preventing resistance.

Although the random MACR strategies, which take advantage of all three ACTs in the simulation, perform significantly better than MFT strategies, MACR strategies seem to have a slightly smaller effect compared to the simple MAC strategies which use only two ACTs. My initial investigations into this behavior did not lead to any obvious reasons for this difference. The expectation in fact is that the opposite would happen: that MACR strategies would be better at delaying resistance than MAC strategies since MACR strategies introduce more variation into the parasites' environment. The difference in the strategies may come in the PK/PD parameters used for the three partner drugs. In the validation analysis in Chapter 5, lumefantrine (4.5-day half-life) was assigned a higher killing rate than piperaquine (28-day half-life) so that AL and DHA-PPQ would have equal efficacies, both around 95%. For this reason, reducing AL treatment from 50% (MAC strategy) to 33% (MACR strategy) may have an effect in lowering average efficacy for patients or in lowering the force of infection during

the early days of infection. But, this needs to be investigated further as the explanation not likely to be this straightforward.

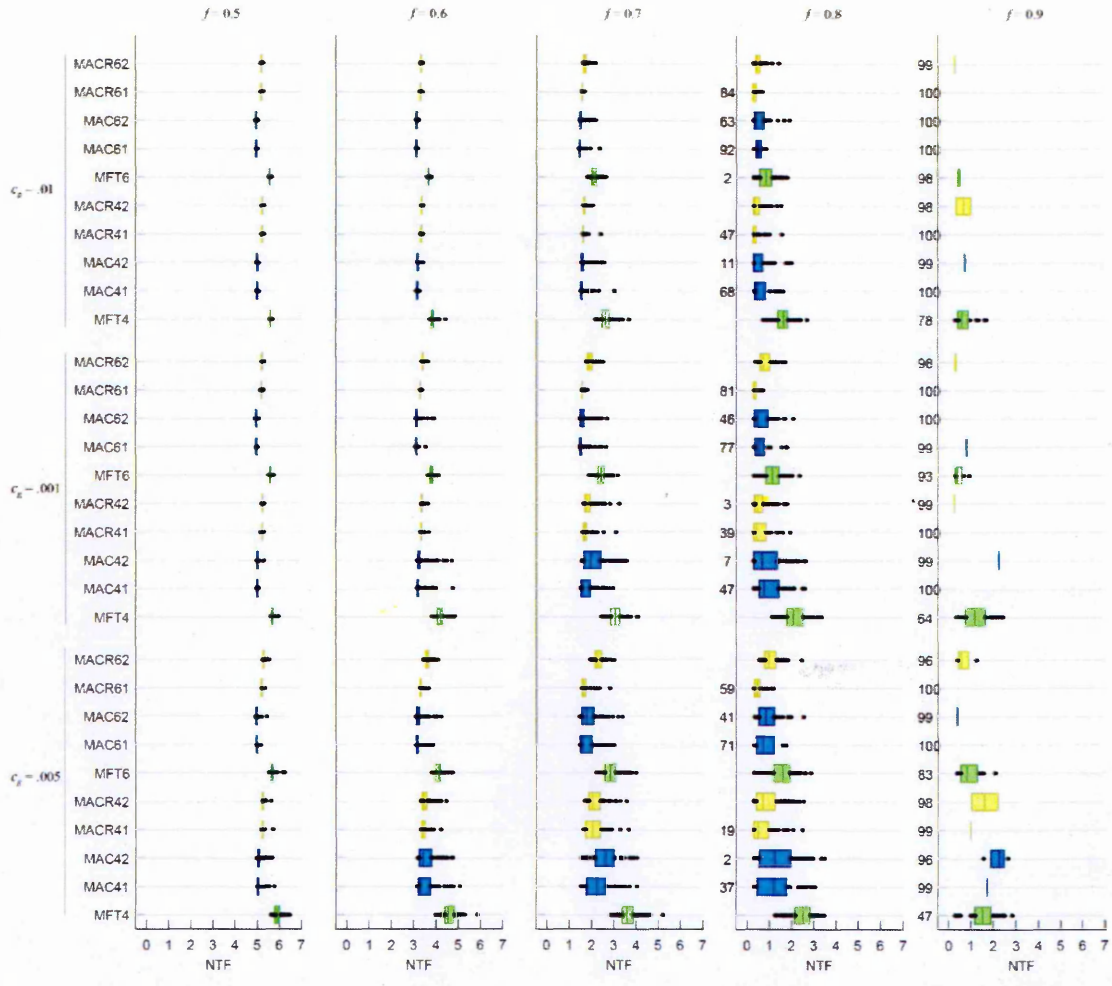

Figure 6.13. Comparisons of MFT and MAC strategies. The chart shows the NTF-values – the annual number of combined treatment failures and non-treatments, per 100 individuals – for different strategies, different costs of resistance (c_R), and different treatment coverages (f). Each row shows the NTF results of 100 model simulations with the colored bars spanning the interquartile range; the green, blue and lime color bars show the results of MFT, MAC and MACR strategies respectively. The definition of MAC41, MAC42, MACR61, and MACR62 are shown in section 6.4. MFT4 and MFT6 are the MFT strategies that employed ACTs with 4 and 6-day dosing respectively. For $f \geq 0.8$ the NTF distributions had a bimodal shape with NTF < 0.5 corresponding to simulations that achieved extinction or near-extinction; the numbers on the left-hand side of each boxplot show the counts of these (near)-extinctions, and the interquartile ranges are plotted only for simulations that did not result in extinction. Simulations assume that three ACTs with 95% efficacy are available and that the three partner drugs have 4.5-day, 9-day, and 28-day half-lives (corresponding to lumefantrine, amodiaquine, and piperaquine, respectively). Population size is 1,000,000.

The potential elimination scenarios for coverage levels of $f = 0.8$ and $f = 0.9$, show that MAC and MACR strategies are associated with more frequent elimination events in the simulations. This is likely due to the high efficacy of individual treatments and the low probability of resistance evolution during individual treatment courses.

6.6 Conclusions

In this chapter, I experimented with a new type of drug-deployment strategy that could be evaluated by the individual-based simulation that I developed for this thesis. This new strategy of "multiple ACT courses" (MAC) per patient seems to act as a good substitute for a triple combination therapy as individual patients in this strategy are given two different ACTs within the first week of a symptomatic malaria infection. As expected for a combination therapy, MAC outperforms both MFT and cycling strategies in that it dramatically reduced the probability of a *de novo* resistance evolution event. Both fixed MAC strategies (the order of the ACTs is predetermined) and random MAC strategies (two out of three ACTs are chosen to be prescribed in random order) are associated with fewer long-term treatment failures than MFT strategies. However, this is the first analysis, to my knowledge, of a population-level strategy employing multiple ACT courses per patient. These are early stage results, and may thus contain important caveats. In Chapter 7, I discuss the potential of MAC strategies to help in the global health response to artemisinin resistance and the types of sensitivity analyses that should be done in future modeling analyses to ensure the robustness of the results obtained in this chapter.

Chapter 7

Discussion

This thesis demonstrates the ways that an individual-based model can be used to evaluate not only population-scale treatment strategies (Chapter 4) but also the long-term outcomes of individual level treatment strategy (Chapter 6) in the context of dealing with antimalarial resistance emerging in the population. This novel microsimulation model provides a unique high-performance framework that allows for drug-resistance evolution and can be run with millions individuals on a personal computer.

7.1 Individual-based Model Development

Chapter 2 describes the software architecture on which the microsimulation model is built. By separating the simulation into components and by giving each component its own functionality, this methodology not only provided the robustness for the framework but also the flexibility and modularity to extend the individual-based model to have more features as more scientific requirements were needed at a later time in the development process (as Chapter 5). The core framework of the simulation is easy to adapt to build up another individual-based model for other diseases, e.g. for influenza, as I did for a side project that is not contained in this thesis [203] or for vector-borne diseases as we hope to do for dengue in Vietnam when dengue vaccination planning is prioritized later this decade [204].

The most important technical developments in this part of my thesis work were the scheduler mechanisms and the object pooling methods that improved speed and memory management. The separate scheduler class was developed so that I could use a purely event-based framework during the model simulation; this also means that the model is asynchronous like other event-based models. (It is possible that these other event-based model used a similar scheduler class to mine, but I did not have access to their source code so the development here is all my own

work). The scheduler-centered simulation allowed for a certain modularity in the functionality in the model so that any new type of event (e.g. a drug non-adherence event, or a biting-rate reduction while feverish event) could be added into the model, scheduled to "occur" when necessary, and thus evaluated as a potentially important factor for transmission. The scheduler also made the simulation much faster by not adding in unnecessary events when individuals were healthy, not at risk for being bitten, and thus not contributing meaningfully to the epidemiological dynamics in the model. Thus, in low transmission settings, model run times were quite fast as the vast majority of individuals avoided infection and did not need to be updated with any relevant events. In high-transmission settings, model run times were much slower as parasite density levels need to be updated frequently and for all infected hosts in these scenarios.

Object pooling allowed me to avoid the long-term drag of memory allocation, freeing, and reallocation. In a model simulation run over twenty years, with a large number of birth and death events, it was important to have a way to manage memory allocation so that individual allocation events were not called too frequently, thus not putting a strain on the operating system's memory management processes.

One important technical shortcoming of the model is that it currently has a one-day time step, thus creating a framework where pharmacokinetics and pharmacodynamics must necessarily be modeling very approximately and coarsely. Initially, this seemed like a good choice for the model development: to hard-code a time step of a single day so that all other processes and parameters could be simplified to how often they occurred "per day." However, once it became clear that the PK/PD dynamics would be a critical component of many of the outcomes and a desirable part of many sensitivity analyses, it was impossible to incorporate more detailed PK/PD dynamics than those observable at a 24-hour level. I cannot say whether this did or did not have an effect on the results. In the process of running the analyses Chapter 4, for example, I found that it was impossible to optimize MFT strategies according to drug half-life. In other

words, it was impossible to state whether an ACT with a short- or long-lived partner drug should be used at a higher or lower frequency in an MFT policy. With more detailed PK/PD modeling, it may turn out the half-life length does have an effect on the optimal distribution patterns when using multiple ACTs. I plan to pursue this question as an extension of my PhD thesis.

One of the biggest changes in the individual-based model that was introduced in Chapter 5 is "partial resistance" feature. This feature was implemented to bring the model closer to the reality that antimalarials still have a certain level of efficacy to resistant parasites. However, the pre-chapter-5 version of the simulation has only two distinct efficacies for naïve and resistant parasites: full efficacy and no efficacy. In the real world, drugs have reduced efficacies that vary by parasite genotype. This is especially important for the artemisinin-resistance *kelch13* genotypes [19,175] as many alleles have been observed in nature and it is likely that they are all partially resistant. An additional feature of multiple resistant alleles will be implemented in the future by defining decreasing drug efficacies that are associated with particular genotypes.

Despite some shortcomings in the original model design and formulation, the model turned out to be a success in modeling the long-term epidemiology of malaria (Chapter 3). The results on multiple first-line therapies appeared to be very robust, and the analyses on multiple ACT courses were the first ones performed for this question and their results appeared to be in agreement with our expectations based on evolutionary theory.

7.2 Benefits of Multiple First-line Therapies

The malaria transmission model that I developed and validated for this thesis provides outcomes in accordance with expectations based on evolutionary theory: that challenging the parasite with an environment presenting simultaneous multiple lethal challenges significantly increases the time the parasite requires to defeat all of them. The analysis suggests that deployment of multiple first-line artemisinin-combination therapies should result in improved population-level treatment outcomes, delayed resistance emergence, and slower resistance

evolution, as was seen in past more general analyses[52,182,183,185]. In addition, the major prevailing concern about MFT strategies – that they would allow recombination to generate multi-drug resistant types earlier than other strategies – proved not to be true in any of our simulations.

As population-level treatment strategies like the ones evaluated here will never be testable in the field, model-based recommendations may be the only evidence available for planning optimal distribution of antimalarial therapies. If the median predicted benefits are a 16% to 41% reduction in treatment failures over a 20-year period and a 40% increase to more than doubling of the useful therapeutic life of ACTs (Figure 4.3, $0.5 \leq f \leq 0.7$)), we may want to consider model-based recommendations as sufficient evidence for managing the distribution and usage patterns of antimalarial drugs. As elimination campaigns move forward, the extra insurance provided by MFT strategies may allow elimination efforts to succeed before a fully artemisinin-resistant genotype emerges.

The key principle at work in the strategy comparisons presented here is the conservation of drug efficacy[205]. As drugs are used more sparingly, the risks of resistance evolution are lowered and drug efficacy is prolonged. An MFT strategy allows individual drugs to be used more sparingly without reducing the total number of patients we intend to treat. The scenario presented in Figure 4.6 specifically considers the conservation of artemisinin efficacy, and the potential for extending the useful therapeutic life of artemisinin drugs by pairing them with other highly-efficacious drugs in an MFT strategy. This conservation approach is logical from an evolutionary perspective, but its ethical dimension will need to be evaluated carefully as it is possible that some patients would be treated with a therapy whose measured efficacy is second best. To improve the chances that a strategy like this meets the highest medical and ethical acceptability criteria, the risks for patients treated with a non-ACT would need to be mitigated, possibly through frequent follow-up and availability of second-line treatments.

As in all past analyses on the dynamics of drug-resistant parasites, measuring fitness costs[206–211] of drug-resistant genotypes is crucial for predicting the spread of resistance. For artemisinin

resistance, the current dynamic picture (2002-2013) of the spread of Kelch 13-propeller resistance-associated alleles in Cambodia is the best starting point for investigating fitness costs. However, the fitness cost of any future hypothetical resistant genotype is impossible to predict. To be conservative, fitness costs in our analyses were varied between 0.1% and 1.0%, as scenarios with much higher fitness costs would result in a bigger advantage of MFT over either cycling or sequential strategy.

In-depth critiques of model structure and validations are necessary when interpreting results from mathematical models, including this one. The model presented here does not take into account fine-scale spatial structure, mosquito dynamics, gametocyte dynamics, genotype-specific drug efficacies, partial drug resistance (in Chapters 3 and 4), or seasonal/climate effects, but it is clear that all of these features should be considered when planning treatment campaigns and elimination strategies. In particular, the model's one-day time step will make some future modifications difficult, e.g. detailed artemisinin action or stage-specific drug activity. For this reason, several lines of research have already begun (in my supervisor's research group, and with my help) to determine if short-term dynamics can be implanted in a separate model and merged into the simulation I developed for this thesis. It is crucial to continually develop and validate models like this one by adding in realistic features that are known to have important effects on malaria transmission and evolution so that each iteration of development brings the model closer to resembling the real-world epidemiology of malaria. Comparison of these results with those of other models will be critical for testing robustness. Analyses in many types of transmission settings will need to be done in order to ensure that specific policy recommendations are optimal. The results in this thesis suggest that MFT's relative benefits are smaller in higher transmission settings, but absolute benefits do not show this consistent pattern.

Potential caveats about the benefits of MFT strategies will need to be addressed and evaluated. First, strategy comparisons will likely be sensitive to the parity of the different available

therapies. In a scenario where one ACT has much higher efficacy than the other two, it may be prudent to utilize the high-efficacy therapy first, as this would lower the parasite population size more quickly (across all hosts) and lower the probability that random mutation generates a drug-resistant genotype. Currently recommended and available ACTs have similar efficacies[212], but this is location-dependent[114]; scenarios where, for example, two treatments with 90% and 98% efficacy have different predicted effects on a desired epidemiological outcome such as elimination will need to be evaluated on a case by case basis. Second, in choosing the optimal strategy we will need to consider the multitude of resistance effects caused by individual loci, an important example being position 76 in the chloroquine resistance transporter gene (*pfcrt*), where the wild-type allele (K) confers lumefantrine resistance and the mutant allele (T) confers amodiaquine resistance [213,214]. Normally, cycling strategies have worse evolutionary outcomes because they drive the evolution of individual resistance types more quickly, but in the case of K76T, amodiaquine resistance driving lumefantrine sensitivity may mitigate this problem. These effects may be present for other loci [215,216].

Implementation, compliance, and operations will be the next important areas of focus if MFT strategies are accepted as the best ways for distributing and prescribing antimalarial drugs. In addition, other factors, such as patient adherence, operational costs, or education programs for a new strategy implementation, would also have large impacts on the outcome. Additional research on health economics is currently an ongoing project of one of my fellow PhD students in order to quantify the costs and benefits of deploying MFT over other strategies. Flexibility and adaptability will be a key attributes of MFT policies if they are to succeed. If we are planning over a 20-year timeframe, transmission reductions resulting from other interventions, economic development, changes in the health care system, and many other political and geographic factors will affect future malaria prevalence. It is crucial that any long-term drug resistance management strategy that we implement is able to adapt to these changes.

Operationally, MFT would have several advantages as it removes the need for large system-wide changes in drug policy and avoids problems of obsolete drug stocks. It is not yet known if randomly assigning therapies should be done by location, day of week, a true randomization scheme, or some other method. Variation in drug purchase patterns from private and public sectors[217,218] will necessitate different implementations, and compliance monitoring will be challenging in contexts with high levels of private sector drug purchases. Nevertheless, some countries have successfully managed the roll-out of multiple ACTs[219–222], and these examples demonstrate the feasibility of locally-determined drug distribution and flexible treatment guidelines that are based on changing epidemiology. A commitment to evaluating the effectiveness of new population-level malaria treatment programs and a willingness to adapt our approach as we continue down this path will be critical for maximizing the benefits of MFT to global malaria policy.

7.3 Benefits of Multiple ACT Courses in Individual Patients

If MFT policies prove too difficult to implement at the population level, perhaps an alternative strategy is to recommend the next closest "MFT-type" strategy for patients. This is something I have called multiple ACT courses (MAC) for individual patients, and I evaluated the population level effects of this simple strategy of (1) lengthening the course of an ACT and (2) increasing the drug variability that the parasite population sees during this time.

The two primary reasons that the medical and public health communities would want to consider using multiple consecutive ACT courses for a single patient's malaria treatment are an increased chance of successful treatment and reduced probability of *de novo* resistance evolution during the course of treatment. This "MAC" treatment essentially mimics a triple combination therapy by forcing the asexual parasite population in the patient's blood to adapt to three different drugs simultaneously. The practical benefit of this "mimicked" combination therapy is that two ACTs can be safely prescribed in succession; in other words, an additional clinical trial establishing safety is not necessary.

From the parasite's perspective, the difference between MAC and MFT is the timeline of encountering different drugs. Both strategies are effective at delaying partner-drug resistance evolution, but in different ways. In an MFT strategy, a PPQ-resistant genotype may escape treatment with DHA-PPQ, after which it will have (1) a chance to establish itself within-host, if that particular patient's sensitive parasites have been killed, and (2) a chance for further spread of escape if the parasite jumps to another host and again undergoes treatment with DHA-PPQ. These probabilities are small, but not negligible. However, in a MAC strategy, neither of these is a possibility. A PPQ-resistant genotype would immediately undergo treatment with the second ACT designated for that course, and in the parasite's jump to the next patient it would be guaranteed to face at least one partner drug that was not piperaquine. For these reasons, MAC strategies seem to be associated with better outcomes in the presence of resistance evolution.

In my analysis, I assumed that different antimalarials drugs are acting independently on the parasite population and that the combined killing rate of different drugs follows the reasoning by Webb JL (1963)[223]. If drug A and B each has 80% parasite killing rate per day, then the additive killing rate is 1 - (1 - 0.8) x (1 - 0.8) = 96%. Webb's method is valid when the effects of two drugs are mutually nonexclusive (e.g., totally independent) and is not valid for mutually exclusive (e.g., similar mechanisms or modes of actions). Hence, to achieve the best performance of MAC, the partner drugs of ACTs should be chosen to have different modes of action of parasite killing as well as independent drug absorption mechanisms. Even in this situation, clinical data and longitudinal patient data would be needed to reconfirm the additive killing effect of two independent antimalarials, or to find the correct killing rate for the particular drug combination. This, and other considerations of drug interactions for efficacy and safety will be crucial for the future analyses of MAC strategies.

To have robust results, a wider range of simulations with different MAC scenarios needs to be run. Specifically, parts of the PK/PD model in the simulation would need to be enhanced,

varied, and revalidated to make sure that the long 6-day courses of treatment evaluated in the different MAC analyses achieve the correct efficacies as seen in patients. Ideally, clinical trials would be run to evaluate MAC in individual patients.

There will also be a need to investigate the difference between MAC and MACR, to see what the different resistance evolution patterns are under the different drug orders that are prescribed. This will necessarily be a theoretical study at the outset, but if MACR strategies prove beneficial in the majority of situations (note that this behavior is not currently observed in my initial analyses), then MACR will face the same implementation challenges as MFT. MACR strategies will also face additional challenges as the order of the ACTs, the combined killing rates of different partner drugs, and the half-life difference may create some unusual situations or results for particular pairs of ACTs. The MACR analysis presented here did not originally meet my expectations that it would be an improvement on MAC, and the comparisons of these two strategies will require significantly more work.

Due to time limitations, I was not able to perform a cost analysis for the MAC. It is true that increasing the number of dosing days from 3 days to 6 days and switching from single ACT to multiple ACTs should increase the treatment cost and operational cost. However, the benefit of preventing drug resistance by applying MAC needs to be quantified as well. Thus, in the future, a health-economic analysis on this topic should be done to evaluate the cost effectiveness of the MAC strategy.

In addition, human behavior is one of the most important factors that could have a large impact on these results. The adherence to a 6-days dosing treatment is crucial for the success of MAC strategy. However, to improve the compliance of patients, more efforts on public training and engagement have to be considered. To analyze the cost and the effect of the public engagement program on the benefit of the MAC strategy, additional health economic analysis will be necessary.

The malaria drug policy analyses presented in this thesis are meant to evaluate several different methods the global health community may use to preserve the efficacy of artemisinin-based drugs, in this crucial time of the early stages of artemisinin resistance spread. The analysis on MFT is mature and robust, and I can confidently recommend this policy as one that would be an improvement of the status quo. The MAC and MACR strategies hold a lot of promise, but further investigation is needed before they can be recommended as national malaria policy.

REFERENCES

1. World Health Organization. *World Malaria Report 2014*. Geneva; 2014.
2. de Zulueta J. Changes in the geographical distribution of malaria throughout history. *Parassitologia*. 29(2-3):193-205.
3. de Zulueta J. Malaria and ecosystems: from prehistory to posteradication. *Parassitologia*. 1994;36(1-2):7-15.
4. Neghina R, Neghina AM, Marincu I, Iacobiciu I. Malaria, a journey in time: in search of the lost myths and forgotten stories. *Am J Med Sci*. 2010;340(6):492-498. doi:10.1097/MAJ.0b013e3181e7fe6c.
5. Cox FEG. History of Human Parasitology. *Clin Microbiol Rev*. 2002;15(4):595-612. doi:10.1128/CMR.15.4.595.
6. Mendis K, Rietveld A, Warsame M, Bosman A, Greenwood B, Wernsdorfer WH. From malaria control to eradication: The WHO perspective. *Trop Med Int Heal*. 2009;14(7):802-809. doi:10.1111/j.1365-3156.2009.02287.x.
7. Hay SI, Guerra C a, Tatem AJ, Noor AM, Snow RW. The global distribution and population at risk of malaria: past, present, and future. *Lancet Infect Dis*. 2004;4(6):327-336. doi:10.1016/S1473-3099(04)01043-6.
8. Cox FE. History of the discovery of the malaria parasites and their vectors. *Parasit Vectors*. 2010;3(1):5. doi:10.1186/1756-3305-3-5.
9. Litsios S. Malaria Control and the Future of International Public Health. In: *The Contextual Determinants of Malaria*. ; 2002:292-328.
10. World Health Organization. *The World Health Report 1999: Making a Difference*. Geneva; 1999.
11. Schlitzer M. Antimalarial drugs - What is in use and what is in the pipeline. *Arch Pharm (Weinheim)*. 2008;341(3):149-163. doi:10.1002/ardp.200700184.
12. Rosenthal PJ, ed. *Anti-Malarial Chemotherapy*. Totowa, NJ, USA: Humana Press; 2001.
13. White N. Antimalarial drug resistance and combination chemotherapy. *Philos Trans R Soc Lond B Biol Sci*. 1999;354(1384):739-749. doi:10.1098/rstb.1999.0426.
14. Wellems TE, Plowe C V. Chloroquine-resistant malaria. *J Infect Dis*. 2001;184(6):770-776. doi:10.1136/bmj.2.5805.108-a.
15. D'Alessandro U, Buttiëns H. History and importance of antimalarial drug resistance. *Trop Med Int Heal*. 2001;6(11):845-848. doi:10.1046/j.1365-3156.2001.00819.x.
16. Farooq U, Mahajan RC. Drug resistance in malaria. *J Vector Borne Dis*. 2004;41(3-4):45-53.
17. Dondorp AMM, Nosten F, Yi P, et al. Artemisinin resistance in Plasmodium falciparum malaria. *N Engl J Med*. 2009;361(5):455-467. doi:10.1056/NEJMoa0808859.
18. Raman J, Mauff K, Muianga P, Mussa A. Five years of antimalarial resistance marker surveillance in Gaza Province, Mozambique, following artemisinin-based combination therapy roll out. *PLoS One*. 2011;6(10):1-8. doi:10.1371/journal.pone.0025992.
19. Ariey F, Witkowski B, Amaratunga C, et al. A molecular marker of artemisinin-resistant Plasmodium falciparum malaria. *Nature*. 2014;505(7481):50-55. doi:10.1038/nature12876.
20. Noedl H, Se Y, Sriwichai S, et al. Artemisinin resistance in Cambodia: a clinical trial designed to address an emerging problem in Southeast Asia. *Clin Infect Dis*. 2010;51(11):e82-e89. doi:10.1086/657120.
21. Noedl H, Se Y, Schaecher K, Smith BL, Socheat D, Fukuda MM. Evidence of artemisinin-resistant malaria in western Cambodia. *N Engl J Med*. 2008;359(24):2619-2620. doi:10.1056/NEJMc0805011.

22. Gilles H, Warrell D. *Bruce-Chwatt's Essential Malariology*. 3rd ed. London: Edward Arnold; 1993.

23. World Health Organization. *World Malaria Report 2015*. Geneva; 2015.

24. White NJ, Pukrittayakamee S, Hien TT, Faiz MA, Mokuolu O a, Dondorp AM. Malaria. *Lancet*. 2013;6736(13). doi:10.1016/S0140-6736(13)60024-0.

25. Kitchen S. Symptomatology: general considerations and falciparum malaria. In: Boyd MF, ed. *Malariology*. 2nd ed. ; 1949:996-1017.

26. Trampuz A, Jereb M, Muzlovic I, Prabhu RM. Clinical review: Severe malaria. *Crit Care*. 2003;7(4):315-323. doi:10.1186/cc2183.

27. World Health Organization. *Guidelines for the Treatment of Malaria, First Edition*. Geneva, Switzerland: World Health Organization; 2006.

28. Day K, Marsh K. Naturally acquired immunity to Plasmodium falciparum. *Immunol Today*. 1991;12(3):A68-A71. doi:10.1016/S0167-5699(05)80020-9.

29. Doolan DL, Dobaño C, Baird JK. Acquired immunity to malaria. *Clin Microbiol Rev*. 2009;22(1):13-36. doi:10.1128/CMR.00025-08.

30. Males S, Gaye O, Garcia A. Long-term asymptomatic carriage of Plasmodium falciparum protects from malaria attacks: a prospective study among Senegalese children. *CID*. 2008;46(4):516-522. doi:10.1086/526529.

31. Greenwood BM. Asymptomatic malaria infections--do they matter? *Parasitol Today*. 1987;3(7):206-214.

32. Enayati a, Hemingway J. Malaria management: past, present, and future. *Annu Rev Entomol*. 2010;55:569-591. doi:10.1146/annurev-ento-112408-085423.

33. Sokhna C, Ndiath MO, Rogier C. The changes in mosquito vector behaviour and the emerging resistance to insecticides will challenge the decline of malaria. *Clin Microbiol Infect*. 2013;19(10):902-907. doi:10.1111/1469-0691.12314.

34. Trape J-F, Tall A, Diagne N, et al. Malaria morbidity and pyrethroid resistance after the introduction of insecticide-treated bednets and artemisinin-based combination therapies: a longitudinal study. *Lancet Infect Dis*. 2011;11(12):925-932. doi:10.1016/S1473-3099(11)70194-3.

35. Corbel V, Akogbeto M, Damien GB, et al. Combination of malaria vector control interventions in pyrethroid resistance area in Benin: a cluster randomised controlled trial. *Lancet Infect Dis*. 2012;12(8):617-626. doi:10.1016/S1473-3099(12)70081-6.

36. Geissbühler Y, Chaki P, Emidi B, et al. Interdependence of domestic malaria prevention measures and mosquito-human interactions in urban Dar es Salaam, Tanzania. *Malar J*. 2007;6:126. doi:10.1186/1475-2875-6-126.

37. Gillies MT. Anopheline mosquitos: vector behaviour and bionomics. In: Wernsdorfer WH, McGregor I, eds. *Malaria: Principles and Practice of Malariology*. Edinburgh, United Kingdom; 1988:453-485.

38. Kleinschmidt I, Schwabe C, Benavente L, et al. Marked increase in child survival after four years of intensive malaria control. *Am J Trop Med Hyg*. 2009;80(6):882-888. doi:80/6/882 [pii].

39. Fegan GW, Noor AM, Akhwale WS, Cousens S, Snow RW. Effect of expanded insecticide-treated bednet coverage on child survival in rural Kenya: a longitudinal study. *Lancet*. 2007;370(9592):1035-1039. doi:10.1016/S0140-6736(07)61477-9.

40. Terlouw DJ, Morgah K, Wolkon A, et al. Impact of mass distribution of free long-lasting insecticidal nets on childhood malaria morbidity: the Togo National Integrated Child Health Campaign. *Malar J*. 2010;9:199. doi:10.1186/1475-2875-9-199.

41. Noor AM, Clements AC a, Gething PW, et al. Spatial prediction of Plasmodium falciparum prevalence in Somalia. *Malar J*. 2008;7:159. doi:10.1186/1475-2875-7-159.

42. Baume C a, Reithinger R, Woldehanna S. Factors associated with use and non-use of mosquito

nets owned in Oromia and Amhara regional states, Ethiopia. *Malar J.* 2009;8:264. doi:10.1186/1475-2875-8-264.

43. Minakawa N, Dida GO, Sonye GO, Futami K, Kaneko S. Unforeseen misuses of bed nets in fishing villages along Lake Victoria. *Malar J.* 2008;7:165. doi:10.1186/1475-2875-7-165.

44. WHO. *Guidelines for the Treatment of Malaria.* Geneva: World Health Organization; 2006.

45. Phyo AP, Nkhoma S, Stepniewska K, et al. Emergence of artemisinin-resistant malaria on the western border of Thailand: A longitudinal study. *Lancet.* 2012;379(12):1960-1966. doi:10.1016/S0140-6736(12)60484-X.

46. Ashley E a, Dhorda M, Fairhurst RM, et al. Spread of Artemisinin Resistance in Plasmodium falciparum Malaria. *N Engl J Med.* 2014;371(5):411-423. doi:10.1056/NEJMoa1314981.

47. Staines HM. *Treatment and Prevention of Malaria: Antimalarial Drug Chemistry, Action and Use.* (Krishna S, ed.). Basel: Springer; 2012.

48. Payne D. Did medicated salt hasten the spread of chloroquine resistance in Plasmodium falciparum? *Parasitol Today.* 1988;4(4):112-115. doi:10.1016/0169-4758(88)90042-7.

49. Newby G, Hwang J, Koita K, et al. Review of Mass Drug Administration for Malaria and Its Operational Challenges. 2015;93(1):125-134. doi:10.4269/ajtmh.14-0254.

50. World Health Organization. *Insecticide-Treated Mosquito Nets : A WHO Position Statement.* Geneva; 2007.

51. WHO. *Global Plan for Artemisinin Containment (GPARC).* Geneva; 2011.

52. Boni MF, Smith DL, Laxminarayan R. Benefits of using multiple first-line therapies against malaria. *Proc Natl Acad Sci U S A.* 2008;105(37):14216-14221. doi:10.1073/pnas.0804628105.

53. Ross R. *The Prevention of Malaria.* London: John Murray; 1911.

54. Fine PE. Ross's a priori pathometry - a perspective. *Proc R Soc Med.* 1975;68(9):547-551.

55. Smith DL, McKenzie FE. Statics and dynamics of malaria infection in Anopheles mosquitoes. *Malar J.* 2004;3(1):13. doi:10.1186/1475-2875-3-13.

56. Macdonald G. *The Epidemiology and Control of Malaria.* London: Oxford University Press; 1957.

57. Macdonald G. The measurement of malaria transmission. *Proc R Soc Med.* 1955;48(4):295-302.

58. Pampana E. *A Textbook of Malaria Eradication.* London: Oxford University Press; 1969.

59. Macdonald G. Epidemiological basis of malaria control. *Bull World Health Organ.* 1956;15(3-5):613-626.

60. Macdonald G, Gockel GW. The malaria parasite rate and Interruption of transmission. *Bull World Health Organ.* 1964;31(6):365-377. doi:10.1016/S1473-3099(04)01043-6.

61. Macdonald G, Cuellar CB, Foll C V. The dynamics of malaria. *Bull World Health Organ.* 1968;38(5):743-755.

62. Dietz K, Molineaux L, Thomas A. A malaria model tested in the African savannah. *Bull World Health Organ.* 1974;50(3-4):347-357.

63. Bekessy A, Molineaux L, Storey J. Estimation of incidence and recovery rates of Plasmodium falciparum parasitaemia from longitudinal data. *Bull World Health Organ.* 1976;54(6):685-693.

64. Cohen JE, Singer B. Malaria in Nigeria: Constrained continuous-time Markov models for discrete-time longitudinal data on human mixed-species infections. *Lect Math Life Sci.* 1979;(12):69-133.

65. Singer B, Cohen JE. Estimating malaria incidence and recovery rates from panel surveys. *Math Biosci.* 1980;49(3-4):273-305. doi:10.1016/0025-5564(80)90084-X.

66. Nájera J a. A critical review of the field application of a mathematical model of malaria eradication. *Bull World Health Organ.* 1974;50(5):449-457.

67. Gonzalez-Guzman J. A mixed program for parasitic disease control. *J Math Biol.* 1980;10(1):53-

64. doi:10.1007/BF00276395.

68. Curtis CF, Otoo LN. A simple model of the build-up of resistance to mixtures of anti-malarial drugs. *Trans R Soc Trop Med Hyg.* 1986;80(6):889-892.

69. Nedelman J. A negative binomial model for sampling mosquitoes in a malaria survey. *Biometrics.* 1983;39(4):1009-1020.

70. Halloran ME, Struchiner CJ, Spielman A. Modeling malaria vaccines. II: Population effects of stage-specific malaria vaccines dependent on natural boosting. *Math Biosci.* 1989;94(1):115-149.

71. Aron JL. Acquired immunity dependent upon exposure in an SIRS epidemic model. *Math Biosci.* 1988;88(1):37-47. doi:10.1016/0025-5564(88)90047-8.

72. Cross AP, Singer B. Modelling the development of resistance of Plasmodium falciparum to anti-malarial drugs. *Trans R Soc Trop Med Hyg.* 1991;85(3):349-355.

73. CLYDE DF, SHUTE GT. Resistance of East African varieties of Plasmodium falciparum to pyrimethamine. *Trans R Soc Trop Med Hyg.* 1954;48(6):495-500.

74. Anderson RM, May RM. *Infectious Diseases of Humans: Dynamics and Control.* Oxford: Oxford University Press; 1991.

75. Dye C. Population genetics of nonclonal, nonrandomly mating malaria parasites. *Parasitol Today.* 1991;7(9):236-240.

76. Dye C, Williams BG. Multigenic drug resistance among inbred malaria parasites. *Proc Biol Sci.* 1997;264(1378):61-67. doi:10.1098/rspb.1997.0009.

77. Hastings IM. A model for the origins and spread of drug-resistant malaria. *Parasitology.* 1997;115 (Pt 2:133-141. doi:10.1017/S0031182097001261.

78. Hastings IM, Mackinnon MJ. The emergence of drug-resistant malaria. *Parasitology.* 1998;117 (Pt 5:411-417.

79. Mackinnon MJ, Hastings IM. The evolution of multiple drug resistance in malaria parasites. *Trans R Soc Trop Med Hyg.* 1998;92(2):188-195.

80. Koella JC, Sørensen FL, Anderson RA. The malaria parasite, Plasmodium falciparum, increases the frequency of multiple feeding of its mosquito vector, Anopheles gambiae. *Proc R Soc B.* 1998;265(1398):763-768. doi:10.1098/rspb.1998.0358.

81. McKenzie FE, Wong RC, Bossert WH. Discrete-event simulation models of Plasmodium falciparum malaria. *Simulation.* 1998;71(4):250.

82. Mason DP, McKenzie FE. Blood-stage dynamics and clinical implications of mixed Plasmodium vivax-Plasmodium falciparum infections. *Am J Trop Med Hyg.* 1999;61(3):367-374.

83. Gu W, Killeen GF, Mbogo CM, Regens JL, Githure JI, Beier JC. An individual-based model of Plasmodium falciparum malaria transmission on the coast of Kenya. *Trans R Soc Trop Med Hyg.* 2003;97(1):43-50.

84. Smith T, Killeen GF, Maire N, et al. Mathematical modeling of the impact of malaria vaccines on the clinical epidemiology and natural history of Plasmodium falciparum malaria: Overview. *Am J Trop Med Hyg.* 2006;75(2 Suppl):1-10.

85. Maire N, Smith T, Ross A, Owusu-Agyei S, Dietz K, Molineaux L. A model for natural immunity to asexual blood stages of Plasmodium falciparum malaria in endemic areas. *Am J Trop Med Hyg.* 2006;75(2 Suppl):19-31.

86. Chitnis N, Smith T, Steketee R. A mathematical model for the dynamics of malaria in mosquitoes feeding on a heterogeneous host population. *J Biol Dyn.* 2008;2(3):259-285. doi:10.1080/17513750701769857.

87. Smith T, Maire N, Ross a, et al. Towards a comprehensive simulation model of malaria epidemiology and control. *Parasitology.* 2008;135(13):1507-1516. doi:10.1017/S0031182008000371.

88. Open Malaria. https://github.com/SwissTPH/openmalaria. Accessed May 26, 2015.

89. Chitnis N, Schapira A, Smith T, Steketee R. Comparing the effectiveness of malaria vector-control interventions through a mathematical model. *Am J Trop Med Hyg.* 2010;83(2):230-240. doi:10.4269/ajtmh.2010.09-0179.

90. Smith T, Maire N, Dietz K, et al. Relationship between the entomologic inoculation rate and the force of infection for Plasmodium Falciparum Malaria. *Trop Med.* 2006;75(Suppl 2):11-18.

91. Ross A, Killeen G, Smith T. Relationships between host infectivity to mosquitoes and asexual parasite density in Plasmodium falciparum. *Am J Trop Med Hyg.* 2006;75(SUPPL. 2):32-37. doi:75/2_suppl/32 [pii].

92. Ross A, Penny M, Maire N, et al. Modelling the epidemiological impact of intermittent preventive treatment against malaria in infants. Hay SI, ed. *PLoS One.* 2008;3(7):e2661. doi:10.1371/journal.pone.0002661.

93. Open Malaria Wiki. https://github.com/SwissTPH/openmalaria/wiki. Accessed December 12, 2015.

94. Filipe J a N, Riley EM, Drakeley CJ, Sutherland CJ, Ghani AC. Determination of the processes driving the acquisition of immunity to malaria using a mathematical transmission model. *PLoS Comput Biol.* 2007;3(12):e255. doi:10.1371/journal.pcbi.0030255.

95. Griffin JT, Hollingsworth TD, Okell LC, et al. Reducing Plasmodium falciparum Malaria Transmission in Africa: A Model-Based Evaluation of Intervention Strategies. *PLoS Med.* 2010;7(8). doi:10.1371/journal.pmed.1000324.

96. Malaria Tool. https://www1.imperial.ac.uk/malariamodelling/toolsdata/tools/. Accessed February 4, 2016.

97. Cameron E, Battle KE, Bhatt S, et al. Defining the relationship between infection prevalence and clinical incidence of Plasmodium falciparum malaria. *Nat Commun.* 2015;6:8170. doi:10.1038/ncomms9170.

98. Griffin JT, Ferguson NM, Ghani AC. Estimates of the changing age-burden of Plasmodium falciparum malaria disease in sub-Saharan Africa. *Nat Commun.* 2014;5:3136. doi:10.1038/ncomms4136.

99. EMOD source code. https://git.idmod.org/projects/EMOD/repos/source-code/browse. Accessed February 4, 2016.

100. Eckhoff P a. A malaria transmission-directed model of mosquito life cycle and ecology. *Malar J.* 2011;10(1):303. doi:10.1186/1475-2875-10-303.

101. Eckhoff P. P. falciparum Infection Durations and Infectiousness Are Shaped by Antigenic Variation and Innate and Adaptive Host Immunity in a Mathematical Model. *PLoS One.* 2012;7(9). doi:10.1371/journal.pone.0044950.

102. Eckhoff P a. Malaria parasite diversity and transmission intensity affect development of parasitological immunity in a mathematical model. *Malar J.* 2012;11(1):419. doi:10.1186/1475-2875-11-419.

103. Gerardin J, Eckhoff P, Wenger E a. Mass campaigns with antimalarial drugs: a modelling comparison of artemether-lumefantrine and DHA-piperaquine with and without primaquine as tools for malaria control and elimination. *BMC Infect Dis.* 2015;15(1):1-14. doi:10.1186/s12879-015-0887-y.

104. Goutelle S, Maurin M, Rougier F, et al. The Hill equation: a review of its capabilities in pharmacological modelling. *Fundam Clin Pharmacol.* 2008;22(6):633-648. doi:10.1111/j.1472-8206.2008.00633.x.

105. EMOD Document. http://idmod.org/idmdoc/. Accessed February 4, 2016.

106. Penny MA, Verity R, Bever CA, et al. Public health impact and cost-effectiveness of the RTS,S/AS01 malaria vaccine: a systematic comparison of predictions from four mathematical models. *Lancet.* 2015;6736(15):1-9. doi:10.1016/S0140-6736(15)00725-4.

107. Gouy I, Fulgham B. The Computer Language Benchmarks Game. http://benchmarksgame.alioth.debian.org/. Accessed January 1, 2005.

108. Fishman GS. *Discrete-Event Simulation*. New York: Springer; 2001.

109. GSL. https://www.gnu.org/software/gsl/.

110. YAML: YAML Ain't Markup Language. http://www.yaml.org/. Accessed May 31, 2015.

111. Boost C++ Libraries. http://www.boost.org. Accessed August 9, 2014.

112. Observer Design Pattern. https://msdn.microsoft.com/en-us/library/ee850490(v=vs.110).aspx. Accessed June 28, 2015.

113. Andreasen V, Lin J, Levin SA. The dynamics of cocirculating influenza strains conferring partial cross-immunity. *J Math Biol*. 1997;35(7):825-842. doi:10.1007/s002850050079.

114. Smithuis F, Kyaw MK, Phe O, et al. Effectiveness of five artemisinin combination regimens with or without primaquine in uncomplicated falciparum malaria: an open-label randomised trial. *Lancet*. 2010;10(10):673-681. doi:10.1016/S1473-3099(10)70187-0.

115. Smith DLL, Dushoff J, Snow RWW, Hay SII. The entomological inoculation rate and Plasmodium falciparum infection in African children. *Nature*. 2005;438(7067):492-495. doi:10.1038/nature04024.

116. Port GR, Boreham PFL. The relationship of host size to feeding by mosquitoes of the Anopheles gambiae Giles complex (Diptera: Culicidae). *Bull Entomol Res*. 1980;70:133-144.

117. Boreham PFL, Lenahan JK, Boulzaguet R, et al. Studies on multiple feeding by Anopheles gambiae s.l. in a Sudan savanna area of north Nigeria. *Trans R Soc Trop Med Hyg*. 1979;73(4):418-423. doi:10.1016/0035-9203(79)90167-6.

118. Eyles DE, Young MD. The duration of untreated or inadequately treated Plasmodium falciparum infections in the human host. *J Natl Mal Soc*. 1951;10(4):327-336.

119. Molineux L, Gramicci G, Molineaux L, Gramiccia G. *The Garki Project: Research on the Epidemiology and Control of Malaria in the Sudan Savanna of West Africa*. World Health Organization; 1980.

120. Lines JD, Wilkes TJ, Lyimo EO. Human malaria infectiousness measured by age-specific sporozoite rates in Anopheles gambiae in Tanzania. *Parasitology*. 1991;102 Pt 2:167-177.

121. Beier JC. Malaria Parasite Development in Mosquitoes. *Annu Rev Entomol*. 1998;43:519-543.

122. McKenzie FE, Bossert WH, Bosserrt W. An integrated model of Plasmodium falciparum dynamics. *J Theor Biol*. 2005;232(3):411-426. doi:10.1016/j.jtbi.2004.08.021.

123. White NJ. Assessment of the pharmacodynamic properties of antimalarial drugs in vivo. *Antimicrob Agents Chemother*. 1997;41(7):1413-1422.

124. Gordeuk V, Thuma P. Iron chelation as a chemotherapeutic strategy for falciparum malaria. *Am J Trop Med Hyg*. 1993;48(2):193-197.

125. Hien TT, White NJ. Qinghaosu. *Lancet*. 1993;341(8845):603-608.

126. Kremsner PG, Winkler S, Brandts C, Graniger W, Bienzle U. Curing of chloroquine-resistant malaria with clindamycin. *Am J Trop Med Hyg*. 1993;49(5):650-654.

127. Meek S, Doberstyn E, Gauzere BA, Thanapanich C, Nordlander E, Phaphaisan S. Treatment of falciparum malaria with quinne and tetracycline or combined mefloquine/sulfadoxine/pyrimethamine on the Thai-Kampuchean border. *Am J Trop Med Hyg*. 1986;35(November 1985):246-250.

128. Pukrittayakamee S, Viravan C, Charoenlarp P, Yeamput C, Wilson RJ, White NJ. Antimalarial effects of rifampin in Plasmodium vivax malaria. *Antimicrob Agents Chemother*. 1994;38(3):511-514. doi:10.1128/AAC.38.3.511.Updated.

129. Rieckmann K, Suebsaeng L, Rooney W. Response of Plasmodium falciparum infections to pyrimethamine-sulfadoxine in Thailand. *Am J Trop Med Hyg*. 1987;37(2):211-216.

130. Kuile F Ter, Nosten F, T. Chongsuphajaisiddhi, et al. Halofantrine versus mefloquine in treatment of multidrug-resistant falciparum malaria. *Lancet*. 1993;341(8852):1044-1049.

131. ter Kuile FO, Nosten F, Thieren M, et al. High-dose mefloquine in the treatment of multidrug-

resistant falciparum malaria. *J Infect Dis.* 1992;166(6):1393-1400.

132. Turaman C, Basco LK, Le Bras J. Evaluating the efficacy of chloroquine in febrile Guinean children infected with Plasmodium falciparum by a simplified in vivo test. *Bull World Heal Org.* 1992;70(4):477-480.

133. Jeffery G. Blood meal volume in Anopheles quadrimaculatus, A. albimanus and Aedes aegypti. *Exp Parasitol.* 1956;375:371-375.

134. Beier JC, Oster CN, Onyango FK, et al. Plasmodium falciparum incidence relative to entomologic inoculation rates at a site proposed for testing malaria vaccines in western Kenya. *Am J Trop Med Hyg.* 1994;50(5):529.

135. Hoffman SL, Oster CN, Plowe C V, et al. Naturally acquired antibodies to sporozoites do not prevent malaria: vaccine development implications. *Science.* 1987;237(4815):639-642.

136. Abdullah S, Adazu K, Masanja H, et al. Patterns of age-specific mortality in children in endemic areas of sub-Saharan Africa. *Am J Trop Med Hyg.* 2007;77(6 Suppl):99.

137. Becher H, Kynast-Wolf G, Sié A, et al. Patterns of malaria: cause-specific and all-cause mortality in a malaria-endemic area of west Africa. *Am J Trop Med Hyg.* 2008;78(1):106-113.

138. Goodman C, Coleman P, Mills A. *Economic Analysis of Malaria Control in Sub-Saharan Africa.* Geneva: Global Forum for Health Research; 2000.

139. Myint HY, Tipmanee P, Nosten F, et al. A systematic overview of published antimalarial drug trials. *Trans R Soc Trop Med Hyg.* 2004;98(2):73-81. doi:10.1016/S0035-9203(03)00014-2.

140. Nsobya SL, Parikh S, Kironde F, et al. Molecular evaluation of the natural history of asymptomatic parasitemia in Ugandan children. *J Infect Dis.* 2004;189(12):2220-2226. doi:10.1086/421281.

141. Kun J, Missinou M, Lell B, Sovric M. New emerging Plasmodium falciparum genotypes in children during the transition phase from asymptomatic parasitemia to malaria. *Am J Trop Med Hyg.* 2002;66(6):653-658.

142. Rabarijaona LP, Randrianarivelojosia M, Raharimalala L a, et al. Longitudinal survey of malaria morbidity over 10 years in Saharevo (Madagascar): further lessons for strengthening malaria control. *Mal J.* 2009;8:190. doi:10.1186/1475-2875-8-190.

143. Wongsrichanalai C, Barcus MJ, Muth S, Sutamihardja A, Wernsdorfer WH. A review of malaria diagnostic tools: microscopy and rapid diagnostic test (RDT). *Am J Trop Med Hyg.* 2007;77(6 Suppl):119-127.

144. Dhillon S. *Clinical Pharmacokinetics.* Pharmaceutical Press; 2006.

145. Hill A. The possible effects of the aggregation of the molecules of haemoglobin on its dissociation curves. *J physiol.* 1910.

146. Simpson J a, Watkins ER, Price RN, Aarons L, Kyle DE, White NJ. Mefloquine pharmacokinetic-pharmacodynamic models: implications for dosing and resistance. *Antimicrob Agents Chemother.* 2000;44(12):3414-3424.

147. Kay K, Hastings IM. Improving pharmacokinetic-pharmacodynamic modeling to investigate anti-infective chemotherapy with application to the current generation of antimalarial drugs. *PLoS Comput Biol.* 2013;9(7):e1003151. doi:10.1371/journal.pcbi.1003151.

148. WHO. *The Use of Antimalarial Drugs. Report of a WHO Informal Consultation.* WHO; 2001.

149. Stepniewska K, Taylor W, Sirima SB, et al. Population pharmacokinetics of artesunate and amodiaquine in African children. *Malar J.* 2009;043:1-13. doi:10.1186/1475-2875-8-200.

150. Byakika-Kibwika P, Lamorde M, Mayanja-Kizza H, Khoo S, Merry C, Van Geertruyden J-P. Artemether-Lumefantrine Combination Therapy for Treatment of Uncomplicated Malaria: The Potential for Complex Interactions with Antiretroviral Drugs in HIV-Infected Individuals. *Malar Res Treat.* 2011;2011:703730. doi:10.4061/2011/703730.

151. Tarning J, Lindegårdh N, Annerberg A, et al. Pitfalls in estimating piperaquine elimination. *Antimicrob Agents Chemother.* 2005;49(12):5127-5128. doi:10.1128/AAC.49.12.5127-

5128.2005.

152. Mwangi TW, Ross A, Snow RW, Marsh K. Case definitions of clinical malaria under different transmission conditions in Kilifi District, Kenya. *J Infect Dis.* 2005;191(11):1932-1939. doi:10.1086/430006.

153. Saúte F, Aponte J, Almeda J, et al. Malaria in southern Mozambique: Incidence of clinical malaria in children living in a rural community in Manhiça district. *Trans R Soc Trop Med Hyg.* 2003;97(6):655-660. doi:10.1016/S0035-9203(03)80097-4.

154. Trape J-F, Rogier C. Combating malaria morbidity and mortality by reducing transmission. *Parasitol Today.* 1996;12(6):236-240. doi:10.1016/0169-4758(96)10015-6.

155. Guinovart C, Bassat Q, Sigaúque B, et al. Malaria in rural Mozambique. Part I: children attending the outpatient clinic. *Malar J.* 2008;7:36. doi:10.1186/1475-2875-7-36.

156. Lindblade KA, Steinhardt L, Samuels A, Kachur SP, Slutsker L. The silent threat: asymptomatic parasitemia and malaria transmission. *Expert Rev Anti Infect Ther.* 2013;11(6):623-639. doi:10.1586/eri.13.45.

157. Yekutiel P. Problems of epidemiology in malaria eradication. *Bull World Heal Org.* 1960;22:669-683.

158. Njama-Meya D, Kamya MR, Dorsey G. Asymptomatic parasitaemia as a risk factor for symptomatic malaria in a cohort of Ugandan children. *Trop Med Int Heal.* 2004;9(8):862-868. doi:10.1111/j.1365-3156.2004.01277.x.

159. Cucunubá ZM, Guerra AP, Rahirant SJ, Rivera JA, Cortés LJ, Nicholls RS. Asymptomatic Plasmodium spp. infection in Tierralta, Colombia. *Mem Inst Oswaldo Cruz.* 2008;103(7):668-673.

160. Beier JC, Killeen GF, Githure JI. Short report: entomologic inoculation rates and Plasmodium falciparum malaria prevalence in Africa. *Am J Trop Med Hyg.* 1999;61(1):109-113.

161. Hay SI, Guerra C a, Tatem AJ, Atkinson PM, Snow RW. Urbanization, malaria transmission and disease burden in Africa. *Nat Rev Microbiol.* 2005;3(1):81-90. doi:10.1038/nrmicro1069.Urbanization.

162. Winskill P, Rowland M, Mtove G, Malima RC, Kirby MJ. Malaria risk factors in north-east Tanzania. *Malar J.* 2011;10:98. doi:10.1186/1475-2875-10-98.

163. Snow R, Marsh K. The consequences of reducing transmission of Plasmodium falciparum in Africa. *Adv Parasitol.* 2002;52:235-265.

164. Marsh K, Snow RW. Malaria transmission and morbidity. *Parassitologia.* 1999;41:241-246.

165. Smith DL, Guerra C a, Snow RW, Hay SI. Standardizing estimates of the Plasmodium falciparum parasite rate. *Malar J.* 2007;6:131. doi:10.1186/1475-2875-6-131.

166. Owusu-Agyei S, Smith T, Beck HP, Amenga-Etego L, Felger I. Molecular epidemiology of Plasmodium falciparum infections among asymptomatic inhabitants of a holoendemic malarious area in northern Ghana. *Trop Med Int Heal.* 2002;7(5):421-428. doi:10.1046/j.1365-3156.2002.00881.x.

167. Arnot D. Unstable malaria in Sudan: the influence of the dry season: clone multiplicity of Plasmodium falciparum infections in individuals exposed to variable levels of disease. *Trans R Soc Trop ....* 1998.

168. Woolhouse M, Dye C, Etard J. Heterogeneities in the transmission of infectious agents: implications for the design of control programs. *Popul Biol.* 1997;94(January):338-342.

169. Feachem RG, Phillips A a, Hwang J, et al. Shrinking the malaria map: progress and prospects. *Lancet.* 2010;376(9752):1566-1578. doi:10.1016/S0140-6736(10)61270-6.

170. Moonen B, Cohen JM, Snow RW, et al. Operational strategies to achieve and maintain malaria elimination. *Lancet.* 2010;376. doi:10.1016/S0140-6736(10)61269-X.

171. Maude RJ, Pontavornpinyo W, Saralamba S, et al. The last man standing is the most resistant: eliminating artemisinin-resistant malaria in Cambodia. *Mal J.* 2009;8:31. doi:10.1186/1475-

2875-8-31.

172. White NJ. Qinghaosu (artemisinin): the price of success. *Science (80-).* 2008;320(5874):330-334. doi:10.1126/science.1155165.

173. Tran TH, Nguyen TT-N, Nguyen HP, et al. In vivo susceptibility of Plasmodium falciparum to artesunate in Binh Phuoc Province, Vietnam. *Malar J.* 2012;11(1):355. doi:10.1186/1475-2875-11-355.

174. Ashley EA, Dhorda M, Fairhurst RM, et al. The spread of artemisinin resistance in falciparum malaria. *N Engl J Med.* 2014;371(5):411-423. doi:10.1056/NEJMoa1314981.

175. Tun KM, Imwong M, Lwin KM, et al. Spread of artemisinin-resistant Plasmodium falciparum in Myanmar: a cross-sectional survey of the K13 molecular marker. *Lancet Infect Dis.* 2015:21-26. doi:10.1016/S1473-3099(15)70032-0.

176. White NJ, Pongtavornpinyo W, Maude RJ, et al. Hyperparasitaemia and low dosing are an important source of anti-malarial drug resistance. *Mal J.* 2009;8:253. doi:10.1186/1475-2875-8-253.

177. Nayyar GM, Breman JG, Newton PN, Herrington J. Poor-quality antimalarial drugs in southeast Asia and sub-Saharan Africa. *Lancet Infect Dis.* 2012;12(6):488-496. doi:10.1016/S1473-3099(12)70064-6.

178. Barnes KI, Watkins WM, White NJ. Antimalarial dosing regimens and drug resistance. *Trends Parasitol.* 2008;24(3):127-134. doi:10.1016/j.pt.2007.11.008.

179. Levins R. *Evolution in Changing Environments*. Princeton, NJ: Princeton University Press; 1968.

180. Bonhoeffer S, Lipsitch M, Levin BR. Evaluating treatment protocols to prevent antibiotic resistance. *Proc Natl Acad Sci USA.* 1997;94(22):12106-12111.

181. Bonhoeffer S. Managing Antibiotic Resistance: What Models Tell Us? In: Dieckmann U, Metz JAJ, Sigmund K, Sabelis MW, eds. *Adaptive Dynamics and Infectious Diseases: In Pursuit of Virulence Management*. Cambridge, UK; 2002:326-338.

182. Bergstrom CT, Lipsitch M, Lo M, Lipsitch M. Ecological theory suggests that antimicrobial cycling will not reduce antimicrobial resistance in hospitals. *Proc Natl Acad Sci USA.* 2004;101:13285-13290.

183. Smith DL, Klein EY, McKenzie FE, Laxminarayan R. Prospective strategies to delay the evolution of anti-malarial drug resistance: weighing the uncertainty. *Malar J.* 2010;9:217. doi:10.1186/1475-2875-9-217.

184. Spiliotopoulou E, Boni MF, Yadav P. Impact of treatment heterogeneity on drug resistance and supply chain costs. *Socio-Econ Plan Sci.* 2013;47(3):158-171. doi:10.1016/j.seps.2013.04.001.

185. Antao T, Hastings IM. Environmental, pharmacological and genetic influences on the spread of drug-resistant malaria. *Proc R Soc L B.* 2011;278(1712):1705-1712. doi:10.1098/rspb.2010.1907.

186. Amin AA, Zurovac D, Kangwana BB, et al. The challenges of changing national malaria drug policy to artemisinin-based combinations in Kenya. *Malar J.* 2007;6:72. doi:10.1186/1475-2875-6-72.

187. Antao T, Hastings I. Policy options for deploying anti-malarial drugs in endemic countries: a population genetics approach. *Mal J.* 2012;11(1):422. doi:10.1186/1475-2875-11-422.

188. Smith DL, Cohen JM, Chiyaka C, et al. A sticky situation: the unexpected stability of malaria elimination. *Phil Trans R Soc L B.* 2013;368:20120145.

189. White NJ, Pukrittayakamee S, Phyo AP, et al. Spiroindolone KAE609 for Falciparum and Vivax Malaria. *N Engl J Med.* 2014;371(5):403-410. doi:10.1056/NEJMoa1315860.

190. Hastings IM, D'Alessandro U. Modelling a Predictable Disaster:: The Rise and Spread of Drug-resistant Malaria. *Parasitol Today.* 2000;16(8):340-347.

191. World Health Organization. Child growth standards: weight-for-age charts. http://www.who.int/childgrowth/standards/weight_for_age/en/. Accessed May 4, 2015.

192. Wijnhoven F. *Information Management: An Informing Approach*. London: Routledge; 2009.

193. Kuhn TS. *Structure of Scientific Revolutions*. 3rd ed. Chicago: University of Chicago Press; 1996.

194. Khim N, Bouchier C, Ekala MT, et al. Countrywide survey shows very high prevalence of Plasmodium falciparum multilocus resistance genotypes in Cambodia. *Antimicrob Agents Chemother*. 2005;49(8):3147-3152. doi:10.1128/AAC.49.8.3147-3152.2005.

195. Reeder JC, Rieckmann KH, Genton B, Lorry K, Wines B, Cowman AF. Point mutations in the dihydrofolate reductase and dihydropteroate synthetase genes and in vitro susceptibility to pyrimethamine and cycloguanil of Plasmodium falciparum isolates from Papua New Guinea. *Am J Trop Med Hyg*. 1996;55(2):209-213.

196. Stepniewska K, Price RN, Sutherland CJ, et al. Plasmodium falciparum gametocyte dynamics in areas of different malaria endemicity. *Malar J*. 2008;7:249. doi:10.1186/1475-2875-7-249.

197. Makanga M. A review of the effects of artemether-lumefantrine on gametocyte carriage and disease transmission. *Malar J*. 2014;13(1):291. doi:10.1186/1475-2875-13-291.

198. Okafor HU, Shu EN, Oguonu T. Therapeutic efficacy and effect on gametocyte carriage of an artemisinin and a non-based combination treatment in children with uncomplicated P. falciparum malaria, living in an area with high-level chloroquine resistance. *J Trop Pediatr*. 2010;56(6):398-406. doi:10.1093/tropej/fmq004.

199. Adjuik M, Agnamey P, Babiker A, et al. Amodiaquine-artesunate versus amodiaquine for uncomplicated Plasmodium falciparum malaria in African children: a randomised, multicentre trial. *Lancet*. 2002;359(9315):1365-1372. doi:10.1016/S0140-6736(02)08348-4.

200. Thanh N V, Toan TQ, Cowman AF, et al. Monitoring for Plasmodium falciparum drug resistance to artemisinin and artesunate in Binh Phuoc Province, Vietnam: 1998-2009. *Malar J*. 2010;9:181. doi:10.1186/1475-2875-9-181.

201. Saralamba S, Pan-Ngum W, Maude RJ, et al. Intrahost modeling of artemisinin resistance in Plasmodium falciparum. *Proc Natl Acad Sci U S A*. 2011;108(1):397-402. doi:10.1073/pnas.1006113108.

202. van Schalkwyk D a, Sutherland CJ. Malaria resistance to non-artemisinin partner drugs: how to reACT. *Lancet Infect Dis*. 2015;3099(15):1-2. doi:10.1016/S1473-3099(15)70080-0.

203. Boni MF, Nguyen TD, de Jong MD, van Doorn HR. Virulence attenuation during an influenza A/H5N1 pandemic. *Philos Trans R Soc Lond B Biol Sci*. 2013;368(1614):20120207. doi:10.1098/rstb.2012.0207.

204. Chao DL, Halstead SB, Halloran ME, Longini IM. Controlling Dengue with Vaccines in Thailand. *PLoS Negl Trop Dis*. 2012;6(10). doi:10.1371/journal.pntd.0001876.

205. Laxminarayan R. Economics of Antibiotic Resistance: A Theory of Optimal Use. *J Env Econ Manag*. 2001;42(2):183-206. doi:10.1006/jeem.2000.1156.

206. Kublin JG, Cortese JF, Njunju EM, et al. Reemergence of chloroquine-sensitive Plasmodium falciparum malaria after cessation of chloroquine use in Malawi. *J Infect Dis*. 2003;187(12):1870-1875. doi:10.1086/375419.

207. Huong NM, Hewitt S, Davis TME, et al. Resistance of Plasmodium falciparum to antimalarial drugs in a highly area of southern Viet Nam : a study in viva and in vitro. *Trans R Soc Trop Med Hyg*. 2001;95(3):325-329.

208. Gharbi M, Flegg J a, Hubert V, et al. Longitudinal study assessing the return of chloroquine susceptibility of Plasmodium falciparum in isolates from travellers returning from West and Central Africa, 2000-2011. *Mal J*. 2013;12(1):35. doi:10.1186/1475-2875-12-35.

209. Mwai L, Ochong E, Abdirahman A, et al. Chloroquine resistance before and after its withdrawal in Kenya. *Mal J*. 2009;8:106. doi:10.1186/1475-2875-8-106.

210. Raman J, Sharp B, Kleinschmidt I, et al. Differential effect of regional drug pressure on dihydrofolate reductase and dihydropteroate synthetase mutations in southern Mozambique. *Am J Trop Med Hyg*. 2008;78(2):256-261.

211. Laufer MK, Thesing PC, Eddington ND, et al. Return of chloroquine antimalarial efficacy in Malawi. *N Engl J Med.* 2006;355(19):1959-1966.

212. Jansen FH, Lesaffre E, Penali LK, Zattera MJG, Die-Kakou H, Bissagnene E. Assessment of the relative advantage of various artesunate-based combination therapies by a multi-treatment bayesian random-effects meta-analysis. *Am J Trop Med Hyg.* 2007;77(6):1005-1009. doi:77/6/1005 [pii].

213. Sisowath C, Petersen I, Veiga MI, et al. In vivo selection of Plasmodium falciparum parasites carrying the chloroquine-susceptible pfcrt K76 allele after treatment with artemether-lumefantrine in Africa. *J Infect Dis.* 2009;199(5):750-757. doi:10.1086/596738.

214. Nzila A, Okombo J, Ohuma E, Al-Thukair A. Update on the in vivo tolerance and in vitro reduced susceptibility to the antimalarial lumefantrine. *J Antimicrob Chemother.* 2012;67(10):2309-2315. doi:10.1093/jac/dks252.

215. Humphreys GS, Merinopoulos I, Ahmed J, et al. Amodiaquine and artemether-lumefantrine select distinct alleles of the Plasmodium falciparum mdr1 gene in Tanzanian children treated for uncomplicated malaria. *Antimicrob Agents Chemother.* 2007;51(3):991-997. doi:10.1128/AAC.00875-06.

216. Veiga MI, Ferreira PE, Malmberg M, et al. pfmdr1 amplification is related to increased Plasmodium falciparum in vitro sensitivity to the bisquinoline piperaquine. *Antimicrob Agents Chemother.* 2012;56(7):3615-3619. doi:10.1128/AAC.06350-11.

217. Talisuna A, Grewal P, Rwakimari JB, Mukasa S, Jagoe G, Banerji J. Cost is killing patients: subsidising effective antimalarials. *Lancet.* 2009;374:1224-1226.

218. Sabot OJ, Mwita A, Cohen JM, et al. Piloting the Global Subsidy: The Impact of Subsidized Artemisinin-Based Combination Therapies Distributed through Private Drug Shops in Rural Tanzania. *PLoS One.* 2009;4(9):e6857. doi:10.1371/journal.pone.0006857.

219. Ministry of Health. *Anti-Malaria Drug Policy for Ghana, 2nd Revised Version.* Accra, Ghana; 2009.

220. Abuaku B, Quaye L, Quashie N, Quashie N, Koram KA. Managing Antimalarial Drug Resistance in Ghana: The Importance of Surveillance. In: Koram KA, Ahorlu CSK, Wilson MD, Yeboah-Manu D, Bosompem KM, eds. *Towards Effective Disease Control in Ghana: Research and Policy Implications.* Accra, Ghana: Sub-Saharan Publishers; 2014:7-18.

221. Kusriastuti R, Surya A. New treatment policy of malaria as a part of malaria control program in Indonesia. *Acta Med Indones.* 2012;44(3):265-259.

222. World Health Organization. *National Malaria Control Programme Review, Republic of Indonesia.* Geneva, Switzerland; 2011.

223. Chou T. Theoretical Basis , Experimental Design , and Computerized Simulation of Synergism and Antagonism in Drug Combination Studies □. 2007;58(3):621-681. doi:10.1124/pr.58.3.10.

APPENDIX

Parameter Description

This section shows the parameters and inputs that were used in the simulation.

```
# total number of days the simulation is run, including the burn-in period which
we normally set to 4000
# days; during the burn-in period, no one receives malaria treatement and the
system sets into a natural
# equilibrium
total_time: 4730


# length of burn-in period
start_treatment_day: 4000


# the day at which the simulation's reporting functionality begins collecting
data for
# the purposes of displaying it
start_collect_data_day: 4000


# probability that a symptomatic and infected individual seeks and receives
antimalarial treatment
p_treatment: 0.600000


# this functionality works, but it was not used in any analyses for the 2015 LGH
paper
number_of_locations: 1


# main scaling parameter for transmission, by location
# the last four terms are ignored when the number of locations is 1
beta: [0.2 , 1.4 , 1.4, 1.4, 1]


# this functionality works, but it was not used in any analyses for the 2015 LGH
paper
# seasonality parameters, by location
seasonal_beta:
  a: [0, 0.25, 0.25, 0.25]
  phi: [200, 200, 200, 200]
```

```
# the last four terms are ignored when the number of locations is 1
population_size_by_location: [100000, 1000 , 1000, 1000, 500]


# probability that an infectious bite on a human causes a blood stage malaria
infection
p_infection_from_an_infectious_bite: 0.1



# the simulation itself uses explicit ages and birthdays
# but for reporting purposes and for age-specific mortality calculations,
individuals are grouped into the following age classes
number_of_age_classes: 15
age_structure: [1, 2, 3, 4, 5, 6, 7, 8, 9, 10, 11, 15, 20, 60, 100]



# this is only used for initializing the population structure at time 0
# the last four rows of the matrix below are ignored when the number of
locations is 1
initial_age_structure: [1, 2, 3, 4, 5, 6, 7, 8, 9, 10, 11, 12, 13, 14, 15, 25,
35, 45, 55, 65, 100]
age_distribution_by_location: [
[0.0334, 0.0300, 0.0329, 0.0324, 0.0332, 0.0314, 0.0316, 0.0310, 0.0285, 0.0256,
0.0298, 0.0212, 0.0321, 0.0228, 0.0230, 0.1906, 0.1403, 0.0966, 0.0605, 0.0344,
0.0387],
[0.0334, 0.0300, 0.0329, 0.0324, 0.0332, 0.0314, 0.0316, 0.0310, 0.0285, 0.0256,
0.0298, 0.0212, 0.0321, 0.0228, 0.0230, 0.1906, 0.1403, 0.0966, 0.0605, 0.0344,
0.0387],
[0.0334, 0.0300, 0.0329, 0.0324, 0.0332, 0.0314, 0.0316, 0.0310, 0.0285, 0.0256,
0.0298, 0.0212, 0.0321, 0.0228, 0.0230, 0.1906, 0.1403, 0.0966, 0.0605, 0.0344,
0.0387],
[0.0334, 0.0300, 0.0329, 0.0324, 0.0332, 0.0314, 0.0316, 0.0310, 0.0285, 0.0256,
0.0298, 0.0212, 0.0321, 0.0228, 0.0230, 0.1906, 0.1403, 0.0966, 0.0605, 0.0344,
0.0387]
]


# below value indicates 37.25 births per 1000 individuals per year
birth_rate: 0.03725


# annual death rate (probability) by age group
death_rate_by_age: [0.053979329, 0.018935757, 0.006867257, 0.001124347,
0.001136455, 0.001606066, 0.001953783, 0.001530096, 0.001299153, 0.001068073,
0.000978264, 0.000978264, 0.0055, 0.0055, 0.04450]
```

```
# number of days to keep track total number of parasites in population
# in other words, the simulation stores 11 days of mosquitoes-biting-on-humans
history
# if an individual is infected today, the infection type and probability will be
based
# on the biting that took place 11 days ago
number_of_tracking_days: 11


# probability of death for patients who are not treated or patients who
experience a treatment failure (due to drug resistance, or otherwise)
mortality_when_treatment_fail_by_age: [0.040,
0.020,0.020,0.020,0.020,0.004,0.004,0.004,0.004,0.004,0.004, 0.001, 0.001,
0.001, 0.001]


# initial conditions for prevalence and drug resistance, by location
# parasite_type_id is the parasite genotype; 0 means completely sensitive to all
drugs
# the parasite_type_id is a bit-string, so types 1, 2, 4, and 8 correspond to
parasites
# that have a resistance to a single drug
initial_parasite_info:
  - location_id: 0
    parasite_info:
      - parasite_type_id: 0
        prevalence: 0.1
#       - parasite_type_id: 2
#         prevalence: 0.1
#       - parasite_type_id: 4
#         prevalence: 0.1
  - location_id: 1
    parasite_info:
      - parasite_type_id: 0
        prevalence: 0.1
  - location_id: 2
    parasite_info:
      - parasite_type_id: 0
        prevalence: 0.1
  - location_id: 3
    parasite_info:
      - parasite_type_id: 0
        prevalence: 0.1
#       - parasite_type_id: 4
#         prevalence: 0.03
```

```
# functional but not used in 2015 LGH paper
# allows for the introduction of a specific parasite type at a specific time
introduce_parasite:
#  - location: 0
#    parasite_info:
#      - time: 4000
#        genotype_id: 1
#        number_of_cases: 5
#      - time: 4000
#        genotype_id: 2
#        number_of_cases: 5
#      - time: 4000
#        genotype_id: 4
#        number_of_cases: 5
#      - time: 4000
#        genotype_id: 8
#        number_of_cases: 5
#


# periodic importation of drug-sensitive parasites; five new cases imported
every seven days
introduce_parasite_periodically:
  - location: 0
    parasite_info:
      - duration: 7
        genotype_id: 0
        number_of_cases: 5


# drug information below
#
# maximum_parasite_killing_rate:
#       e.g. 0.999 means the drug can kill 99.9% of parasites in 1 day if a
person has
#       the highest possible drug concentration
#
# n:
#       the slope of the linear portion of the conentration-effect curve
#
# EC50:
#       the drug concentration which produces 50% of the parasite killing
achieved at maximum-concentration
#       ( the expected starting concentration is 1.0 )
#
# age_specific_drug_concentration_sd:
#       the actual drug concentration, per individual, will be drawn from a
normal distribution with mean=1 and this sd.
```

```
#
# k:
#       parameter that describes the change in the mutation probability when
drug levels are intermediate
#       - set k=0.5 for a simple linear model where mutation probablity
decreases linearly with drug concentration
#       - set k=2 or k=4 for a piecewise-linear model where mutation probability
increases from high concentrations
#               to intermediate concentrations, and then decreases linearly from
intermediate concentrations to zero
#
drugInfo:
  1:  # artemisinin (used for artemether, artesunate, and dihydroartemisinin)
    half_life: 0.0
    maximum_parasite_killing_rate: 0.999
    n: 25
    EC50: 0.7
    age_specific_drug_concentration_sd:
[0.4,0.4,0.4,0.4,0.4,0.4,0.4,0.4,0.4,0.4,0.4,0.4,0.4,0.4,0.4,0.4]
    mutation_probability: 0.005
    mutation_position: [0]
    k: 4
    resistance_cost_multiple_infection: 0.01
    isArtermisininDerivative: 1
  2: # lumefantrine - use this for a standard simulation
    half_life: 4.5
    maximum_parasite_killing_rate: 0.99
    n: 20
    EC50: 0.65
    age_specific_drug_concentration_sd:
[0.4,0.4,0.4,0.4,0.4,0.4,0.4,0.4,0.4,0.4,0.4,0.4,0.4,0.4,0.4,0.4]
    mutation_probability: 0.005
    mutation_position: [1]
    k: 4
    resistance_cost_multiple_infection: 0.01
    isArtermisininDerivative: 0
  3: # lumefantrine - for advanced users only
    half_life: 4.5
    maximum_parasite_killing_rate: 0.99
    n: 20
    EC50: 0.65
    age_specific_drug_concentration_sd:
[0.4,0.4,0.4,0.4,0.4,0.4,0.4,0.4,0.4,0.4,0.4,0.4,0.4,0.4,0.4,0.4]
    mutation_probability: 0.005
    mutation_position: [2]
    k: 4
    resistance_cost_multiple_infection: 0.01
    isArtermisininDerivative: 0
  4: # lumefantrine - for advanced users only
    half_life: 4.5
```

```
    maximum_parasite_killing_rate: 0.99
    n: 20
    EC50: 0.65
    age_specific_drug_concentration_sd:
[0.4,0.4,0.4,0.4,0.4,0.4,0.4,0.4,0.4,0.4,0.4,0.4,0.4,0.4,0.4]
    mutation_probability: 0.005
    mutation_position: [3]
    k: 4
    resistance_cost_multiple_infection: 0.01
    isArtermisininDerivative: 0
  5: # amodiaquine - for advanced users only
    half_life: 9.0
    maximum_parasite_killing_rate: 0.95
    n: 19
    EC50: 0.65
    age_specific_drug_concentration_sd:
[0.4,0.4,0.4,0.4,0.4,0.4,0.4,0.4,0.4,0.4,0.4,0.4,0.4,0.4,0.4]
    mutation_probability: 0.00
    mutation_position: [1]
    k: 4
    resistance_cost_multiple_infection: 0.01
    isArtermisininDerivative: 0
  6: # amodiaquine - use this for a standard simulation
    half_life: 9.0
    maximum_parasite_killing_rate: 0.95
    n: 19
    EC50: 0.65
    age_specific_drug_concentration_sd:
[0.4,0.4,0.4,0.4,0.4,0.4,0.4,0.4,0.4,0.4,0.4,0.4,0.4,0.4,0.4]
    mutation_probability: 0.005
    mutation_position: [2]
    k: 4
    resistance_cost_multiple_infection: 0.01
    isArtermisininDerivative: 0
  7: # amodiaquine - for advanced users only
    half_life: 9.0
    maximum_parasite_killing_rate: 0.95
    n: 19
    EC50: 0.65
    age_specific_drug_concentration_sd:
[0.4,0.4,0.4,0.4,0.4,0.4,0.4,0.4,0.4,0.4,0.4,0.4,0.4,0.4,0.4]
    mutation_probability: 0.005
    mutation_position: [3]
    k: 4
    resistance_cost_multiple_infection: 0.01
    isArtermisininDerivative: 0
  8: # piperaquine - for advanced users only
    half_life: 28.0
    maximum_parasite_killing_rate: 0.9
    n: 15
```

```
    EC50: 0.65
    age_specific_drug_concentration_sd:
[0.4,0.4,0.4,0.4,0.4,0.4,0.4,0.4,0.4,0.4,0.4,0.4,0.4,0.4,0.4]
    mutation_probability: 0.005
    mutation_position: [1]
    k: 4
    resistance_cost_multiple_infection: 0.01
    isArtermisininDerivative: 0
  9: # piperaquine - for advanced users only
    half_life: 28.0
    maximum_parasite_killing_rate: 0.9
    n: 15
    EC50: 0.65
    age_specific_drug_concentration_sd:
[0.4,0.4,0.4,0.4,0.4,0.4,0.4,0.4,0.4,0.4,0.4,0.4,0.4,0.4,0.4]
    mutation_probability: 0.005
    mutation_position: [2]
    k: 4
    resistance_cost_multiple_infection: 0.01
    isArtermisininDerivative: 0
 10: # piperaquine - use this for a standard simulation
    half_life: 28.0
    maximum_parasite_killing_rate: 0.9
    n: 15
    EC50: 0.65
    age_specific_drug_concentration_sd:
[0.4,0.4,0.4,0.4,0.4,0.4,0.4,0.4,0.4,0.4,0.4,0.4,0.4,0.4,0.4]
    mutation_probability: 0.005
    mutation_position: [3]
    k: 4
    resistance_cost_multiple_infection: 0.01
    isArtermisininDerivative: 0

# therapy info
# the drug_ids that make up the therapy, and the number of days that the therapy
is prescribed for
# testing day tells you the follow-up point at which it is determined if
treatment failed or not
TherapyInfo:
  1:
    drug_id: [1,2]
    dosing_days:  3
    testing_day: 28
  2:
    drug_id: [1,3]
    dosing_days:  3
    testing_day: 28
  3:
    drug_id: [1,4]
    dosing_days: 3
```

```
    testing_day: 28
  4:
    drug_id: [1,5]
    dosing_days: 3
    testing_day: 28
  5:
    drug_id: [1,6]
    dosing_days: 3
    testing_day: 28
  6:
    drug_id: [1,7]
    dosing_days: 3
    testing_day: 28
  7:
    drug_id: [1,8]
    dosing_days: 3
    testing_day: 28
  8:
    drug_id: [1,9]
    dosing_days: 3
    testing_day: 28
  9:
    drug_id: [1,10]
    dosing_days: 3
    testing_day: 28
  10:
    drug_id: [1,2]
    dosing_days: 3
    testing_day: 28
  11:
    drug_id: [1,6]
    dosing_days: 3
    testing_day: 28
  12:
    drug_id: [1,10]
    dosing_days: 3
    testing_day: 28


# drug-deployment strategy - simply uncomment below to turn on a particular
strategy
StrategyInfo:
  #strategyName can be SFTStrategy / CyclingStrategy / MFTStrategy /
AdaptiveCyclingStrategy
#  strategyName: SFTStrategy
#  strategyName: CyclingStrategy
  strategyName: MFTStrategy
#  strategyName: AdaptiveCyclingStrategy
```

```
  SFTStrategy:
    therapyID: [10]


  # cycle three ACTs in and out every five years
  CyclingStrategy:
    therapyID: [10,11,12]
    cycling_time: 1825

  # deploy three ACTs simultaneously
  MFTStrategy:
    therapyID: [10,11,12]
    distribution: [0.33334,0.33333,0.33333]


  # cycle three ACTs in and out - switch between ACTs when the fraction of
patients experiencing
  # treatment failure get to the trigger value below
  # there is a one-year delay until the actual switch is made in the field
(delay_until_actual_trigger)
  AdaptiveCyclingStrategy:
    therapyID: [10,11,12]
    trigger_value: 0.1
    delay_until_actual_trigger: 1
    turn_off_days: 50



# this number use to detemine whether a therapy is "useful" or not and it is
used to calculate
# the useful therapeutic duration of a therapy
TF_rate: 0.1


# definitions of some log parasite density levels
#
parasite_density_level:
  log_parasite_density_cured:        -2.699    # corresponds to 10,000 total
parasites (0.002 per µl)
  log_parasite_density_from_liver:    -2.000   # corresponds to 50,000 total
parasites (0.01 per µl)
  log_parasite_density_asymptomatic: 3         # corresponds to 1000 parasites
per microliter of blood
  log_parasite_density_clinical:     4.301     # corresponds to 20,000 parasites
per microliter of blood
  log_parasite_density_detectable:   1.000     # corresponds to 10 parasites per
microliter of blood
  log_parasite_density_pyrogenic:    3.398     # corresponds to 2500 parasites
per microliter of blood
```

```
immune_system_information:

  #rate at which antimalarial immune function increases when a host is
parasitaemic
  b1: 0.00125

  #rate at which antimalarial immune function decreases when a host is
parasitaemic
  b2: 0.0025

  # durations of infection of naive and fully-immune hosts.
  # these parameters are used to calculate max and min killing rate by immune
system
  duration_for_naive: 300
  duration_for_fully_immune: 60


  # initial conditions for the immune function of the population at time zero
  mean_initial_condition: 0.1
  sd_initial_condition: 0.1

  # (per year) age-dependent faster acquisition of immunity from age 1 to age 10
  immune_inflation_rate: 0.01


  # mix and max probabilities of experiencing symptoms as a result of a new
infection
  # the actual probability will depend on the host's immunity
  min_clinical_probability: 0.05
  max_clinical_probability: 0.99


  # slope of sigmoidal prob-v-immunity function (parameter z in supplement of
2015 LGH paper)
  immune_effect_on_progression_to_clinical: 4

  # age at which immune function is mature
  age_mature_immunity: 10

  # parameter kappa in supplement of 2015 LGH paper
  factor_effect_age_mature_immunity : 1


# days from end of liver-stage infection to appearance of symptoms
days_to_clinical_under_five: 4
days_to_clinical_over_five: 6
```

```
# days that parasites develop mature gametocyte after exiting liverstage
# please read the documentation carefully - there are no explicit gametocytes in
# v3.0.2 of the simulation
days_mature_gametocyte_under_five: 4
days_mature_gametocyte_over_five: 6


# probability that a patient completes a course of treatment
p_compliance: 1


# this functionality works. It is used when p_compliance (above) is less than 1.
# It was not used in any analyses for the 2015 LGH paper where p_compliance is
always 1.
# this guarantees that the minimum number of dosing days for a poorly-complying
# patient is still 1
min_dosing_days: 1


# relative biting rates for individuals; uncomment "distribution: Exponential"
to use an
# exponentially distributed biting rate
relative_bitting_info:
  max_relative_biting_value: 35
  number_of_biting_levels: 100
  biting_level_distribution:
  #  distribution: Exponential
    distribution: Gamma
    Exponential:
      scale: 0.17
    Gamma:
      mean: 5
      sd: 10



# this functionality works, but it was not used in any analyses for the 2015 LGH
paper
percentMovement: [
[0.0,   0.01,   0.01 ],
[0.01,  0.01,   0.01],
[0.01,  0.04,   0.02]
]


meanDaysToReturn: [
```

```
[3,   3,  3 ],
[7,   7,  7 ],
[14,  14, 14 ]
]


# do not change this
# this paramater was used in a different model version where gametocytes were
# modeled explicitly.  In v3.0.2, this need to be set to 0.2.
gametocyte_level_under_artemisinin_action: 0.2


# these values are based on Ross 2006 - these parameters determine the
probability a mosquito
# becomes infected based on the host's asexual parasitaemia level
relative_infectivity:
  sigma: 3.91
  ro: 0.00031
  # on average 1 mosquito take 3 microliters of blood per bloodeal
  blood_meal_volume: 3


# probability to relapse after no treatment, or a treatment failure due to drug
resistance
p_relapse: 0.01


# number of days before a relapse can occur
relapse_duration: 30


# relapse rate - used to increase the parasite density after a treatment failure
(at the drug clearance day)
# multiply by sqrt(20) per day
relapseRate: 4.4721


# minimum update frequency for a host's attributes (esp. parasite density) is
every 7 days, or
# more frequently if other events are occurring at this time
update_frequency: 7


#report to GUI and console every 30 days
report_frequency: 30


# if an infected and asymptomatic host is bitten and infected by a new
# parasite clone, this setting allows the new infection to cause symptoms
allow_new_coinfection_to_cause_symtoms: true
```

```yaml
# this functionality works, but it was not used in any analyses for the 2015 LGH
paper
spatial_information:
  max_relative_moving_value: 35
  number_of_moving_levels: 100
  moving_level_distribution:
  #  distribution: Exponential
    distribution: Gamma
    Exponential:
      scale: 0.17
    Gamma:
      mean: 5
      sd: 10
  circulation_percent: 0.0
  length_of_stay:
    mean: 5
    sd: 10

# this functionality works, but it was not used in any analyses for the 2015 LGH
paper
spatial_external_population_information:
  max_relative_moving_value: 35
  number_of_moving_levels: 100
  moving_level_distribution:
  #  distribution: Exponential
    distribution: Gamma
    Exponential:
      scale: 0.17
    Gamma:
      mean: 5
      sd: 10
  circulation_percent: [0.0, 0.01, 0.01, 0.01, 0.01 ]
  length_of_stay:
    # drawn from gamma distribution?
    mean: 5
    sd: 10
  daily_EIR: [0.01,0.01,0.01,0.01,0.1]
  seasonal_EIR:
    a: [0.25,0.25,0.25,0.25]
    phi: [200,200,200,200]

# this functionality works, but it was not used in any analyses for the 2015 LGH
paper
tme_info:
  tme_starting_day: 0
  mda_coverage: [0.8, 0.8, 0.8, 0.8]
  mda_duration: [4, 4, 4, 4]
```

```
# free recombination among the drug resistance loci
using_free_recombination: true
#using_free_recombination: false


# the current treatment failure rate as observed in the population is not really
# today's treatment failure rate, as these data are never assembled that quickly
in
# real life; rather, it is the average treatment failure rate observed over the
# past 60 days
tf_window_size: 60


# special function to make the mean biting rate (across hosts) depend on age
using_age_dependent_bitting_level: false


# special function which makes the probability of an infection (resulting
# from an infectious mosquito bite) age-dependent
using_variable_probability_infectious_bites_cause_infection: false
```